POWER
REACTOR
TECHNOLOGY

A Quarterly Technical Progress Review

Prepared for DIVISION OF TECHNICAL INFORMATION, USAEC, by

W. H. ZINN and J. R. DIETRICH, GENERAL NUCLEAR ENGINEERING CORPORATION

June 1962

● VOLUME 5

● NUMBER 3

TECHNICAL PROGRESS REVIEWS

To meet the needs of industry for concise summaries of current atomic developments, the Atomic Energy Commission is publishing this series, Technical Progress Reviews. Issued quarterly, each of the reviews digests and evaluates the latest findings in a specific area of nuclear technology and science.

The four journals published in this series are:

Nuclear Safety, Wm. B. Cottrell, W. H. Jordan, and associates, Oak Ridge National Laboratory

Power Reactor Technology, W. H. Zinn and J. R. Dietrich, General Nuclear Engineering Corporation

Reactor Materials, R. W. Dayton, E. M. Simons, and associates, Battelle Memorial Institute

Reactor Fuel Processing, Stephen Lawroski and associates, Chemical Engineering Division, Argonne National Laboratory

Each journal may be purchased ($2.00 per year for subscription and individual issues $0.55) from the Superintendent of Documents, U. S. Government Printing Office, Washington 25, D. C. See back cover for remittance instructions and foreign postage requirements.

Availability of Reports Cited in This Review

Unclassified AEC reports are available for inspection at AEC depository libraries and are sold by the Office of Technical Services, Department of Commerce, Washington 25, D. C. Some of the reports cited are not available owing to their preliminary nature; however, the information contained in them will eventually be made available in formal progress or topical reports.

Unclassified reports issued by other Government agencies or private organizations should be requested from the originator.

Unclassified British and Canadian reports may be inspected at AEC depository libraries. British reports are sold by the British Information Service, 45 Rockefeller Plaza, New York, N. Y.; Canadian reports (AECL series) are sold by the Scientific Document Distribution Office, Atomic Energy of Canada, Ltd., Chalk River, Ontario, Canada.

Classified U. S. and foreign reports identified in this journal as Classified may be purchased by properly cleared Access Permit Holders from the Division of Technical Information Extension, U. S. Atomic Energy Commission, P. O. Box 1001, Oak Ridge, Tenn. Such reports may be inspected at classified AEC depository libraries.

POWER
REACTOR
TECHNOLOGY

A REVIEW OF RECENT DEVELOPMENTS

● JUNE 1962

● VOLUME 5

● NUMBER 3

Foreword

This quarterly review of reactor development has been prepared at the request of the Division of Technical Information of the U. S. Atomic Energy Commission. Its purpose is to assist interested organizations in the task of keeping abreast of new results in reactor technology for civilian application.

Power Reactor Technology contains reviews of selected recently published reports that are judged noteworthy, in the fields of power-reactor research and development, power-reactor applications, design practice, and operating experience. It is not meant to be a comprehensive abstract of all material published during the quarter, nor is it meant to be a treatise on any part of the subject. However, related articles are often treated together to yield reviews having some breadth of scope, and from time to time background material is added to place recent developments in perspective.

The intention is to cover the various areas of reactor development from the general viewpoint of the reactor designer rather than from the more detailed points of view of specialists in the individual areas. To whatever extent the coverage of *Power Reactor Technology* may occasionally overlap the fields of the other Technical Progress Reviews, the overlaps will be motivated by this objective of viewing current progress through the eyes of the reactor designer.

A degree of critical appraisal and some interpretation of results are often necessary to define the significance of reported work. Any such appraisals or interpretations represent only the opinions of the reviewers and the editor of *Power Reactor Technology*, who are General Nuclear Engineering Corporation personnel. Readers are urged to consult the original references in order to obtain all the background of the work reported and to obtain the interpretation of the results given by the original authors.

W. H. ZINN, President
J. R. DIETRICH, Vice President and Editor
General Nuclear Engineering Corporation

Contents

Contents (Continued)

Section

I

Fuel Cycles
and Fuel Utilization

Discussions on the questions of fuel cycles and nuclear fuel utilization have appeared in two published papers[1,2] (one in the United Kingdom and one in the United States). The author of each paper is associated with governmental planning of nuclear fuel applications in his country, but the papers are not intended to reflect official policy.

The question of nuclear fuel utilization, as it relates to nuclear fuel resources, has been discussed on several occasions in the past in *Power Reactor Technology* (Vol. 2, No. 3, pages 1 to 12; Vol. 3, No. 2, pages 21 to 29; Vol. 4, No. 1, pages 5 to 10; and Vol. 4, No. 2, pages 1 to 3). The conclusion appears to be inescapable that thermal-neutron power reactors of current types, in both the United States and Great Britain, utilize so small a fraction of the energy which is potentially available in nuclear fuel that they do not represent long-term solutions to the problem of nuclear power. The first step toward more effective fuel utilization will probably be the recycling of plutonium, but the gains achieved in this way are not large unless the effective conversion ratios of the reactors to which it is applied are relatively high. In principle, the breeder reactor with plutonium (or U^{233}) recycle is an adequate answer to the problem of long-term nuclear fuel supply, but at the present time the practical and economic aspects of breeder reactors and of recycling bred fissionable isotopes have not been proved. In arriving at policies for the development of breeder reactors and for the interim utilization of nuclear fuels, the following questions seem to be important:

1. How soon will nuclear power become generally competitive with conventional power?

2. How rapidly will the quantity of nuclear fuel committed to low-utilization plants increase once these plants do become generally competitive?

3. How much can the utilization of fuel be improved in reactors of current types by straightforward developments of technology?

4. Are there other reactor types which might utilize nuclear fuel more effectively than current types but which would have economic advantages over the breeder reactors?

The papers mentioned above contain information bearing on some of these questions.

The rate of growth of nuclear generating capacity, relative to total installed capacity, is greater in the United Kingdom than in the United States. The planned nuclear capacity for 1967 amounts to some 4000 Mw(e). This is equal to, or somewhat greater than, the expected annual rate of increase of total generating capacity. In reference 1, J. L. Gillams of the Economics and Programming Branch of the United Kingdom Atomic Energy Authority (UKAEA) suggests that the large-base-load nuclear stations should break even with conventional stations at about the end of the decade. Reference 1 does not give an estimate of the rate of increase of nuclear capacity after that time but does give the following qualitative appraisal:

> The rate of nuclear installation seems likely to grow during the 1970's so that first the national base load and later some of the more intermittent demands are met with nuclear stations. As cheaper and more advanced nuclear stations are developed, this should lead to a small but definite reduction in the overall cost of power. If energy demands in the less developed countries follow the rapid rate of the Western industrial nations, an economic way of using nuclear fuels will one day be essential. And then, as cheaper uranium ore reserves are exhausted, it will become necessary to burn at greater efficiencies, and the breeder systems will come into their own, if indeed they have not already done so in straight competition with converters.

In considering breeder reactors, the reference, by implication, limits itself to the fast breeder, and calls attention to the rather large inventory of fissionable isotope required per unit of installed electrical capacity. Despite the rapid accumulation of plutonium inventory from the thermal-neutron power reactors, the inventory requirement might be hard to meet if a nation's power system were suddenly shifted from low-enrichment thermal-neutron reactors to fast breeders. Further, the rate at which inventory can be built up by the net breeding gain is relatively slow because of the long doubling times of breeder reactors. For these reasons reference 1 concludes:

> With the long doubling times with which practical breeders are likely to increase their original fissile inventory, this implies that the first breeder reactors must be brought into operation several decades before any serious shortage of nuclear fuel occurs. This is a most important argument for devoting resources to breeder development today. Nevertheless the immediate incentive to develop breeder reactors is the hope that they will generate power at lower costs than thermal converters fed with cheap uranium. If that were not the case, the development of the breeder could be allowed to proceed at a slower rate more akin to the expected rise in future uranium costs.

This conclusion as to the urgency (or the lack of it) for the development of breeder reactors may be more appropriate for the United Kingdom, in which the planning and selection of reactor types to supply the national grid is under the firm control of a government agency, than for the United States. When it is recognized that the construction of a nuclear plant represents a commitment for 20 to 30 years to a particular kind of fuel and a particular degree of fuel utilization, it is easy to imagine that the wasteful application of nuclear fuels could progress to an undesirable extent before economic forces would correct the situation in a free economy.

In reference 2, Donald W. Kuhn and Ray D. Walton, Jr., of the Technical Policy Branch, Division of Operations Analysis and Forecasting, USAEC, treat some of the more detailed questions of plutonium recycle. They give estimates of the fuel utilization attainable with a boiling-H_2O reactor and with a fast-breeder reactor, and they describe past and present work with experimental reactors directed toward breeding and plutonium recycle.

In estimating the possible fuel utilization with the boiling-H_2O reactor, Kuhn and Walton make use of a previous study, by Greebler et al., which was reported at the 1958 Geneva Conference.[3] The reactor utilizes UO_2 (with recycled PuO_2) as fuel at an H_2O-to-UO_2 volume ratio of 2.0. The reactor is assumed to be in an equilibrium fuel cycle, in which the discharge exposure of the fuel is 8800 Mwd/metric ton of uranium. Fuel is discharged and reloaded in an idealized small-batch system; each batch consists of 20 per cent of the total core volume. The feed fuel contains uranium enriched to 0.952 at.% U^{235} plus the recycled plutonium; the discharged fuel contains uranium that is 0.653 at.% U^{235}. The plutonium isotopes are removed from the discharged fuel by chemical separation processes and are recycled to the new fuel. After the chemical separation step, the partially depleted uranium is recycled to the diffusion plant, where, along with a feed of virgin natural uranium, it is reenriched to the 0.952 at.% level required for fresh reactor feed. In this equilibrium cycle, 0.572 metric ton of uranium appears in diffusion-plant tails, and 0.019 metric ton of uranium is consumed, in the reactor and in processing losses of uranium outside the reactor, per metric ton of uranium put into the reactor as fresh feed. The uranium utilization is therefore $8800/(0.572 + 0.019) = 14,900$ Mwd/metric ton of uranium consumed. This utilization is equivalent to the fissioning of 1.63 per cent of the natural uranium fed into the cycle. Further characteristics of the reactor and the fuel cycle are summarized in Table I-1.

In a fast-breeder reactor, the utilization can be quite high, and, in present concepts of the system, the fuel is recycled many times before it is finally used up. In a system of this kind, the actual level of fuel utilization is determined primarily by the processing losses per cycle and by the average number of processing cycles experienced by a typical fuel sample during its lifetime. On the basis of an average burnup of 2 per cent of the uranium atoms per exposure cycle, the estimates[2] are (1) that about 25 per cent of the uranium could be fissioned if the losses amount to 2 per cent per processing cycle and (2) that about 60 per cent could be fissioned if the losses were no greater than

Table I-1   CHARACTERISTICS OF BOILING-H_2O
REACTOR USED FOR FUEL-UTILIZATION
ESTIMATES[2,3]

Reactor type	Boiling H_2O
Pressure	1015 psia (546.4°F saturation)
Core size	Cylinder, 10.3 ft in diameter by 8.6 ft in length
Power	630 Mw(t)
Fuel	UO_2 with recycled PuO_2, at 95% of the theoretical UO_2 density
Fuel-rod diameter	0.494 in. (cold)
Cladding	0.030-in. Zircaloy-2
Volume ratio: H_2O/fuel	2.0
Volume fractions:	
Fuel	0.30728
Water	0.61455
Cladding	0.07817
Average steam void	15% of water volume
Fuel-replacement scheme	20% of core per cycle
Discharge exposure level	8800 Mwd/metric ton of U
k_{eff} before fuel discharge	1.04 (without Xe and Sm)
Irrecoverable processing losses	0.4% per cycle
Ratio: kg of U discharged/kg of U charged	0.985
U^{235} content of U in fresh fuel	0.952 at.%
U^{235} content of U in spent fuel	0.653 at.%
Composition of spent fuel (in at.%, where 100% is sum of U + Pu atoms):	
U^{235}	0.641
Pu^{239}	0.525
Pu^{240}	0.324
Pu^{241}	0.18
Pu^{242}	0.80

0.4 per cent per cycle. These energy yields are not affected strongly by the reactor breeding ratio, provided that it is substantially greater than unity.

The reference quotes some experience with fabrication costs of fuel elements containing plutonium. Although these figures apply to special situations and are of limited general significance, they are nevertheless of some interest. The costs for a loading of 36 plutonium-aluminum fuel assemblies for the Materials Testing Reactor were about $525,000 for fuel-element development and $210,000 for fabrication. The reference states that a current Hanford cost estimate for fabricating an equivalent amount of fuel with presently available

techniques is $150,000 or approximately $25,000 per kilogram of contained plutonium. The Plutonium Recycle Test Reactor utilizes, in its present loading, some UO_2 fuel elements and some elements of 1.8 wt.% plutonium–aluminum alloy, both Zircaloy clad. The reference quotes fabrication cost estimates of $3500 per UO_2 fuel element and $3900 per plutonium fuel element. These estimates are based on the techniques used to fabricate the last fuel element of each type for the first core.

A study of fuel burnup in H_2O-moderated reactors is reported in reference 4. This study is of interest in connection with fuel utilization, although it was not directed specifically at that question. It examines the reactivity relations, conversion ratios, and lifetime characteristics of single-batch H_2O-moderated reactors fueled with UO_2, giving special attention to lattices having low moderator-to-fuel ratios. Earlier work on this project, which treated lattices of uranium metal in H_2O, was reviewed in the December 1960 issue of *Power Reactor Technology*, Vol. 4, No. 1, pages 6 and 7.

Figure I-1 shows the calculated variation of initial conversion ratio (ICR) with hydrogen-to-uranium atom ratio for lattices of 0.4-in. UO_2 rods of several enrichments. As is to be expected, the conversion ratio increases with decreasing enrichment and with decreasing hydrogen-to-uranium ratio, since both of these variations increase the ratio of neutron absorption in U^{238} to that in U^{235}. When considerations of reactivity are interjected by requiring that
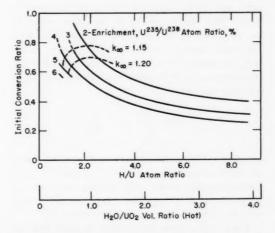
Fig. I-1   Initial conversion ratios and loci of k_∞ values for H_2O-UO_2 reactors.[4]
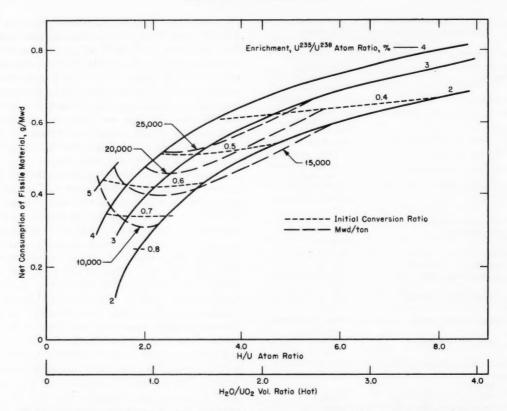
Fig. I-2   Net consumption of fissile material (in grams per megawatt-day) for very large H_2O-UO_2 reactors.[4]

the lattice have some specified value of k_∞ (the infinite multiplication constant), a single combination of enrichment and hydrogen-to-uranium ratio will then yield the maximum conversion ratio. This maximum value becomes lower as the required k_∞ is increased because the extra neutrons required to increase k_∞ must, in effect, be taken from the neutrons available for conversion. This relation may be expressed in the following way:

$$ICR = \frac{\eta_{25}\epsilon}{k_\infty} - 1 - \frac{A_p}{A_{25}}$$

where η_{25} is the number of neutrons produced per neutron absorbed in U^{235}, ϵ is the U^{238} fast-fission factor, and A_p/A_{25} is the ratio of the parasitic absorption rate (all materials except U^{235} and U^{238}) to the absorption rate in U^{235}.

When the conversion ratio is high, the net consumption of fissile material, per unit of energy produced by the reactor, is low. This

trend is shown in Fig. I-2, where net consumption is plotted as a function of hydrogen-to-uranium ratio with parametric curves giving the initial conversion ratio and the reactivity lifetime. This figure applies to a very large reactor in which the loss of neutrons by leakage is negligible. Other characteristics of the reactor are given in Table I-2. It is evident from Fig. I-2 that, as the reactivity lifetime is increased, the ICR decreases and the net fuel consumption increases. This results mainly from the increase in initial k_∞ which is necessary to yield the longer reactivity lifetime. It is fairly evident from the figure that high conversion ratio is incompatible with very long reactivity lifetime in a single-batch reactor of this kind.

For the relatively modest reactivity lifetime of 10,000 Mwd/ton, the net consumption of fissile material is rather low, approximately 0.31 g/Mwd. This value, which is approximately one-fourth of the consumption that would apply

Table I-2   CHARACTERISTICS OF H$_2$O-MODERATED REACTOR USED FOR INVESTIGATION OF UO$_2$-H$_2$O LATTICES[4]

Moderator-coolant	H$_2$O
Temperature	550°F
H$_2$O density	0.75 g/cm^3
Fuel	UO$_2$ rods, 0.400 in. in diameter
Cladding	Zirconium
Volume ratio: (cladding and structure)/fuel	0.74
Average power level	5 kw/linear foot of fuel rod
Fuel reloading scheme	Full-core batch

if pure U^{235} were burned without conversion of U^{238}, is compatible with the indicated initial conversion ratio of about 0.75. It corresponds to the destruction of approximately 0.86 g of U^{235} per megawatt-day and a net production of about 0.55 g of fissile plutonium (Pu^{239} + Pu^{241}) per megawatt-day. In supplying the slightly enriched U^{235} feed for such a reactor, the diffusion plant would discard about 0.38 g of U^{235} per megawatt-day in the tails. If this U^{235} is considered to be wasted, then the net consumption of fissile isotopes per megawatt-day increases to 0.31 + 0.38 = 0.69 g. This increase illustrates the importance of the U^{235} loss in the diffusion-plant tails in increasing the effective consumption of fissile isotope.

Although the analyses reported in reference 4 do not give an estimate of the fuel utilization attainable with plutonium recycle, they do indicate that the maximum usable conversion ratios in H$_2$O-moderated reactors are not extremely high, even before plutonium isotopes have built up. When the lower value of η for Pu^{239} in a thermal-neutron spectrum is taken into account, it seems probable that the value of utilization estimated in reference 2 (14,900 Mwd/metric ton of virgin uranium) is near the maximum that can be achieved practically in an H$_2$O-moderated reactor.

References

1. J. L. Gillams, Uranium, Plutonium, and Nuclear Breeders Long-Term Prospects for Nuclear Power in Britain, British Report DPR/INF/263, August 1961; also in the May 1961 issue of *Discovery*.

2. D. W. Kuhn and R. D. Walton, Jr., Long Term Utilization of Uranium and Thorium, USAEC Report TID-13901, October 1961.

3. P. Greebler et al., Recycle of Plutonium in Low-Enrichment Light-Water Reactors, *Proceedings of the Second United Nations International Conference on the Peaceful Uses of Atomic Energy, Geneva, 1958*, Vol. 13, pp. 251–264, United Nations, New York, 1958.

4. J. Bengston et al., Lifetime Characteristics and Economics of Slightly Enriched Uranium Dioxide in Water Lattices, USAEC Report CEND-145, Combustion Engineering, Inc., Sept. 30, 1961.

Reactor Physics

Critical and Exponential Experiments

An investigation of D_2O-moderated lattices made up of R-3/Adam type fuel assemblies is being carried out at Savannah River Laboratory (SRL). The earlier room-temperature measurements of material buckling in the Process Development Pile[1] (PDP) have now been supplemented by measurements at elevated temperature in the Laboratory's High Temperature Exponential Facility (PSE).[2] The latter experiments were performed for a range of D_2O moderator temperatures from 20 to 220°C, with three different lattice pitches (one of which was the R-3/Adam design pitch).

Fuel assemblies that will later be used in the R-3/Adam reactor were furnished to SRL for the experiments. These assemblies are clusters of 19 Zircaloy-2-clad fuel rods of sintered natural-uranium oxide pellets. The fuel rods are 1.70 cm in diameter, and the average intra-assembly center-to-center spacing of the rods is 2.176 cm. The Zircaloy-2-clad tubes have an inside diameter of 1.72 cm and an outside diameter of 1.86 cm. Each tube is approximately 75 cm long; for the experiments two lengths of tubes were joined together to make assemblies that were approximately 150 cm in length. A gap of 4.5 cm, in which no fuel was present, existed at the junction of the two tubes.

Buckling measurements were made in the high-temperature exponential facility for three square lattice pitches: (1) 27 cm (the design pitch of the R-3/Adam reactor), (2) 24 cm, and (3) 30 cm. For the 30- and 27-cm pitches, 21 fuel assemblies were arranged in a five-by-five array with one assembly removed from each corner. For the 24-cm pitch, 24 assemblies were arranged in a six-by-six array with three

assemblies removed from each corner. The experimental portion of the investigation consisted of determining the axial flux distributions for each of the arrays at selected moderator temperatures within the range 20 to 220°C. The room-temperature radial buckling for the PSE had previously been determined by intercomparison measurements between the PDP and the PSE. A series of least-squares fits of the experimentally determined transverse flux distributions was used to ascertain the values of arguments of $A \sinh{(\kappa_z)}$, the function used to describe the axial flux distribution. The material bucklings were then calculated by means of the following:

$$B_m^2 = 8.45m^{-2} - \kappa_z^2 - (\delta B_r^2 + \delta \kappa_z^2)$$

where δB_r^2 is the change in radial buckling with temperature and $\delta \kappa_z^2$ is a correlation term used to account for the change in length, due to changes in temperature, of the aluminum support tube which holds the foils. The measurements previously made in the PDP served as check points for the room-temperature exponential measurements.

Activation foils were also used to determine the thermal-migration areas for the lattice of 27 cm pitch. At 20°C the thermal-migration area was found to be 183 cm^2, and at 217°C it was 263 cm^2.

The Zero Power Reactor III (ZPR-III) was used to perform criticality studies[3,4] of a dilute oxide fast-reactor core at two values of the oxygen-to-uranium atomic ratio. A similar study with a core using an intermediate oxygen-to-uranium atomic ratio of 1:1 was previously reported and was reviewed in the March 1962 issue of *Power Reactor Technology*, Vol. 5, No. 2. In the studies described in reference 3, the use of two alumina plates per plate of ura-

nium gave a uranium-to-oxygen atomic ratio of 1:1.90 so as to simulate a uranium oxide fuel. Reference 4 reports the results of critical experiments in which the oxygen was eliminated.

The experiments previously reported and those in reference 4 were undertaken to determine whether the discrepancy in calculated and measured critical mass (24 to 40 per cent) could be attributed to deficiencies in the theoretical treatment of the oxygen. Since approximately the same discrepancy was noted in all three experiments, with widely different oxygen contents, it cannot be attributed to the effects of oxygen, but is now thought to be due to inaccuracy in the cross-section data used in the calculation of large dilute fast-reactor cores.

Studies[5] were conducted on service core 1 of the N.S. *Savannah* at the Babcock and Wilcox Critical Experimental Laboratory to determine: (1) fast-neutron-flux distributions at the pressure vessel wall, and (2) in-core neutron-flux distributions for a number of control-rod configurations. The first set of measurements was made in order to provide a limited amount of information on fast-neutron distributions immediately outside the core. These data will subsequently be used in the correlation of potential radiation-damage effects to the pressure vessel, as determined from carbon steel samples that will be irradiated during actual reactor operation in a test well outside the *Savannah* core. In-core flux distribution measurements for various control-rod configurations and reactor operating conditions were performed using manganese-copper activation wires. Some of these measurements have been analyzed using a three-dimensional (TKO), diffusion-theory IBM-704 code. Within the mesh-point limitations imposed by the IBM-704 storage capabilities, the calculations were found to agree rather well with the experimental data.

Reference 6 presents a semiempirical method of estimating the material bucklings for slightly enriched uranium-water lattices. The method is based on a correlation between one-group theory calculations and experimental data gathered for uranium-rod light-water lattices, in which enrichments of 1, 2, and 3 per cent U^{235} were used. With the exception of η, the parameters necessary to calculate the material bucklings were determined by the use of an IBM-7090 code (IDIOT). Calculated values of η were adjusted to give agreement with experimentally measured values, and those empirically modified values of η were then used in the calculations of the material bucklings. Maximum bucklings and minimum critical masses for water-reflected lattices of enriched-uranium rods in light water, as determined by this method, are given for fuel enrichments of 2.0, 3.063, and 5.0 per cent U^{235}.

The same method of calculation was used[7] to determine a number of additional critical parameters that are useful in establishing nuclear safety in the handling and storage of slightly enriched uranium fuel elements. The parameters include critical mass, critical slab thickness, critical slab geometry, critical volume, and critical mass per unit area. These parameters are reported as functions of water-to-uranium volume ratio, rod diameter, and U^{235} enrichment.

Reference 8 contains a summary of critical and exponential experiments performed in support of the Spectral Shift Control Reactor (SSCR) Basic Physics Program. The critical experiments were performed with UO_2 fuel rods of 4 per cent enrichment in moderators containing 70 mole % D_2O, 70 mole % D_2O with dissolved boric acid, and 50 mole % D_2O with boric acid. In all lattices the nonmoderator-to-moderator volume ratio was 1.0. The following measurements were made for all arrays: critical mass, critical buckling, thermal-disadvantage factor, and cadmium ratio of U^{235}. Measurements of the neutron spectra are given for lattices containing 70 and 76.7 mole % D_2O, and measurements of epithermal absorption in U^{238} which were made by several techniques are also reported.

For the room-temperature exponential experiments, highly enriched $(U^{235} + Th)O_2$ fuel rods were used in moderators that ranged between 50 and 80 mole % D_2O. The volume ratio of nonmoderator to moderator for all the exponentials was 1.0. The cadmium ratio of U^{235}, the cadmium ratio of thorium in lattices having moderators of 53, 71, and 80 mole % D_2O, and the material bucklings were the three primary quantities measured in the exponential experiments.

Reference 9 describes an investigation of the void coefficient of reactivity in natural uranium—D_2O lattices at SRL by both exponential experiments and theoretical calculations. The fuel elements used in this investigation

were assemblies of either two or four coaxial tubes of natural-uranium metal arranged in several lattices to simulate the fuel-element design and the lattice spacings which have been proposed for a boiling-D_2O-cooled power reactor. Although there was some uncertainty in the experimental reactivity values and in the theoretical calculation of resonance capture, the agreement between theory and experiment was satisfactory (<1.5 per cent Δk_∞ deviation). Since both theory and experiment predict large positive void coefficients of reactivity in boiling-D_2O-moderated reactors, consideration of the fuel-element designs and lattice spacings used in this study would be prohibited for a power reactor of practical size.

The Lawrence Radiation Laboratory has completed a series of experiments with bare graphite-moderated assemblies of various carbon-to-U^{235} ratios. The preliminary results of this series of experiments are given in reference 10. The Hot Box critical facility was used with fuel elements of 2- and 4-mil thickness. Critical buckling was measured over a temperature range of 45 to 1205°F and for carbon-to-U^{235} ratios ranging from 1185:1 to 21,690:1. The preliminary data indicate that the rate of change of critical buckling with temperature $[(\Delta B^2/B^2)/\Delta B]$ decreases with temperature for all carbon-to-U^{235} ratios. At a constant temperature the same quantity increases with an increase in the carbon-to-U^{235} ratio and approaches an asymptotic value of about 2 per cent per 100°F at very high carbon-to-U^{235} ratios. A more comprehensive description and analysis of the experiments will appear in a subsequent report.

Reference 11 presents an empirical method of estimating the minimum critical mass, in spherical geometry, of enriched-uranium rods in light water, and is intended to be used to evaluate the minimum safe configurations in chemical separations processes. The capture by U^{238} in the resonance and epithermal regions is represented by a uniformly distributed neutron poison with an effective thermal absorption cross section of 1.61 barns. A number of empirical equations which are presented in the reference permit a rapid and conservative estimation of the minimum critical mass for all possible rod sizes and all possible water-to-uranium volume ratios. The critical mass predicted by this method is always conservatively less than, or equal to, the experimental value.

Exponential experiments are described in reference 12 for uranium metal lattices moderated by heavy water, graphite, and diphenyl. The fuel elements were in the form of 1-in.-diameter 4-in.-long slugs of three enrichments: 0.4962, 0.7205, and 0.9124 per cent U^{235}. Experimental values of resonance capture, thermal utilization, material buckling, and local flux distributions are reported for the several lattice arrangements and moderators used. A theoretical comparison is also included, for which a two-group diffusion theory was used. Maxwellian-averaged thermal cross sections were used for D_2O- and graphite-moderated lattices, and Wigner-Wilkins-averaged cross sections were used in the more closely packed diphenyl-moderated lattice. Fast-group constants were evaluated with the FORM code, and local self-shielding and thermal group constants were determined with an S_n code. Although the calculated intracell flux distributions and thermal utilization (f) agreed reasonably well with experiment, the calculated material bucklings were consistently larger than the measured values.

In support of the Organic-Moderated Reactor concept, reference 13 presents a theoretical investigation of three metal-plate fuel assemblies in a critical facility moderated by Santowax R. Experimental data are available for one of the core arrangements. The fuel elements are in the form of 100-mil plates of slightly enriched uranium, clad with 40-mil aluminum. Two calculational schemes were used for the analysis of the critical cores. The first method, a two-group one-dimensional cylindrical model, overestimated the reactivity by about $2\frac{1}{2}$ per cent $\Delta k/k$. The second scheme, a multigroup calculation using 15 groups, agreed with the experimental reactivity within 0.7 per cent $\Delta k/k$. In addition to reactivity calculations, the report discusses thermal utilization (cell homogenization), flux distributions, temperature and void coefficients, fuel orientation effects, and flux flattening by means of a variable moderator-to-fuel ratio.

A survey[14] that contains abstracts of unclassified reports on criticality calculations, exponential and critical experiments, safety regulations and limits for critical experiments, and safety criteria for handling and storing of fissionable materials is available.[14] A total of 1145 references were abstracted, and their coverage extends through Dec. 31, 1961.

Effect of Absorber Temperature Distribution on Resonance Absorption

References 15 and 16 give the results of analytical studies of the effect of temperature distribution within a fuel rod on the resonance absorption of incident neutrons. In both references a parabolic temperature distribution is assumed, with the maximum temperature (T_c) at the center of the fuel element. The flux variation through the fuel element was computed by the methods of Case, De Hoffmann, and Placzek. In general, an effective uniform temperature (T_{eff}) can be defined which is a function of the fuel-element geometry and the temperatures at the surface (T_s) and at the center (T_c) of the fuel element. Reference 15 gives the following expression for T_{eff}:

$$T_{eff} = T_s + A(T_c - T_s)$$

where $A = \frac{2}{3}$ for slab geometry, $\frac{1}{3}$ for spherical geometry, and $\frac{4}{9}$ for cylindrical geometry; T_{eff} is defined as that temperature which will yield the same neutron absorption (resonance) as the actual nonuniform temperature distribution.

Reference 16 contains a more theoretical and detailed treatment of the problem and includes a general expression that will permit the evaluation of the effective temperature for any given neutron-flux distribution.

Neutron Spectra in Graphite Lattices

Reference 17 is a report on the results of neutron-energy-spectrum measurements that were made, by a time-of-flight spectrometer, on a uranium-graphite lattice at several different lattice temperatures. The subcritical lattice, which consisted of natural-uranium slugs that were 1.15 in. in diameter on an 8-in.-square pitch in graphite, was fed from a reactor. The neutron beam was extracted, in a direction parallel to the fuel channels, from a position near the center of the lattice and midway between two fuel channels.
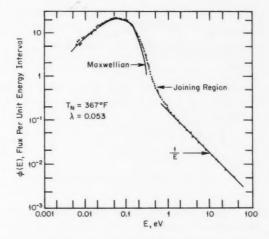
Fig. II-1   Neutron spectrum[17] with lattice at 321°C.

A typical spectrum is shown in Fig. II-1.* As is usual in reasonably well-moderated cases, the observed spectrum can be divided into three characteristic regions. In the lowest of these, the flux distribution is Maxwellian:

$$\phi_M(E) \propto \frac{E}{E_0^2} \exp\left(-\frac{E}{E_0}\right)$$

where E_0 is the energy at the peak of the distribution. The upper range of the spectrum, often referred to as the tail, has the usual $1/E$ distribution:

$$\phi_T(E) = \frac{\lambda}{E}$$

where λ is a constant, chosen to normalize the spectrum in such a way that $\int_0^\infty \phi_M(E) = 1$. Between the Maxwellian and the $1/E$ regions is a transition, or joining, region whose shape cannot be described by a simple relation. The characteristics of the joining region can be examined by subtracting the Maxwellian portion of the spectrum and considering the remainder, $\phi'(E)$:

$$\phi'(E) = \phi(E) - \phi_M(E)$$

If the quantity $E\phi'(E)/\lambda$ is plotted as a function of E/kT_N (where T_N is the neutron temperature,

*Figures II-1 and II-2 and Table II-1 are reprinted here by permission from the United Kingdom Atomic Energy Authority.[17]
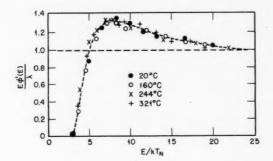
Fig. II-2   Joining-region spectra.[17]

i.e., the temperature that characterizes the Maxwellian component of the spectrum), the curve is independent of the moderator temperature.[17] Such a curve is shown in Fig. II-2.

Frequently, in taking account of the spectrum for practical reactor problems, the joining portion of the spectrum is omitted; however, its effect is approximated by assuming that the spectrum consists of a Maxwellian distribution joined to a $1/E$ tail which drops abruptly to zero at some energy, μkT, such that the absorption rate for a $1/v$ absorber in the fictitious spectrum is the same as its absorption rate in the real spectrum. The significance of Fig. II-2, in which the points for various moderator temperatures fall nearly on a single curve, is that the parameter μ in such an approximation would be nearly independent of moderator temperature.

The experimentally determined neutron temperatures and the values of λ and μ are given in Table II-1 for the four different moderator temperatures investigated. The neutron temperatures are higher than those predicted by the heavy-gas thermalization model when a mass of 12 is used for the carbon atom in graphite. The reference gives the effective masses of the carbon atom which are consistent with the observed temperatures and the heavy-

Table II-1   RESULTS OF NEUTRON-SPECTRUM MEASUREMENTS IN A URANIUM-GRAPHITE LATTICE[17]

Lattice temp. (T_M), °C	Neutron temp. (T_N), °C	λ	μ
20	74 ± 2	0.065 ± 0.001	3.6 ± 0.1
160	210 ± 3	0.060 ± 0.001	3.5 ± 0.1
244	290 ± 4	0.057 ± 0.001	3.1 ± 0.1
321	367 ± 4	0.053 ± 0.001	3.1 ± 0.1

gas model. The effective mass decreases from 30 to about 19 as the moderator temperature is raised from 20 to 321°C.

The reference also discusses the principles of the measurements, the sources of error, and the corrections that were applied.

References

1. W. E. Graves, R-3/Adam Lattice Buckling Measurements in the Process Development Pile, USAEC Report DP-598, Savannah River Laboratory, July 1961.

2. N. P. Baumann, PSE-SE Measurements on R-3/Adam Lattices, USAEC Report DP-613, Savannah River Laboratory, September 1961.

3. A. L. Hess et al., Critical Studies of a 450-Liter Uranium Oxide Fast Reactor Core (ZPR-III Assembly 29), USAEC Report ANL-6336, Argonne National Laboratory, November 1960.

4. J. M. Gasidlo et al., Critical Studies of a Dilute Fast Reactor Core (ZPR-III Assembly 31), USAEC Report ANL-6338, Argonne National Laboratory, October 1961.

5. A. L. McKinney (Ed.), Nuclear Merchant Ship Reactor Project. Extended Zero Power Tests, N.S. *Savannah* Core I. Final Report, USAEC Report BAW-1203(Vol. 1), Babcock and Wilcox Co., January 1961.

6. C. L. Brown, A Semi-Empirical Method of Estimating Material Bucklings for Slightly Enriched Uranium-Water Lattices, USAEC Report HW-68405, Hanford Atomic Products Operation, March 1961.

7. C. L. Brown, Calculated Critical Parameters for Slightly Enriched Uranium Rods in Light Water, USAEC Report HW-69273, Hanford Atomic Products Operation, April 1961.

8. Babcock and Wilcox Co., Spectral Shift Control Reactor Basic Physics Program, Quarterly Technical Report No. 4, April–June 1961, USAEC Report BAW-1221.

9. W. B. Rogers, Jr., Exponential Void Coefficient Measurements for Natural Uranium Tubes in D_2O, USAEC Report DP-643, Savannah River Laboratory, September 1961.

10. R. G. Finke, Preliminary Results of High-Temperature Bare U^{235}-C Critical Assembly Measurements, USAEC Report UCRL-6504, University of California Lawrence Radiation Laboratory, June 1961.

11. B. G. Owen and H. W. Haskey, Minimum Mass in Uranium-Metal Water Lattices, British Report PG-Report-257, 1961.

12. R. W. Campbell and C. H. Skeen, Exponential Experiments with Heavy-Water, Graphite-, and Diphenyl-Moderated, Uranium Metal Lattices,

USAEC Report NAA-SR-6446, Atomics International, Sept. 15, 1961.

13. R. A. Blaine and J. L. Watts, Calculated Nuclear Properties of Low-Enrichment Metal-Plate Lattices in the OMR Critical Assembly, USAEC Report NAA-SR-6330, Atomics International, Aug. 15, 1961.

14. R. L. Scott, Criticality, a Bibliography of Unclassified Literature, USAEC Report TID-3306, March 1961.

15. G. Rowlands, Atomic Energy Research Establishment, Harwell, August 1961. (Unpublished)

16. A. Reichel, The Effect of Nonuniform Fuel Rod Temperatures on Effective Resonance Integrals, British Report AEEW-R-76, June 1961.

17. M. S. Coates and D. B. Gayther, Time of Flight Measurements of Neutron Spectra in a Graphite Uranium Lattice at Different Temperatures, British Report AERE-R-3829, September 1961.

Heat Transfer:
International Conference

New developments in the theory and practice of heat transfer were summarized in a series of about 125 papers presented at the 1961 International Heat Transfer Conference held August 28 to September 1, 1961, at the University of Colorado. The papers are published by the ASME in five volumes (Parts I to V), each volume bearing the general title, *International Developments in Heat Transfer*. A review is presented here of those papers which are of specific interest in nuclear engineering applications. Each conference paper referred to is identified by its paper number as it appears in the five-part publication by the ASME.

Contact Resistance

Reference 1 describes the experimental work performed and the data obtained in an investigation of the thermal contact resistance at the interface of uranium and Magnox test specimens under various conditions. This work was performed as part of the British effort to improve the over-all heat-transfer performance of the CO_2-cooled graphite-moderated power reactors being built in Great Britain at the present time; these reactors incorporate cylindrical metallic uranium fuel rods canned in a magnesium alloy that is known as Magnox A12. Measurements were carried out with an apparatus using small cylindrical specimens of uranium and Magnox placed with their flat faces in contact. The experimental program included the effect of such parameters as interface temperature, interface gas, interface gas pressure, contact pressure, surface uranium oxide layer thickness, and surface uranium nitride layer thickness. Data are presented which give the effects of these parameters on the contact-interface resistance to heat flow.

The heat transfer across an interface involves two parallel heat-flow paths: (1) conduction through the metal contact spots between the two surfaces (total contact area is normally only a small fraction of the nominal area) and (2) conduction across the fluid film that normally fills the spaces between the surfaces (radiation here is negligible). The data show that at low contact pressures the interface resistances for an argon atmosphere are appreciably higher than those for a helium atmosphere, whereas the resistances measured in vacuum are even higher than those in argon. However, at the higher contact pressures, the resistances for helium, argon, and vacuum tend to approach each other. Under these conditions the contact becomes very intimate, and virtually all the heat is transferred by conduction through the contact spots. The data show that the presence of a uranium oxide film of 3×10^{-4} in. thickness increases the resistance by a factor of about 3 compared with the case of an unoxidized surface.

Reference 2 also treats the problem of thermal conductance of metal contacts but uses a more basic approach than reference 1. As two normally rough flat surfaces in contact are pressed together under an increasing load, the contact spots increase in size, at first by elastic and then by plastic deformation. Experiments show that, unless surfaces are extremely smooth, the loads which can be supported by elastic deformation are extremely small. Hence it can be assumed that the pressure over each contact spot is equal to the indentation yield pressure of the softer metal, i.e., the Meyer hardness value M. A simple thermal-conductance theory is first reviewed in the reference, based on the proposition that M is independent of the contact-spot loading. To check the adequacy of the theory and to evaluate the parameters involved, experimental values of conduct-

ance versus load were obtained for contacts of steel and brass, steel and aluminum, brass and aluminum, and brass and brass. The interface fluids were air, glycerol, and water. Machined surfaces were used, and they had a regularly pitched ridging or waviness in one direction which was due to the periodic nature of the machining process. The roughness of a surface was defined in terms of λ, the wavelength of surface irregularity. Four different surface roughnesses were used in the experiments, varying from $\lambda = 0.0280$ to 0.0029 in. Comparison of the experimental data with the functional relations indicated by the theory shows good agreement with respect to the contribution of the fluid-film conductance to the over-all conductance process. However, deficiencies in the theory with regard to the contact-spot conductance term are evident. In particular, the plots of contact-spot conductance versus pressure exhibit slopes considerably greater than $\frac{1}{2}$ (as given by the theory). Moreover, the superiority of the finer (small λ) surfaces over the coarser surfaces, which is due to the larger number of contact spots, is not as great as predicted. Various possible explanations for the discrepancies between experiment and theory were considered; it was concluded, on the basis of observed results of microindentation hardness tests, that there is an apparent increase in the hardness of metals at low loads. Such an effect has also been indicated by other experiments. To correlate the heat-transfer data obtained, reference 2 extends the simple conductance theory to include the effects of very high microhardness, dependent both on pressure and on surface texture. The postulated form of the microhardness variation contains adjustable constants that were selected to obtain agreement with the experimental data. The maximum hardnesses indicated by the data fits are extremely high. No explanation could be offered for this; the only claim that could be made for the "superhardness" hypothesis used is its value in correlating the heat-transfer data.

Once-Through Boilers

In the design of heat exchangers for the gas cooled nuclear-power stations in Great Britain, consideration has been given to the possible use of "once-through" systems where water entering the tubes of the evaporating section may be completely evaporated by the time it leaves. In the thermal design of these evaporators, a knowledge of the heat-transfer coefficient is required over the entire range of quality of the steam-water mixture, from 0 to 100 per cent. Experiments that are described in reference 3 were made on the evaporation of high-quality two-phase mixtures flowing in a horizontal hairpin tube that was 1.6 in. in inside diameter. A wide variety of flow rates, steam pressures, and quality conditions was investigated, but at relatively low heat fluxes. For each test condition the whole transition region, from the portion characterized by high boiling coefficients to that characterized by low superheated-steam coefficients, which occurred along the length of the test section, was studied. It was not possible to obtain a satisfactory correlation of the high coefficient values prior to transition, but the general changes in the coefficient with respect to steam pressure, flow rate, and heat flux were qualitatively explained by existing correlations. In the experiments the transition generally began at steam qualities between 94 and 98 per cent; as the 100 per cent quality condition was approached, the coefficients reached the anticipated values for dry saturated steam.

Three main regimes, occurring at progressively higher qualities, are involved during the complete evaporation of liquids flowing in tubes: (1) the nucleate boiling region; (2) the mist-annular region wherein water is dispersed as fine droplets in the vapor-phase stream and wets the tube walls; and (3) the liquid-deficient region where the walls become dry. From the many local temperature measurements made, it appears that the water film of the mist-annular regime does not disappear suddenly but recedes progressively, starting at the top of the tube and finally finishing at the bottom. The fact that the film can exist in an intermediate condition, i.e., partly up the sides of the tube walls, can be explained by the action of surface-tension forces.

Bubble Growth and Pool Boiling

Reference 4 presents the results of an experimental study of the rate of growth of bubbles in binary liquid mixtures. The immediate objective was to evaluate the adequacy of a recent

theory by Scriven[5] which predicts bubble growth rates in such mixtures; from a long-range viewpoint, it is hoped that research on the microscopic details of boiling may lead eventually to a much-needed understanding of the macroscopic behavior of boiling liquids.

The form chosen by Scriven for expressing the growth of a bubble is

$$R = 2\beta \sqrt{\alpha\theta}$$

where R = bubble radius
α = liquid thermal diffusivity
θ = time
β = coefficient dependent on properties of the liquid and vapor and on the degree of superheat, ΔT, at the heating surface

Values of β have been computed for the system water-glycol for ΔT's of 4, 8, 15, 18, and 30°C.

Boiling-bubble growth rates in mixtures of water and ethylene glycol were measured at 1 atm. Boiling took place at an artificial nucleation site that was 0.004 in. in diameter in a vertical copper surface, at 4, 8, and 18°C superheat. Measurements were made from motion pictures taken with a high-speed camera through a metallographic microscope. The photographs were made with 3 diameters magnification, at 6000 frames/sec, using a d-c arc for light. The resulting diameters (D) and time measurements were fitted, via a least-squares method, to an equation of the form: $D \propto \theta^x$.

The exponent x averaged about 0.4 rather than the theoretical value of 0.5 and showed a decided statistical variation. The coefficient β in the growth equation also varied statistically, but it assumed maximum values for pure water and pure glycol and reached a minimum value at about 5 wt.% water, as predicted by Scriven. Quantitatively the data gave coefficients that were smaller than predicted.

Information concerning pool boiling has generally been limited to the use of a small-diameter heated wire as the heated surface. To provide information for intensely heated surfaces of sizes and geometries comparable with those used in practical applications, an experimental investigation of pool boiling from a downward-facing flat disk has been made and is reported in reference 6. For such a surface it might be expected that both the burnout limit and the film coefficient of heat transfer would be very low, inasmuch as the downward-facing surface must inevitably be covered with a steam blanket. The result of the experiment was substantially contrary to such expectations. The curve obtained by plotting heat flux against temperature difference is quite similar to that for boiling from electrically heated wires. Close photographic observations showed that, up to the burnout limit, the heating surface was not completely steam blanketed because at least a part of the surface was intermittently swept by water when the steam film left the surface to escape into the atmosphere. However, after the burnout limit was reached, c o m p l e t e steam-film blanketing occurred in spite of the violent motion of the bubbles emerging from the persisting steam blanket.

An analysis of the critical heat flux in pool boiling is presented in reference 7. The hydrodynamic crisis referred to in reference 7 occurs when the vapor-generation rate at the heat-transfer surface becomes so large as to prevent the flow of liquid to the interface; this results in the well-known burnout phenomenon. The similarity between nucleate boiling and the process of gas bubbling from a porous surface immersed in a liquid is discussed; the hydrodynamic phenomenon comparable to burnout has been referred to as "flooding."

Because of the effects of surface-tension forces, a certain o v e r p r e s s u r e is required just to force the gas through the porous plate. In the process of bubbling, the effect of the pressure drop, Δp, due to surface tension is analogous to the effect of the superheat temperature difference, ΔT, in boiling. Reference 7 points out the similarity in the data plots of Δp versus "superficial" vapor velocity (related to volumetric gas flow through the porous plate) and of ΔT versus a heat-flux density parameter (which plays the same role in boiling as does the superficial vapor velocity in bubbling). It is pointed out that the superficial vapor velocity at flooding appears to be related to the difference in density of the liquid and the vapor in the same manner as the heat-flux density parameter at burnout. Other similarities between burnout and flooding are discussed with respect to the parameter groupings used for data correlations.

Reference 7 refers to the work of Kutateladze et al.,[8,9] who, in postulating that the boiling crisis is a purely hydrodynamic phenomenon, identified the important dimensionless groups from similarity considerations applied to the

equations of motion and energy. From experimental data, Kutateladze determined the value of the empirical constant for the important dimensionless grouping involved. Reference 7 presents this correlation of Kutateladze as well as Borishanski's[10] extension of the analysis; good agreement is indicated with a collection of 117 data points.

Reference 7 presents an analysis of the burnout phenomenon in pool boiling from a horizontal heating surface (facing upward). The problem is formulated by considering the combined effects of Taylor and Helmholtz instabilities of the two-phase mixture. As a result of this instability analysis, reference 7 derives the upper- and lower-bound values for the important dimensionless grouping of Kutateladze. The two extremes correspond, approximately, to the spread of the experimental data (the 117 data points previously referred to) and compare well with the constant found by Borishanski's extension of the work of Kutateladze.

The foregoing analysis applies for the saturated liquid. If the liquid is subcooled, it is postulated in reference 7 that the same hydrodynamic crisis occurs but that there also occurs a transfer of heat from the interface, which is taken to be at the saturation temperature, to the subcooled bulk liquid. The theoretical results obtained on critical heat flux from the idealized sequence of events postulated therein are in good agreement with the available data for different liquids, pressures, and degrees of subcooling.

Previous studies by Zuber and Tribus on transition boiling were reviewed in the September 1958 issue of *Power Reactor Technology*, Vol. 1, No. 4, pages 7–9.

Burnout in Two-Phase Flow

Reference 11 is a brief review of the results of Russian experimental work on critical heat fluxes for water flowing through tubes. A list of references from the Russian literature is presented and is referred to in the discussion. Aladyev et al. point out[11] that, on the basis of the available experimental evidence, the initiation of boiling burnout can be markedly affected by such factors as the heat-flux distribution around the channel perimeter and along its length, the geometrical dimensions of the channel heated, and the compressibility of the medium in the section preceding the experimental one. The effects of these factors on the critical heat flux q_{BO} are reported in the paper. The reference presents a sketch of the apparatus used in many of the tests, wherein a so-called expander is placed near the inlet of the electrically heated test section. The expander is a reservoir chamber that is tapped off the main stream piping just upstream of the test section. By varying the medium or the condition of the medium in the expander, a variable amount of compressibility could be introduced just upstream of the test section. Figure III-1 is a plot of q_{BO} versus steam quality x_{ex} at the outlet (or in the cross section where burnout usually occurs) for the cases of: (1) the expander filled with a compressible medium such as superheated steam or nitrogen; (2) the expander filled with water heated to near its saturation temperature; and (3) the expander filled with cold water. For case 3 the water in the
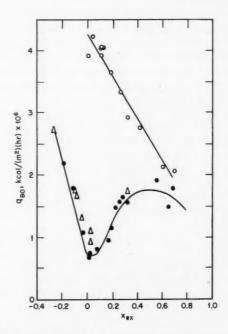

Fig. III-1   Critical heat flux under pulsating and non-pulsating conditions.[11] Pressure = 100 atm; mass flow = 400 kg/(m²)(sec); test-section inside diameter = 8 mm. ●, expander filled with compressible fluid (steam or nitrogen); pulsations noted. △, expander filled with saturated water; pulsations noted. ○, expander filled with cold water; no pulsations.

expander was practically incompressible; for case 2 the compressibility of the water in the expander was about 12.5 times greater than for case 3.

The marked effect of upstream compressibility on q_{BO}, as indicated in Fig. III-1, is accounted for as follows: The steam generation within the intensely heated tube can result in periodic disturbances followed by corresponding changes in the hydraulic resistance of the tube. The fluctuations depend on conditions in the upstream section between the heated channel and throttle (or pump). If this section is filled with a noncompressible medium and the resistance fluctuations of the channel are small compared to the pressure drop in the throttle, they cannot greatly affect the amount of water flow through the heated channel. However, with a compressible medium in the upstream section, the resistance fluctuations in the heated channel cause periodic compressions of this medium and temporary decrease of the flow velocity in the heated tube, ultimately resulting in burnout.

The pressure pulsations can be quite large; cyclic pulses of up to 30 atm with about a 1-sec period were measured in one set of experiments. Under such conditions, throttles (or orifices) between the expander and heated channel were effective only if the throttle pressure drop was quite large.

It is obvious that, in the investigation of the conditions leading to boiling burnout in heated channels and in the correlation of burnout data, consideration must be given to the existence of different types of conditions, namely, (1) those with unhindered flow-rate pulsations referred to as "pulsating" conditions and (2) those with limited pulsations referred to as "nonpulsating" conditions.

The effect of channel diameter on q_{BO} is not definitely known; in most cases with subcooled inlet conditions, q_{BO} has been found to increase somewhat when the inner tube diameter was decreased from 8 to 3 mm. The effect of channel length depends markedly on whether pulsating or nonpulsating conditions prevail. Figure III-2 presents data on q_{BO} obtained using tubes of the same diameter but different heated length, with unhindered pulsations. The critical heat flux decreases markedly with increased length over almost the entire range of conditions investigated. However, for the nonpulsating conditions (data not shown in reference 11), q_{BO} remains
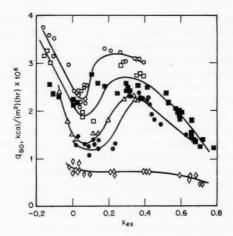
Fig. III-2   Effect of heated tube length on burnout heat flux under pulsating conditions.[11] Pressure = 100 atm; mass flow = 800 kg/(m^2)(sec); test-section inside diameter = 8 mm. Length/diameter ratios: $\bigcirc$, 15; $\square$, 20; $\triangle$, 30; $\bullet$, 50; $\blacksquare$, 20; $\diamondsuit$, 188.

practically unaffected by the change in length-to-diameter ratio.

Increasing the pressure (and hence decreasing the difference between steam and water density) lowers the perturbations caused by boiling and diminishes the effect of channel length on q_{BO}. As the mass velocity and kinetic head of the flow are increased, the perturbation effects on the flow diminish and the differences between the values of q_{BO} for the pulsating and the nonpulsating conditions tend to decrease.

Figure III-3 shows that, under nonpulsating conditions, q_{BO} decreases almost linearly with increasing x_{ex} for a given mass velocity W_g. However, the separate lines for the various W_g values intersect; this means that in a definite range of x_{ex} the critical heat fluxes increase with increasing velocity, but in another range of x_{ex} the opposite effect is obtained. Hence there are also values of x_{ex} of such a magnitude that the change of velocity within certain limits has little or no effect on q_{BO}. The inverse dependence of q_{BO} on W_g exhibited in Fig. III-3 for $x_{ex} \simeq 0$ seems to be due to partial tearing off of the liquid film from the tube walls. Reference 11 contains another plot similar to Fig. III-3 but for the higher pressure of 170 atm; in this case the inverse dependence of q_{BO} on W_g is exhibited for $x_{ex} \simeq 0.3$.

Reference 11 also briefly discusses the effects on q_{BO} of thickness and roughness of the

heating surface and of uneven heat flux around the perimeter and along the channel length. Experimental data are presented as obtained at different pressures, velocities, and degrees of subcooling.

As part of an experimental program to study fog cooling for power reactors, reference 13 describes some of the work completed on heat transfer in two-phase (water and steam) flow systems. The success in interpreting experimental data on two-phase flow, both with and without heat transfer, has been quite limited. Because the relative importance of the different variables involved is not understood, extrapolations, and even interpolations, present unknown dangers. A thorough experimental program is planned not only to determine the magnitude of the burnout heat flux, or of any other limiting factor, but also to provide for a parametric variation of all physical quantities of possible importance. The reference is devoted to a preliminary approach, mainly on burnout data, and the conclusions arrived at are only tentative.

The reference[13] enumerates the many definitions of critical heat flux used by the various investigators and recommends caution in comparing "burnout heat fluxes" that were obtained in different laboratories with different instrumentation.

The burnout data reported in reference 13 were obtained in round tubes for the following ranges of variables:

1. With a pressure of 70 kg/cm^2 and a constant length, diameters of 3, 4, 5, 6, 8, and 10 mm were used.
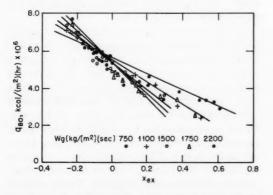
Fig. III-3   Effect of mass flow on burnout heat flux.[11] Pressure = 80 atm; test-section inside diameter = 8 mm.
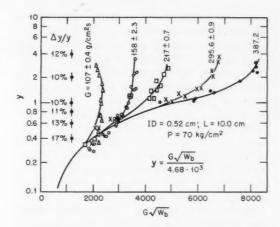
Fig. III-4   Correlation of data on burnout heat flux for constant tube diameter and length and at constant pressure.[13] Here $y = (1 - x)/(x + a)$, where x = steam quality, lb/lb, and a = (liquid specific volume)/(gas specific volume − liquid specific volume).

2. With a pressure of 70 kg/cm^2 and a constant diameter, lengths of 10, 20, 40, and 80 cm were used.

3. Pressures of 40, 55, 70, and 85 kg/cm^2 were used with a constant diameter and a constant length.

In each case, four to six flow rates were explored, and, for each flow rate, a number of steam qualities were explored. The total number of burnout heat-flux data reported in reference 13 is about 1700. The degree of data correlation is very high, as illustrated in Fig. III-4. Here the quantity y is plotted as a function of the product $G\sqrt{W_b}$ for constant tube diameter and length and for a constant pressure. The quantity y is proportional to the concentration of the liquid phase at burnout, when the slip ratio is unity. G is the mass velocity, and W_b is the burnout heat flux. From such plots it was deduced[13] that (1) the burnout heat flux is not a single-valued function of y and hence of steam quality; (2) a maximum of W_b is reached at a certain quality; and (3) in a certain range the burnout heat flux is correlated to y and flow rate (at constant diameter, length, and pressure) through a very simple relation given by $G\sqrt{W_b} = ay$. At a certain point, there is a departure from this functional relation, and different variations are obtained with different velocities (see Fig. III-4). The fact that there is a single value of W_b for two different exit

qualities around the m a x i m u m suggests the possibility of two different flow regimes.

A careful analysis was devoted to the maximum values of W_b measured in the experiments. The maxima have an element in common: the mean inlet velocity seems to be a constant at constant pressure and seems to be independent of the values of diameter, length, and flow rate. This suggests that the maximum must be related to some kind of instability and to a change in flow pattern at the inlet of the heated tube. This hypothesis was substantiated by the consideration of results given in reference 14 for distinguishing between different flow patterns. It is evident then that the often-used principle, that burnout is a function of local variables only, is suspect. Further considerations in reference 13 suggest that e x p e r i m e n t s in the quality region carried out with subcooled inlet water cannot be compared with those made with inlet-quality conditions.

Transient Boiling

Reference 15 gives experimental values of surface temperature and volume of vapor produced in transient pool boiling of water at atmospheric pressure. Heat energy was generated electrically in a metal ribbon that was immersed in a glass-walled tank of water for photographic measurements; the energy was generated uniformly in the ribbon at an exponentially increasing rate. The subcooling of the pool was varied between 2 and 112°F, and the period of the transient pulse ranged between 5 and 80 msec. These periods are representative of those in a nuclear reactor experiencing a prompt-critical excursion. The nature of the results being obtained in this experimental program was described previously in the March 1961 issue of *Power Reactor Technology*, Vol. 4, No. 2, pages 26 and 27.

Steam Condensation

References 16 to 20 treat the problem of condensation of pure vapors (notably steam) and add to the experimental data available in the l i t e r a t u r e on this important heat-transfer process. Reference 16 is an experimental investigation on the influence of tube angle on heat transfer by condensing pure saturated vapors outside inclined tubes. Vapors of three

alcohols (methanol, 2-propanol, and 1-butanol) were condensed filmwise on the outsides of copper tubes. Tubes 2 m long were used, with three different diameters: $\frac{3}{4}$, 1, and $1\frac{1}{2}$ in. For the horizontal and vertical tube orientations, the experimental results are in good agreement with the well-known modifications of Nusselt's original theory on the subject. The variation in heat-transfer coefficient with angle of inclination from the horizontal is small until an angle of about 60° is attained; most of the v a r i a t i o n occurs between about 60 and 90° (vertical). From the viewpoint of heat transfer, the optimum angle of inclination of long tubes is near the horizontal in the range of heat loads investigated. The applicability of existing correlation equations for condensing on the outside of inclined tubes is confirmed.

Reference 17 reports on investigations of the condensation of steam in its flow within a horizontal tube, wherein the steam flow significantly affects the condensate film being formed on the interior surface of the tube. In this case the movement of the liquid film is downward and in the direction of the steam flow and represents a quite complicated behavior. Further, the condensed fluid accumulates at the bottom of the tube cross section and rises to some height in the tube; the liquid level then varies along the tube length. The usual heat-exchange equations are not applicable in this case. Reference 17 deals with an application of the Reynolds analogy between heat transfer and fluid friction pertinent to the condensation of flowing vapor within a tube. From this point of view, both local and mean values of heat-transfer coefficient were obtained for comparison with experimental results. The agreement between calculations and experiment is satisfactory.

An experimental investigation of the maintenance of dropwise condensation (as contrasted to film condensation), by injection of waxes with a suitable carrier material into the steam, is reported in reference 18. It was found that a high value of heat-transfer coefficient could be maintained by the cleaning action of the wax, which replenished the surface layers and maintained a nonwetting condition. The wiping action of liquid drops rolling across the condensing surface is the basis of the low thermal resistance in dropwise condensation. From motion-picture studies of dropwise condensation, it was determined in reference 18 that there is a delay between track formation (track of "bare"

metal maintained by the movement and resultant wiping action of the drops) and the first condensation. This delay may increase the thermal resistance at high frequencies of track formation.

Reference 19 reports studies of the dropwise condensation of steam by high-speed motion pictures taken through a microscope. Three different sizes of copper surfaces were used as the condensing surface. Dropwise condensation was induced by adding 0.005 wt.% cupric oleate to the feed water in the steam-supply boiler. The useful life of this promoter in a recycle system is stated to be at least 10,000 hr. The ΔT varied from 0.4 to 47°F, and the heat flux varied from about 5000 to 85,000 Btu/(hr)(sq ft of surface area). Heat balances indicated good experimental accuracy. For the large surface (8 in. high by 3 in. wide), a set of runs in filmwise condensation showed excellent agreement with Nusselt's equation. It was found that the drops grow mainly by numerous coalescences. Each coalescence results in a vibration of the new drop, sweeping up the nearby liquid film. Condensation takes place mainly on the swept areas and only slightly on the drops. The heat flux through the liquid-free metal surface left bare by the coalescence is at first enormous; it then decreases as liquid forms. When the liquid film that is formed on the swept area reaches a critical thickness of about 0.5 μ, the film fractures to form new drops.

Reference 20 is a report on the investigation of heat transfer during steam condensation at atmospheric pressure over a single tube with no significant velocity of flow across the surface. The variables covered include tube diameter and inclination, heat load, mode of condensation (filmwise or dropwise), and the presence of a noncondensable gas in several concentrations. With a noncondensable gas present, steam-side heat-transfer coefficients depended on the quantity of venting and on the position of the vent in the condenser.

Air and Water Flow Experiments

The similarities between nucleate boiling and the behavior of gas bubbles emanating from a porous surface, and between the burnout and the flooding phenomena. have been mentioned above. The results of experimental investigations of various gas-bubbling processes are

presented in reference 21. These experiments were performed to gain insight into the boiling process and into the phenomena of critical heat fluxes. Part I of the reference is specifically concerned with the rise of air bubbles in a stagnant column of water; the air was supplied through a porous plate at the bottom of the water column. The several flow regimes observed as the gas flow rate through the liquid is increased are described. The quantitative results are presented as plots of superficial gas velocity (given as the ratio of the gas-volume flow rate to the area of the flow cross section) versus mean void fraction in the liquid column. The effects of agglomeration and of transition from the bubbly flow regime to the slug flow regime are clearly evident in these plots. The experimental results obtained, as well as results obtained by other investigators, are compared with the results of a simplified analysis for the bubbly flow regime. It is concluded that:[21]

1. The bubbly flow regime is basically unstable and always tends to develop into the slug flow regime. However, it is possible to retard this transition by introducing suitable additives to the liquid.

2. Partial agglomeration gives rise to transitional flow patterns which are virtually impossible to describe analytically.

3. For the bubbly flow regime in a stagnant liquid or with countercurrent flow, there are in general either two possible void fractions, for a given liquid flow rate and bubble size, or none. Which is obtained depends on whether the superficial gas velocity is below or above a certain critical velocity. If this critical velocity is exceeded, a sudden change in flow pattern to slug flow occurs.

4. For cocurrent upward flow of a two-phase mixture, with negligible wall shear stress, there is always a possible solution in either the bubbly or slug flow regime. Which pattern occurs depends on the method of introduction of the phases and the degree of agglomeration.

Part II of reference 21 describes a study of the phenomena that occur when air is blown through the walls of a horizontal porous tube submerged in a pool of water. High-speed moving pictures were taken of the flow patterns surrounding the tube for various air flow rates. Three different flow patterns ("bubbly," "patchy," and "blanketed") were obtained, depending on the normal average air velocity from

the tube surface. The results are used both to explain hydrodynamic aspects of pool boiling and to support the treatment of the burnout heat flux as a purely hydrodynamic phenomenon.

Part III of the reference describes some of the results obtained in an air-water analog study of the hydrodynamics of two-phase flow in tubes. Porous tubes ($\frac{3}{8}$, $\frac{5}{8}$, and $\frac{7}{8}$ in. in diameter) were used to obtain a continuous addition of air bubbles to a flowing stream so as to simulate the formation of steam bubbles on the walls of a forced-convection boiling system. A clear picture of the various flow regimes was obtained, and quantitative measurements were made of the parameters that give rise to transition from one regime to another. Pressure-drop characteristics were found to depend on the prevailing flow regime, which was studied visually. For the bubbly flow regime with constant bubble generation at the walls, a similarity criterion was found to be the ratio of the gas (or vapor) flux at the walls to the single-phase liquid velocity. For this flow regime and for a given fluid and tube geometry, the total two-phase pressure drop (friction plus acceleration pressure drop) is related[21] to the single-phase pressure drop solely in terms of this ratio. Typical data for the nonbubbly flow regime are also presented to emphasize the fact that it is meaningless to correlate data for one regime against a theory derived for another (inasmuch as the important independent variables may be quite different).

Superheated Steam

The experimental results of heat-transfer investigations for the flow of superheated steam in an annulus are presented in references 22 and 23. In reference 23 the steam flow velocity ranged up to the sonic level. In reference 22 the pressure extended from 20 to 1075 psi, whereas the investigations of reference 23 were confined to relatively low steam pressures (20 to 50 psig). Data correlations that were obtained and comparisons with the traditional correlation equations are discussed; also included are the measured effects of entrance length. Measurements were also made in reference 23 of the recovery factor, which is important for the high-speed flows used therein. The recovery factor is applied for determination of the adiabatic wall temperature, which is

then used in place of the fluid temperature in the application of the normal heat-transfer equations. Comparisons are made in reference 23 of the measured recovery factors with those obtained in theoretical analyses and in previous experimental investigations with air.

Supercritical Fluids

Reference 24 presents a comparison of predicted and experimentally determined heat-transfer characteristics for supercritical water (5000 psi) flowing at high mass flow rates through round tubes. Two distinctly different modes of heat transfer were observed: (1) the "normal" mode for which the experimental and predicted heat-transfer data are quantitatively compared and (2) a mode for which a "boiling-like" mechanism is postulated and discussed qualitatively. The test results obtained at low heat fluxes, wherein the wall-to-bulk-fluid temperature differences are small, were used to determine the variation of a fluid-property parameter with temperature; comparison is made with the property parameter determined on the basis of extrapolations of presently available fluid-property (viscosity, specific heat, thermal conductivity) measurements. A review of some of the results described in reference 24 was previously given in the June 1958 issue of *Power Reactor Technology*, Vol. 1, No. 3, page 18.

The results of an experimental investigation of local heat transfer to supercritical carbon dioxide, flowing turbulently in a pipe, are reported in reference 25. The range of temperatures and pressures used covers a wide variation of the physical properties of carbon dioxide; conditions involving rather large transverse variations of fluid properties across the boundary layer (due to large transverse temperature gradients) were included. Suitable correlation of all data was accomplished by including multiplicative factors in the usual correlation equation; each factor accounts for the transverse variation of an individual fluid property (viscosity, specific heat, thermal conductivity).

Fuel-Rod Clusters

References 26 to 28 deal with the crucial aspects of the flow and heat-transfer processes

occurring in fuel-rod-cluster configurations of practical interest in gas-cooled power reactors. The specific arrangement investigated is the seven-rod cluster (six in a regular hexagonal pattern surrounding the seventh central rod) positioned within a flow channel. The coolant gas flows parallel to the heated rods. The resulting flow geometry, which consists of parallel, interconnecting, noncircular paths, gives rise to peripheral variations in local heat-transfer coefficient and to nonuniformity of gas flow and gas temperature over the flow cross-sectional area. In reference 26 the ratio (center-to-center distance)/(rod diameter) for the parallel rods was 1.015; the rod surfaces formed flow passages of tricuspid-shaped cross section. The flow channel into which the rod cluster was centrally positioned was hexagonal, with circumferential segments of tubing attached to the sides of the hexagon to simulate the adjacent rods of a larger array. Average and local (with respect to the peripheral position on the surface of the rods) heat-transfer coefficients, pressure drops and velocity profiles were measured under established hydrodynamic conditions.

The measured average heat-transfer coefficients were approximately equal to those for smooth round tubes; however, the peripheral variation of the local coefficients at a Reynolds number of 20,000 was −50 per cent to +30 per cent of the average values. The data were taken under the following forced-convection conditions: (1) Reynolds number from 10,000 to 60,000; (2) rod heat flux from 400 to 1000 Btu/(hr)(sq ft); and (3) rod surface temperature from 100 to 160°F. Fanning-friction factors were approximately 5 per cent higher than those for smooth tubes over a Reynolds number range from 3000 to 30,000. The velocity structure of the flowing gas was determined at a Reynolds number of 20,000. The peripheral variation of the local-to-bulk mean velocity ratio was found to be very nearly that of the local-to-average heat-transfer coefficient ratio.

The work reported in reference 27 covers the initial stages of an extensive investigation of the heat-transfer and fluid-flow aspects of roughened surfaces and their application to a seven-rod cluster. Twenty-one different roughened surfaces were surveyed in an atmospheric air rig. The pressure drop and the heat-transfer data are expressed in terms of Reynolds number, Stanton number, and friction factor; the

Reynolds number ranged from 0.5×10^5 to 5×10^5. A method was developed which selects the better surfaces for future development. This method involves the use of two plots: (1) a plot of friction factor versus Stanton number for all the surfaces investigated at a representative value of Reynolds number $(1.1 \times 10^5$ in this case) and (2) a plot, for the surfaces thus shown to have the better heat-transfer performances, of the ratio (Stanton number)/(friction factor) versus Reynolds number. Fluid-friction characteristics of a seven-rod cluster assembly with different spacings and surfaces were also measured. Detailed velocity traverses were made across the flow passage at varying positions along the length of the cluster to determine whether any rod or group of rods was being starved of coolant.

Reference 28 reports on the first of a series of experiments investigating the heat-transfer characteristics of rod clusters under various conditions of rod spacing, gas flow, power generation, and rod constraint. Two experimental techniques were utilized in obtaining the desired data. The first approach involved the direct measurement of rod surface temperatures using an electrically heated model of a seven-rod cluster. The second utilized data on mass removal from naphthalene-coated rods to obtain heat-transfer coefficient distributions.

The rod-cluster geometry, which was patterned after the fuel element planned for the Experimental Gas-Cooled Reactor (EGCR), consisted of seven stainless-steel tubes (0.8 in. in outside diameter) arranged on a regular hexagonal pattern and contained within a 3.83-in.-ID precision-bore pyrex channel. The tubes were individually heated by the passage of an alternating current through the tube walls. A central spacer was included which maintained the positions of the tubes, at a point halfway down the tube length, with a minimum of flow obstruction. The use of atmospheric air at relatively low temperatures as the test fluid (adequately simulating helium at reactor temperatures and pressures) enabled open-circuit operation. The circumferential variation of the tube surface temperature, which was measured at several axial positions by means of movable thermocouple probes contacting the inside surfaces of the tubes, was of the order of ±10 per cent around the mean value. The amplitude of these variations was found to be significantly less than that predicted by the theoretical analy-

sis of Deissler and Taylor;[29] a circumferential displacement of the profile maxima and minima from the anticipated locations was also noted; this suggested the existence of a swirl component in the axial flow. The mid-cluster spacer had a marked influence on the heat transfer immediately downstream, implying an increased turbulence level arising from the spacer itself and interruption of the boundary layer; these results are not inconsistent with entrance-region data for air in circular tubes.

The measurements on the mass removal from naphthalene-coated rods were applied, through the analogy relations, to the determination of local heat-transfer coefficients for the seven-rod cluster. For a geometry identical to that used in the heat-transfer studies, it was found that circumferential profiles of the j factor (analogous heat-transfer and mass-transfer parameter) showed a greater variation around the mean for the mass-transfer data than for the heat-transfer data. At the same time, a comparison of the mean j factors for mass transfer and for heat transfer showed only a 10 per cent disparity. The circumferential patterns in the mass-transfer profiles were qualitatively related to heat-transfer coefficient distributions on single rods oriented transversely to the flow; this implied the existence of a strong crossflow over the rod cluster. A further study by the mass-transfer technique into the effect of rod spacing on the circumferential heat-transfer distributions showed least variation in the profile for the situation in which the surface of the peripheral tubes in the cluster was equidistant from the channel wall and the surface of the central tube.

Time-Variable Reactor Power

Reference 30 presents a theoretical analysis of the heat-exchange dynamics in a forced-convection-cooled heterogeneous nuclear reactor. The two significant features of the problem are that (1) the fundamental time variation is exponential and (2) the axial power distribution is sinusoidal. In the analysis the thin-plate approximation (fuel-temperature distribution invariant in direction transverse to the flow) is used, and the local heat-transfer coefficient from the fuel to the bulk coolant is taken as

constant. The specific contribution of reference 30 is the extension of the work of Doggett and Arnold[31] for an axially unreflected core to the important case of a chopped-sine distribution that is characteristic of end-reflected reactors. Rigorous and exact solutions of the local heat-balance equations are presented in the form of analytical expressions for the fuel and coolant temperatures as functions of time and axial position. Distributions for general reactor time variation are obtainable by superposing the analytical solutions contained therein. The solutions contain two- and three-parameter integrals that are expressed in terms of tabulated one-parameter functions suitable for desk calculator computations. Asymptotic forms for long times, small reciprocal periods, small or large fuel-to-coolant heat-capacity ratios, and bare cores are given and are compared with previously published solutions. During the transient the point of maximum metal temperature shifts from its initial steady-state position to a position nearer the center of the core.

Pebble Beds and Fluidized Beds

References 32 to 36 are concerned with the packing and heat-transfer characteristics of pebble or fluidized beds. This work is of interest in view of the several projected nuclear reactors that have their nuclear fuel arranged in the form of packed beds of spherical solid particles. Reference 32 presents the elements of an approximate theory for the transfer of heat between a wall and a particulate fluidized bed. An attempt is made to emphasize the principal factors involved in the phenomena and to demonstrate the validity of the theory by qualitative comparisons with the observed experimental results of other investigators. Reference 33 treats the problem of radially effective thermal conductivities in packed beds with both stagnant and flowing fluids. The work reported in the literature is summarized, and, in addition, the results of additional experimental work performed by the authors are presented. The measurements in reference 33 were made in a 60-mm steam-jacketed copper tube which was packed with four sizes of glass beads and through which air was passed downward and heated. The method of obtaining the radially ef-

fective thermal conductivities from the measurement results is described. A theoretically derived equation is applied to correlate satisfactorily almost all the experimental data, including those previously reported for various shapes of solids. It is also shown that the stagnant conductivities for very wide ranges of experimental conditions can be predicted with quite good accuracy.

Reference 34 presents theoretical equations and a calculational procedure for the prediction of over-all heat-transfer coefficients in packed beds through which fluids are flowing. This involves determinations of both the radially effective thermal conductivity and the apparent wall film coefficient of the packed bed; from the theoretical equations for these two heat-transfer coefficients, Nusselt numbers for the over-all coefficient are calculated. The agreement between the computed and observed values is good not only for gas-solid systems but also for liquid-solid systems, indicating the adequacy of the theoretical equations for any fluid-solid system.

Reference 35 reports detailed investigations of the local packing and heat-transfer processes in packed beds of homogeneous spheres. The local packing configurations that occur in a randomly stacked bed were examined, both as a function of position in the bed and as a function of the size of container. It was concluded that only incomplete rhombohedral packing configurations exist when smooth hard homogeneous spheres are randomly stacked into smooth hard containers and that the distribution of the incompleteness is random throughout the bed. Experiments were carried out for measuring the distribution of the local heat-transfer coefficient over the surface area of a sphere when immersed in a rhombohedral array. A range of Reynolds numbers of from 8000 to 60,000 was covered in these experiments.

The investigation reported in reference 36 was undertaken to establish the validity and determine the limitations of the cyclic method of measuring heat-transfer coefficients for the flow of gas through matrices such as porous solids or beds of solid particles. As contrasted to the commonly used "single-blow technique," in which a step change of fluid inlet temperature is introduced, reference 36 utilized the technique involving sinusoidal variation of the fluid inlet temperature. The heat-transfer coefficient could then be calculated from measurements of the ratio of the amplitude of the sinusoidally varying fluid temperature at outlet to that at inlet. The sinusoidally varying air temperature was obtained by use of an electric heater placed in the air stream. The air-stream temperatures were measured by resistance thermometers, each forming a leg of a Wheatstone bridge that was balanced for the mean resistance; the out-of-balance current was photographically recorded through the use of a fast-response galvanometer. The speed of response of the thermometers to the air-temperature variations was experimentally determined to be satisfactory for the fastest cycling speeds.

All the matrices were made up with 10-mm-diameter steel ball bearings which were put into the containers at random. In two of the matrices, measures were taken to achieve uniform porosity and, in particular, to eliminate the excess porosity normally occurring at the walls of the container. Over 200 test runs were made. The velocity of approach varied from 4 to 16.5 ft/sec, and the frequency of temperature variation was from 0.16 to 80 cycles/min. In general, no variation was found in the results with frequency of cycling or with temperature amplitude.

Greater values of heat-transfer coefficient were obtained for the matrices in which the wall effect was eliminated. Differences in packing arrangement and in porosity appear also to have an effect on heat transfer. However, a correlation equation is presented which is considered to be a fair representation of the majority of the more reliable results obtained for random packing.

Friction factors were also measured and were found to vary in the same way as the Stanton number. It is possible, therefore, that measurements of the pressure drop would give a good indication of what heat transfer might be expected.

No valid objection could be discovered in the use of the cyclic method for obtaining heat-transfer coefficients. Results obtained at high frequencies were shown, from a study of the theoretically derived curves relating amplitude ratio to heat-transfer coefficient, to be less subject to experimental errors. At the lowest cycling speeds, the sensitivity of experimental errors was found to result in an apparent variation of the heat-transfer coefficient with frequency. At high frequencies the upstream-to-downstream temperature amplitude ratio

increases exponentially with the Stanton number and the length of matrix and inversely with the mean equivalent diameter of the flow passage. In certain circumstances the downstream temperature amplitude thus becomes too small to measure; this constitutes probably the chief disadvantage and practical limitation of the cyclic method.

Properties of Helium

Reference 37 reports on the measurement of the Prandtl number of helium at atmospheric pressure over the temperature range 270 to 640°K. Consistently with predicted monatomic gas behavior, the Prandtl number was found to remain constant at 0.659 over the measured temperature range, the data points showing a scatter not exceeding ±0.5 per cent. It is further shown in reference 37 that the modified Buckingham potential model for helium predicts Prandtl numbers in good agreement with the measured values. Also, viscosity predictions based on the modified Buckingham potential agree to within 1 per cent of the available measured values (up to 680°K). For this reason the modified Buckingham potential was selected, in combination with the reported values of helium constant-pressure heat capacity, to obtain thermal conductivities from the measured Prandtl numbers. The values of thermal conductivity so obtained are compared with other experimental data and with the several semiempirical prediction schemes, including the National Bureau of Standards curve. It is concluded that, as in the case of viscosity, the modified Buckingham potential provides predictions that best agree with the experimental data above 575°K (up to 775°K). In view of the excellent agreement indicated above, predictions are presented[37] for the viscosity, thermal conductivity, and Prandtl number for helium, as based on the modified Buckingham potential. The predictions are in table form at regular temperature intervals from 200 to 1850°K.

Natural Convection

References 38 to 40 deal with the problem of heat transfer by the natural-convection mechanism. The results of an experimental investigation are reported in reference 38 for natural-convection heat transfer within horizontal cylindrical annuli. Five sets of concentric tubes of different inside-to-outside diameter ratios were used. Flow patterns, temperature profiles, and over-all heat-transfer correlations were determined for air, water, and silicone fluid. The over-all heat transfer was correlated in terms of an effective thermal conductivity. A review of previously published investigations is included, together with a comparison of the test data. Various types of flow instabilities were observed. For small ratios of gap width to inside diameter, Benard type cells were observed near the top at values of Rayleigh number above 1600−2000. With larger diameter ratios, an increase in Rayleigh number led to flow instabilities near the 135° position which were transferred to the top section as sideways oscillations. Reference 39 presents explicit finite difference equations that permit the direct computation of the transient and/or steady-state velocity and temperature fields in natural-convection processes. The finite difference equations are derived from the partial differential equations describing the conservation of mass, momentum, and energy. Exploratory calculations on an IBM-704 computer yielded results in agreement with existing steady-state solutions and experimental data. The method presented in reference 39 does not require the strict idealizations of boundary conditions necessary to obtain analytical solutions.

Reference 40 is concerned with the natural-convection process for fluids having a distributed heat source and a vertical temperature gradient, contained in long vertical cells of circular or rectangular cross section. Experiments were carried out on two such containers, heat being generated by passing an electric current through a 20 per cent solution of zinc chloride. Cooling water was passed upward over only two of the vertical walls of the rectangular container to give an approximate two-dimensional system, but over the entire curved surface of the vertical cylindrical container to give an axially symmetric system. The effects of various coolant flow rates, heat-generation rates, and shapes of apparatus were determined. Velocities were measured by tracers and temperatures by thermocouples and an interferometer. From a comparison with the experimental results, it is concluded that the theory of Woodrow[41] successfully predicts the form of the temperature profiles. At low heat-generation rates, the temperature differences

are approximately correct in the cylindrical cell, but the central velocities are much lower than predicted in both cells. Sinuosities and eddies that exist are not predicted by the simple theory, but it may be that the experiments were conducted in a transitional regime.

References

1. P. D. Sanderson (U. K.), Heat Transfer from the Uranium Fuel to the Magnox Can in a Gas-Cooled Reactor, Paper No. 7 at the 1961 International Heat Transfer Conference.*

2. L. C. Laming (U. K.), Thermal Conductance of Machined Metal Contacts, Paper No. 8 at the 1961 International Heat Transfer Conference.

3. C. Rounthwaite and M. Clouston (U. K.), Heat Transfer During Evaporation of High Quality Water-Steam Mixtures Flowing in Horizontal Tubes, Paper No. 23 at the 1961 International Heat Transfer Conference.

4. J. E. Benjamin and J. W. Westwater (U. S.), Bubble Growth in Nucleate Boiling of a Binary Mixture, Paper No. 24 at the 1961 International Heat Transfer Conference.

5. L. E. Scriven, On the Dynamics of Phase Growth, *Chem. Eng. Sci.*, 10: 1–13 (1959).

6. S. Ishigai et al., (Japan), Boiling Heat Transfer from a Flat Surface Facing Downward, Paper No. 26 at the 1961 International Heat Transfer Conference.

7. N. Zuber et al. (U. S.), The Hydrodynamic Crisis in Pool Boiling of Saturated and Subcooled Liquids, Paper No. 27 at the 1961 International Heat Transfer Conference.

8. S. S. Kutateladze, On the Transition to Film Boiling Under Natural Convection, *Kotloturbostroenie*, 3: 10 (1948).

9. S. S. Kutateladze, A Hydrodynamic Theory of Changes in a Boiling Process Under Free Convection, *Izvest. Akad. Nauk S.S.S.R., Otdel. Tekh. Nauk*, 4: 529 (1951).

10. V. M. Borishanski, An Equation Generalizing Experimental Data on the Cessation of Bubble Boiling in a Large Volume of Liquid, *Zhur. Tekh. Fiz.*, 25: 252 (1956).

11. I. T. Aladyev et al. (U.S.S.R.), Boiling Crisis in Tubes, Paper No. 28 at the 1961 International Heat Transfer Conference.

12. B. W. LeTourneau, DNB Correlation, in Technical Progress Report, Reactor Physics, Engineering and Mathematics, for the Period April 1, 1961 to July 1, 1961. USAEC Report WAPD-MRJ-14,

13. M. Silvestri (Italy), Two-Phase (Steam and Water) Flow and Heat Transfer, Paper No. 39 at the 1961 International Heat Transfer Conference.

14. H. S. Isbin et al., Two-Phase Steam-Water Pressure Drop, Nuclear Engineering and Science Conference, Chicago, 1958.

15. H. A. Johnson et al. (U. S.), Transient Pool Boiling of Water at Atmospheric Pressure, Paper No. 29 at the 1961 International Heat Transfer Conference.

16. G. Selin (Sweden), Heat Transfer by Condensing Pure Vapours Outside Inclined Tubes, Paper No. 33 at the 1961 International Heat Transfer Conference.

17. E. P. Ananiev et al. (U.S.S.R.), Heat Transfer in the Presence of Steam Condensation in a Horizontal Tube, Paper No. 34 at the 1961 International Heat Transfer Conference.

18. R. G. H. Watson et al. (U. K.), Dropwise Condensation of Steam, Paper No. 35 at the 1961 International Heat Transfer Conference.

19. J. F. Welch and J. W. Westwater (U. S.), Microscopic Study of Dropwise Condensation, Paper No. 36 at the 1961 International Heat Transfer Conference.

20. H. Hampson (U. K.), The Condensation of Steam on a Tube with Filmwise or Dropwise Condensation and in the Presence of a Noncondensable Gas, Paper No. 37 at the 1961 International Heat Transfer Conference.

21. G. B. Wallis (U. K.), Some Hydrodynamic Aspects of Two-Phase Flow and Boiling, Paper No. 38 at the 1961 International Heat Transfer Conference.

22. J. G. Collier and P. M. C. Lacey (U. K.), Heat Transfer to High Pressure Superheated Steam in an Annulus, Paper No. 40 at the 1961 International Heat Transfer Conference.

23. A. W. Scott and R. M. G. Meek (U. K.), Heat Transfer Investigations for the Flow of Steam Ranging Up to Sonic Velocity, Paper No. 42 at the 1961 International Heat Transfer Conference.

24. K. Goldmann (U. S.), Heat Transfer to Supercritical Water at 5000 psi Flowing at High Mass Flow Rates, Paper No. 66 at the 1961 International Heat Transfer Conference.

25. B. S. Petukhov et al. (U.S.S.R.), An Investigation of Heat Transfer to Fluids Flowing in Pipes Under Supercritical Conditions, Paper No. 67 at the 1961 International Heat Transfer Conference.

26. L. D. Palmer and L. L. Swanson (U. S.), Measurements of Heat-Transfer Coefficients, Friction Factors, and Velocity Profiles for Air Flowing Parallel to Closely Spaced Rods, Paper No. 63 at the 1961 International Heat Transfer Conference.

27. A. Draycott and K. R. Lawther (Australia), Improvement of Fuel Element Heat Transfer by Use of Roughened Surfaces and the Application to a

Westinghouse Electric Corp., Bettis Atomic Power Laboratory. (Classified)

---

*Papers that were presented at this conference appear in the American Society of Mechanical Engineers' publication, *International Developments in Heat Transfer.*

7-Rod Cluster, Paper No. 64 at the 1961 International Heat Transfer Conference.

28. H. W. Hoffman et al. (U. S.), Heat Transfer with Axial Flow in Rod Clusters, Paper No. 65 at the 1961 International Heat Transfer Conference.

29. R. G. Deissler and M. F. Taylor, Analysis of Axial Turbulent Flow and Heat Transfer Through Banks of Rods or Tubes, in Reactor Heat Transfer Conference of 1956, USAEC Report TID-4729 (Pt. 1), Book 2, pp. 416–461, November 1957.

30. W. O. Doggett and R. H. Shultz, Jr. (U. S.), Transient Heat Transfer in a Convection Cooled Heterogeneous Nuclear Reactor, Paper No. 74 at the 1961 International Heat Transfer Conference.

31. W. O. Doggett and E. L. Arnold, Axial Temperature Distribution for a Nuclear Reactor with Sinusoidal Space and Exponential Time Varying Power Generation (to appear in *J. Heat Transfer*).

32. S. S. Zabrodsky (U.S.S.R.), Heat Transfer by a Fluidized Bed, Paper No. 89 at the 1961 International Heat Transfer Conference.

33. S. Yagi et al. (Japan), Radially Effective Thermal Conductivities in Packed Beds, Paper No. 90 at the 1961 International Heat Transfer Conference.

34. S. Yagi and D. Kunii (Japan), Studies on Heat Transfer in Packed Beds, Paper No. 91 at the 1961 International Heat Transfer Conference.

35. J. Wadsworth (U. S.), An Experimental Investigation of the Local Packing and Heat Transfer Processes in Packed Beds of Homogeneous Spheres, Paper No. 92 at the 1961 International Heat Transfer Conference.

36. R. M. G. Meek (U. K.), The Measurement of Heat-Transfer Coefficients in Packed Beds by the Cyclic Method, Paper No. 93 at the 1961 International Heat Transfer Conference.

37. P. D. Stroom et al. (U. S.), Helium Prandtl Number Measurements and Calculated Viscosity and Thermal Conductivity, Paper No. 105 at the 1961 International Heat Transfer Conference.

38. Chen-Ya Liu et al. (U. S.), Natural Convection Heat Transfer in Long Horizontal Cylindrical Annuli, Paper No. 117 at the 1961 International Heat Transfer Conference.

39. J. D. Hellums and S. W. Churchill (U. S.), Computation of Natural Convection by Finite Difference Methods, Paper No. 118 at the 1961 International Heat Transfer Conference.

40. D. Wilkie and S. A. Fisher (U. K.), Natural Convection in a Liquid Containing a Distributed Heat Source, Paper No. 119 at the 1961 International Heat Transfer Conference.

41. J. Woodrow, Free Convection in Heat Generating Fluid (Laminar Flow), British Report AERE-E/R-1267, October 1953.

Shielding

Barytes Concrete

High-density concrete is sometimes used for the biological shield of a power reactor to reduce the shield thickness. This reduction in thickness may be to save space, to reduce shield penetration lengths, or, in some cases, to reduce shielding costs or plant costs. Higher-density concretes are obtained by the use of high-density aggregates such as iron punchings, limonite ore, magnetite ore, and barytes ore. A report on barytes concrete has been issued by Oak Ridge National Laboratory.[1] The report is divided into two sections: (1) the mix criteria and (2) the attenuation characteristics.

The use of the concrete is the determining factor for the best mix criteria. In the case of barytes concrete, the usual application is as a biological shield, but the concrete may also serve structural needs in which strength is important. Finally, the requirements of attenuating neutrons of intermediate energies may make a reasonably high water content desirable. The reference[1] treats the effects of aggregate gradation, cement-to-aggregate ratio, and water content on the workability, compressive strength, and density. The density increases as the maximum size of the aggregate increases while the compressive strength is held at approximately 3200 psi. The increase in density is due mostly to the increase in percentage of the denser aggregate relative to the less dense cement. Other data show that, for a fixed maximum aggregate size, the density reaches a maximum as the cement-to-aggregate volume ratio is varied. The densities predicted by the data are contingent on the use of the recommended gradations.

The second section of the report is chiefly concerned with neutron attenuation. The fast neutrons (of energy greater than 2 Mev) are slowed down principally by inelastic scattering.

After the fast neutrons are inelastically scattered, they are re-emitted at intermediate energies in the range about 1 Mev. In this energy range the hydrogen in water is important for slowing the neutrons down to thermal energies, at which they may be absorbed. A criterion for a good neutron shield is that the intermediate-energy neutron removal cross section be as large as, or larger than, the fast-neutron removal cross section.

The Lid Tank Facility at Oak Ridge National Laboratory was used to measure the neutron-attenuation characteristics of barytes aggregate. Six aluminum cans were used to hold the test materials in the facility. The fast-neutron removal cross section was measured, in turn, for the barytes aggregate, for the aggregate plus cement, and for the barytes concrete. The removal cross sections and the mass attenuation coefficients that were measured are shown in Table IV-1. The measurements included the

Table IV-1   MEASURED FAST-NEUTRON REMOVAL CROSS SECTIONS[1]

Material	Density, g/cm^3	Σ_R, cm^{-1}	Σ_R/ρ, cm^2/g
Barytes aggregate	2.68	0.0662	0.0247
Barytes aggregate and cement	2.67	0.0633	0.0245
Barytes concrete	3.30	0.0993	0.0301

usual thermal-neutron distribution measurements, from which the removal cross sections were derived, and the fast-neutron dose distribution, as measured by a Hurst type dosimeter. Fast-neutron removal cross sections derived from the dose measurements were found to be a little larger than those shown in Table IV-1.

A check of how well the composite removal cross section could be calculated from the

measured removal cross sections of the individual elements was made by calculating the removal cross sections for the barytes aggregate and the barytes concrete. The calculated mass attenuation coefficients were 0.0265 and 0.0313 cm^2/g for the barytes aggregate and barytes concrete, respectively, a little larger than the measured values. It is interesting to note that the calculated values were in practically exact agreement with those derived from the fast-neutron dose measurements. The intermediate-energy neutron removal cross section for these materials was found to be larger than the fast-neutron removal cross section.

The agreement between calculation and measurement that is observed in this investigation is of considerable importance because it shows that the information and methods can be applied to other types of concretes and that the removal cross section can be calculated from the composition. This bears out the results of experiments on ordinary concrete.[2]

Fission-Product Heating

The analyses of shutdown and emergency cooling problems in nuclear reactors require a knowledge of the heat that is released by the fission products. Several authors have taken experimental and theoretical data and have combined them to get representative curves of the energy emitted per fission-second as a function of time after an instantaneous fission.[3,4] Curves are given in reference 3 for gamma and beta emission and in reference 4 for gamma emission. Reference 3 also gives the beta decay rate as a function of time after shutdown for several reactor operating times; reference 4 gives similar information for gammas and for the total absorbable energy following steady operation of 1000-hr duration. The results of other authors are compared in reference 4.

The equations necessary for the determination of the decay rate of the fission products after an arbitrary operating history are prescribed in reference 3. For efficient use the method should be programmed for a digital computer.

Another method of determining the fission-product decay rate after constant or variable power conditions of long duration has been reported in reference 5. In this report the 1000-hr

constant power decay curves of reference 4 have been represented by a sum of exponentials, and coefficients for fits by four and seven exponentials are given. The resulting integral equation that represents the heat generation is derived and is represented by a set of linear first-order differential equations that can be solved conveniently on an analog computer.

Shield Design for Gas-Cooled Reactors

A group at Harwell has written a report on methods of calculation for use in the design of shields for gas-cooled, graphite-moderated, natural-uranium reactors.[6] The methods presented include neutron- and gamma-radiation attenuation, nuclear heating, coolant activation, and radiation streaming in ducts. Basic constants that are used in the shielding calculations for the materials in the Calder Hall No. 1 Reactor (graphite, iron, and concrete) are also presented. The methods recommended attempt to satisfy four requirements: (1) accuracy, (2) ease of application, (3) minimum use of empirical formulas, and (4) standardization of methods. The authors point out that the recommended methods are not meant to be final and that there is room for improvement.

Most of the basic methods are those commonly used by shield designers. The differences that occur involve the choices of constants, energy groups, and geometrical representations. One exception is the introduction of a new method for calculating the neutron distribution in the shield. The method is basically a multigroup diffusion calculation with the source distribution determined by a semiempirical removal theory. The major difference of this method from other methods of calculating the thermal-neutron distribution is the use of six energy groups in the multigroup representation. A suitable choice of energy intervals allows one to take into account the scattering resonances that may allow neutrons to stream through large thicknesses of shielding without much attenuation.

To check the multigroup method, the distribution in the Calder Hall No. 1 Reactor was measured by drilling a 2-in. hole through the 7-ft-thick biological shield on the reactor mid-plane. The comparison of the calculated

thermal-neutron flux with the measured flux is shown in the reference. The results show good agreement when consideration is given to the uncertainties in the constants and to the fact that a two-group core calculation was used to get the initial neutron source. A further check was made by use of the experimental thermal-neutron fluxes that were measured in the charge-face of the British Experimental Pile O (BEPO) Reactor. The calculated results agree extremely well in the graphite reflector, through the steel thermal shield, and, for the first few centimeters, into the barytes concrete biological shield; beyond this point both the magnitude and shape of the calculated thermal-flux curve diverge from the experimental results.

The distribution of the gamma dose rate was measured during the drilling into the Calder Hall shield. A comparison of the calculated results was again made with the experimental results; in this case the calculated results were slightly higher than the measured.

Although the calculation methods presented in reference 6 are for a specific type of reactor, many of the methods are applicable to other types. Geometric attenuation is a relatively unimportant characteristic of large natural-uranium graphite-moderated reactors but will have to be more carefully considered when the methods are applied to other types of reactors. In a way this characteristic has been a help in proving out the methods because the effect of geometry could almost be removed from consideration.

Gamma-Ray Heat Generation in Hallam Biological Shields

The calculated gamma-ray heat generation in the biological shields of the Hallam Nuclear Power Facility has been reported in reference 7. The radial biological shield is ordinary concrete, and the top axial shield is iron-limonite concrete. A presentation and a discussion of the methods used in the calculations are included in the report. Extensive use is made of computing machine codes, and the codes are well referenced.

In the calculations of the gamma-ray heat generation, the most important requirement is

a correct calculation of the neutron distribution (particularly of the thermal-neutron distribution). A multigroup, one-dimensional, diffusion equation code was used to calculate the thermal-neutron distribution. Four energy groups were utilized in the calculation, and the nuclear constants are reported in tabular form. The capture gamma source distribution was derived from the neutron distribution, and the energy absorbed in the concrete biological shields was calculated from all capture and core gamma sources. The sources were represented by 10 gamma-energy groups. In the radial shield the major contribution to heat generation is from capture gammas produced in the concrete. The Na^{24} decay gammas from the sodium coolant are the major contributors in the axial shield.

Duct Studies

The calculation of neutron transmission through ducts in reactor shields is a problem of practical importance which has not been solved except in some special cases. Experimental and analytical work on the problem has been done under the Military Compact Reactor Program, and the results are reported in reference 8.

The experimental facility consists of a 40-curie polonium-beryllium source in an oil-filled source tank. The shield slab through which the ducts penetrated was placed adjacent to the outside surface of the source tank. The shields consist of a 12-in. slab of steel followed by a 12-in. slab of paraffin. Both the fast-neutron dose rates and the thermal-neutron fluxes were measured at several locations on the outside surface of the shield.

For three of the 13 configurations studied, some analytical results were obtained by a Monte Carlo duct code (ADONIS) for comparison with the experimental data. The author, after considering the uncertainties in both the experimental data and the Monte Carlo results, states that the agreement is satisfactory.

References

1. W. J. Grantham, Jr., Barytes Concrete for Radiation Shielding: Mix Criteria and Attenuation Characteristics, USAEC Report ORNL-3130, Oak Ridge National Laboratory, July 25, 1961.
2. E. P. Blizard and J. M. Miller, Radiation Attenuation Characteristics of Structural Concrete, USAEC

Report ORNL-2193, Oak Ridge National Laboratory, Aug. 29, 1958.

3. W. E. Knabe and G. E. Putnam, The Activity of the Fission Products of U^{235}, USAEC Report APEX-448, General Electric Co., Aircraft Nuclear Propulsion Dept., Oct. 31, 1958.

4. I. J. MacBean, Energy Release from Fission Product Decay, British Report AERE-R-3033, September 1959.

5. R. Potter and J. Graham, A Representation of Fission Product Heating Under Variable Power Conditions, British Report AEEW-R-33, March 1961.

6. A. F. Avery et al., Methods of calculation for Use in the Design of Shields for Power Reactors, British Report AERE-R-3216, May 1960.

7. S. Berger, Gamma-Ray Heat Generation in the HNPF Biological Shields, USAEC Report NAA-SR-6244, Atomics International, July 30, 1961.

8. R. Schamberger, Military Compact Reactor Program Duct Studies, USAEC Report NDA-Memo-2143-14, United Nuclear Corp., July 25, 1961.

Materials

Uranium Metal

A thorough examination of fuel slugs from the first loading of the Experimental Breeder Reactor No. 1 (EBR-I) has been reported from Argonne.[1] This reactor first operated in 1951; fuel was removed for examination in June 1952 and in January 1954, at which time a maximum burnup of 0.3 at.% had been attained. The fuel was highly enriched uranium metal in the beta-quenched alpha-annealed condition. Maximum metal temperatures were in the 395°C range. Measurements at the two exposure times revealed that the length of the slugs increased with burnup up to 0.05 at.%. As burnup increased from 0.2 to 0.3 at.%, the slugs shortened and ultimately became shorter than their original length. Diameter changes were the inverse of the length changes, and density decreased linearly with burnup. It was not found possible to relate chemical composition, isotopic composition, dilatometric measurements, etc., to length changes.

More recent irradiations have been carried out by Atomics International[2] in both the Sodium Reactor Experiment and the Materials Testing Reactor (MTR) with generally similar experimental results. However, the difference in burnup rate in the two reactors resulted in a higher total swelling in the MTR at temperatures below 500°C. A relation was apparent between creep strength and swelling, although the correlation involves a temperature correction between in-pile and out-of-pile tests. Tests were carried out to a burnup of 0.68 at.% on uranium−2 wt.% zirconium, uranium−1.5 wt.% molybdenum, thorium−11 wt.% uranium, uranium in the cast and beta-quenched form, and uranium as alpha rolled and beta quenched. Tests on a uranium−10 wt.% molybdenum alloy went to 2.0 at.% burnup. Center fuel temperatures were between 368 and 660°C in these tests, and swelling (per cent $\Delta V/V$) as high as 12 per cent was measured.

Zirconium and Niobium Alloys

Douglass[3] has reviewed recent work on zirconium and niobium alloys intended for use in boiling- or pressurized-water reactors, or in steam, at temperatures above those which are used in present practice. For zirconium alloys he concludes that a radical breakthrough would be required to produce materials that would withstand steam at temperatures above those employed today. Two aspects of zirconium-alloy behavior are important in high-temperature water or steam: the limited time to transition, or the onset of "breakaway" corrosion, at higher temperatures, and the several deleterious effects of hydrogen absorption. Recent work on these problems has provided important information but, as yet, little progress toward solutions. Values given by Douglass for the time to breakaway for Zircaloy-2 are as follows:

Temp., °F	Medium	Time for transition, days
550	Water	1800 ± 200
680	Water	110
750	Steam	40
850	Steam	10
900	Steam	2

Although there has been a great deal of study of the effects of hydrogen on the mechanical properties of unirradiated zirconium, apparently the combined effects of irradiation and hydrogen

have not been adequately studied. An excerpt from reference 3 reports the following experience:

> A pertinent experience with irradiated Zircaloy-2 channels in VBWR sheds valuable qualitative information on this problem. Ogawa and Brandt report[*] that certain channels which performed well during irradiation exhibited failures of small holding tabs during subsequent out-of-pile handling. The channels were therefore removed and stored in a fuel storage pool. The channels were to be scrapped, and in an effort to reduce the storage space, the channels were collapsed to a smaller volume by striking them with a heavy pipe under water. Those portions which had been across from the fuel failed in a completely brittle manner when the 57-pound weight was dropped from a height of 12 inches. Areas above and below the fuel did not fail during the "pipe-drop" test but merely deformed plastically. Further examination revealed the presence of 45 ppm of hydrogen in the irradiated area and about $20-82$ ppm of hydrogen in the ductile portions. Most of the brittleness may be attributed to the radiation damage, but it is felt that the brittleness associated with a given amount of hydrogen is much greater when subjected to irradiation (in this case 7.5×10^{20} nvt thermal and 8.9×10^{20} nvt epithermal and fast).

An incident of this type may serve as a valuable warning regarding the behavior of zirconium under certain conditions. However, since an impressive number of miles of zirconium-alloy-clad fuel elements have already operated successfully in nuclear reactors, pessimism regarding the performance of the materials at "conventional" temperatures does not appear to be justified.

The possibility of niobium alloys for use in steam at 750°F or above may be more promising. A niobium—8.9 per cent vanadium alloy followed a parabolic law for 3000 hr in 1050° superheated steam, although the total weight gain was high. Although breakaway can occur with the niobium alloys, hydrogen pickup is not a problem with the better alloys. Oxygen diffusion is much more serious, however, with niobium than with zirconium. Although much remains to be done in niobium-alloy development, it is obvious that the far greater cost of the metal will restrict its use in power reactors unless near perfection is attained or unless the price is brought down. Niobium, and particularly niobium-vanadium alloys, cannot be considered low-cross-section materials, although they are significantly better than the stainless steels in this respect. For space power systems, the cost and neutron absorption factors are relatively unimportant, and the promising behavior of niobium in high-temperature liquid metals may lead to its use in these specialized applications.

Considerable work on zirconium alloys for superheated steam has been done at Argonne National Laboratory. The work is not connected with a specific reactor program but is intended to produce a superheater alloy that will operate at 540°C (1004°F) and 600 psi. A large number of binary and some ternary alloys have been tested in autoclaves at the above conditions. Several interesting alloys have been found; one was a 3 per cent nickel*—$\frac{1}{2}$ per cent iron alloy that showed a weight-gain rate of 1.1 mg/(dm^2)(day) in 540°C superheated steam.[4] Zircaloy-2 is so rapidly corroded under these conditions that no quantitative comparison is possible. Although the corrosion rates are promising, difficulties with hydrogen absorption will probably increase as the temperature of exposure to H_2O is increased.

Aluminum Corrosion

As a reactor material, aluminum is unusual because it combines a low neutron-absorption cross section with low cost, ready availability, and a fully developed fabrication technology. These, in combination with other thermal and mechanical properties, have made aluminum a standard fuel-element cladding material for research and testing reactors. For such reactors the temperatures are not high enough to give rise to corrosion difficulties—the major drawback of the metal. For the High-Flux Isotope Reactor (HFIR), the heat fluxes [1.52×10^6 Btu/(hr)(sq ft)] and the possible maximum water coolant temperature (236°F at hot spot) are high enough to raise questions as to the behavior of

---

*Listed as personal communication in reference 3.

*The virtues of Zircaloy-4 are attributed to its very low nickel content, 0.007 per cent maximum. A group at Bettis has found that, below 454°C (850°F) in steam, Zircaloy-4 with low nickel is superior but that, above this temperature, Zircaloy-2 is superior.[5] Evidently this rule applies to the high-nickel zirconium alloys.

aluminum, even for the short fuel cycle of only two weeks. The corrosion product at these temperatures is boehmite, alpha $Al_2O_3 \cdot H_2O$, which is adherent and thickens rapidly enough to act as an increasingly important thermal barrier. The performances of the aluminum alloys 1100 and 6061 were therefore investigated at ORNL[6] in rigs that provided coolant temperatures up to 250°F, flow rates up to 51 ft/sec, and heat fluxes as high as 2.06×10^6 Btu/(hr)(sq ft).

It was found that both of the alloys were satisfactory if the pH of the coolant was held at 5.0 to 5.5 with nitric acid. The greatest penetration was 1.5 mils in 10 days at these conditions. However, in pure water, which is a more convenient coolant, corrosive attack was excessive. The corrosion-product layer had a thermal conductivity of 1.5 ± 0.4 Btu/(hr)(sq ft)(°F/ft). The 6061 alloy was preferred to the commercially pure metal (1100 alloy) because of its better strength characteristics, and it was concluded that 6061 has a high probability of being satisfactory in the HFIR.

Although the above conditions may represent an approach to the upper limit for test reactor operations, there has been considerable interest in the past few years in extending the use of aluminum cladding into the power-reactor range to temperatures of 360°C (680°F). The limitation here is again inadequate corrosion resistance. An indication of the long times necessary to test materials intended for prolonged reactor operation is given by the fact that, although the first successful results with a 1 per cent nickel alloy (X-8001, previously M-388) were reported by Draley and Ruther[7] in 1955, results of long-time (seven months) tests have only recently been reported from Argonne.[8] Dynamic out-of-pile loops were employed in these tests, and the effects of pH, ratios of surface area to water volume, surface boiling, and other variables were investigated.

In the tests that lasted seven months, no indication of catastrophic attack was found.[8] Phosphoric acid added to the water up to a pH of 5.5 decreased the corrosion rate by a factor of 2 and the metal loss by a factor of 4 at 260°C (500°F). At lower pH the attack became localized, and, although the corrosion rates were lower, pitting was excessive. The metal loss rate decreased as the ratio of surface area of sample to volume of water in the test loop increased. Surface boiling increased corrosion, but not to a serious extent. The loop opera-

tion indicated that deposition of alumina occurs on other metal surfaces in the system and may be a problem.

In an aluminum-alloy development program at Hanford,[9] titanium- and silicon-containing alloys were investigated in addition to the nickel and nickel-iron systems that are usually considered for resistance to corrosion by high-temperature water. Testing was restricted to low-flow autoclave work. It appeared that similar corrosion behavior could be secured from a wide range of nickel-iron concentrations. These alloys were not greatly affected by casting and fabrication techniques. It was also found that corrosion penetration increased to a maximum at between 320 and 350°C (608 and 662°F) and then decreased with increasing temperature.

Radiation Effects in Steels

Two recent compilations of materials data should be of considerable value to the reactor designer. The first covers the effects of irradiation on the mechanical properties of the stainless steels.[10] The information was abstracted from USAEC, AECL, and AERE reports dating back to 1948. Twenty-one alloys are covered, including the common 300- and 400-series stainless steels, boron—stainless steel (1 per cent), AM-350, 17-7-PH, 17-4-PH, and Stainless W. Strength, ductility, fatigue, and impact data are provided to the limits of the available information. Much of the information is presented in graphic form, and the original sources are clearly identified.

The companion report[11] covers similar irradiated properties for 23 carbon and low-alloy steels for data collected from American, Canadian, and British reports over the same period.

Because of the relative scarcity of long-term irradiation data and because extensions of the information can be made only slowly, irradiation effects tend to place artificial restraints on the selection of materials. Thus the designer might be tempted to, or forced to, select a material for an application in a radiation field on the basis of how much information is available on its response to irradiation, and he might thereby eliminate a material that would be more suitable in other respects. Compilations like those in references 10 and 11 assure, at least, that the designer will be aware of the data that do exist.

Boron Carbide Control Rods

Theoretical determinations of the useful lifetime of a B_4C-in-tubes control rod are reported in reference 12. This is the type of rod that was installed in the Dresden reactor to replace the original boron—stainless steel rods which were found to contain cracks. The boron carbide rod consists of boron carbide that is contained in round tubes of type 304 stainless steel. These tubes are held in a cruciform assembly by a sheath of type 304 stainless steel, as indicated in Fig. V-1. The size of the cruciform in this particular case is determined by the requirement that it be suitable for replacement of the original Dresden rods.

The lifetime of a boron carbide control rod may be limited either by depreciation of its nuclear worth or by the buildup of internal gas pressure as helium is formed by the $B^{10}(n,\alpha)Li^7$ reaction. The nuclear lifetime is maximized when the maximum amount of B_4C is packed into tubes having the least possible wall thickness, but this approach simultaneously minimizes the life of the tube as determined by gas-pressure buildup. The reference treats the problem of balancing these two considerations to arrive at a design which yields the maximum useful lifetime. Obviously the design and the lifetime estimate will depend on the fractional release of the helium by the B_4C particles. It is assumed in reference 12 that this fractional release will lie between 10 and 40 per cent,
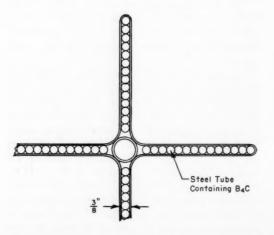
and the lifetime is estimated as a function of this variable. It is concluded that lifetimes of 10 or more years are achievable through the proper selection of tubing material and B_4C density values and that the B_4C densities required for maximum lifetimes are in a range that can be obtained by vibratory compaction followed by swaging.

References

1. W. F. Murphy et al., Examination of Uranium from the First Core of the EBR-I, USAEC Report ANL-6113, Argonne National Laboratory, September 1961.
2. G. G. Bentle, Irradiation Swelling of Uranium and Uranium Alloys, USAEC Report NAA-SR-4893, Atomics International, Sept. 30, 1961.
3. D. L. Douglass, Corrosion Problems in the Use of Zirconium and Columbium Alloys in Nuclear Reactors, *Corrosion*, 17(12): 589t (December 1961).
4. Sherman Greenberg, Zirconium Alloys for Use in Superheated Steam, *J. Nuclear Materials*, 4(3): 334 (August/September 1961).
5. J. N. Chirigos et al., Development of Zircaloy-4, in *Fuel Element Fabrication*, Vol. 1, Chap. 4, p. 19, Academic Press, London and New York, 1961.
6. J. C. Griess et al., Effect of Heat Flux on the Corrosion of Aluminum by Water. Part III. Final Report on Tests Relative to the High-Flux Isotope Reactor, USAEC Report ORNL-3230, Oak Ridge National Laboratory, December 1961.
7. J. E. Draley and W. E. Ruther, Corrosion Resistant Aluminum Above 200°C, USAEC Report ANL-5430, Argonne National Laboratory, July 15, 1955.
8. N. R. Grant, Summary of Corrosion Investigations of High-Temperature Aluminum Alloys, October 1957—December 1959, USAEC Report ANL-6204, Argonne National Laboratory, September 1961.
9. H. C. Bowen, Development of Corrosion-Resistant Aluminum Alloys for High-Temperature Water Service, USAEC Report HW-68253, Hanford Atomic Products Operation, March 1961.
10. R. E. Schreiber (Comp.), Mechanical Properties of Irradiated Stainless Steels, USAEC Report DP-579, Savannah River Laboratory, September 1961.
11. R. E. Schreiber (Comp.), Mechanical Properties of Irradiated Plain Carbon and Alloy Steels, USAEC Report DP-581, Savannah River Laboratory, October 1961.
12. F. H. Megerth, Determination of Lifetime of the B_4C-in-Tubes Control Rod, USAEC Report GEAP-3764, General Electric Co., Atomic Power Equipment Dept., July 19, 1961.

Fig. V-1   Cross section of B_4C-in-tubes control rod.[12]

Components: Pump, Valve, and Turbine Leakage

Pumps

The leakage of water from the primary system of either a D_2O-cooled or an H_2O-cooled power reactor is a serious consideration because it poses problems of contamination and waste disposal. Substantial leakage rates are particularly serious in the D_2O-cooled systems because the D_2O is expensive and because the tritium content of irradiated D_2O aggravates the waste-disposal problem. It seems a bit paradoxical that, whereas zero-leakage canned-motor pumps are used almost without exception on existing large pressurized-H_2O reactors, studies and plans directed toward the construction of D_2O-cooled reactors usually emphasize the choice of limited-leakage pumps employing shaft seals of one kind or another. A partial explanation may be that most of the D_2O designs presently under construction have primary system pressures somewhat lower than those in the pressurized-H_2O plants. A further explanation appears to be that, whereas large limited-leakage pumps may be postulated for reactors to be built in the future, they are not in fact available for reactors being built today. The Yankee reactor, for example, uses four canned-motor pumps; each has a capacity of 23,700 gal/min and operates at 2000 psi and 545°F. No doubt the size requirements will be still higher for future large reactors of the pressurized-H_2O type. According to reference 1, the largest limited-leakage pumps built so far which are capable of operation at these conditions have capacities of 14,000 gal/min. Nevertheless the possibility of cost savings through the use of limited-leakage pumps continues to be of interest.

The requirements for main coolant pumps for pressurized-H_2O service are reviewed in references 1 and 2, and some of the pumps built to date for both conventional and nuclear plants

are described. Also, reference 2 summarizes pump experience to date in a number of nuclear plants. Estimates in reference 1 show that the limited-leakage pump should have a cost advantage, for 40,000 gal/min pumps, of about \$225,000 per pump in multiple-pump orders. The limited-leakage pump uses about 10 per cent less power because of its higher electrical efficiency. The application of this information to the Yankee reactor shows that, if limited-leakage pumps were substituted for canned-motor pumps, the net plant output would be raised by about 0.7 per cent and there would be a similar saving in initial plant cost. The waste-disposal system would have to be enlarged to accommodate pump leakage, negating some of the savings. Further cost comparisons are given.[1,2]

In reference 1 both the present capabilities and the seal development programs of manufacturers are reviewed. The conclusion[1] is that, because of low anticipated sales volume, manufacturers' development programs are on a very limited scale which is insufficient for the development of a high-temperature, high-pressure seal that would be suitable for use in 40,000 gal/min pumps for pressurized-H_2O service. Initiation by the AEC of a program for development of a suitable seal is recommended.[1]

Other possible areas of improvement in pump cost are through use of less expensive materials than those presently used, through relaxation of inspection and test requirements for major pump components such as castings, through elimination of seal welds on canned-motor pumps, and through improvement of canned-motor design to increase the electrical efficiency.

Reference 3 is a Sargent and Lundy report on an investigation of the leakage characteristics of various seals that might be used in D_2O systems for turbine shafts, pump shafts, and valve

stems. The pump-shaft seal leakage tests were conducted at Savannah River Laboratory. Commercially available mechanical shaft seals were tested. These mechanical seals were furnished by Durametallic, Borg-Warner, and Crane, and were types PTO, D, and 8B, respectively. Four seals for 2-, $2\frac{5}{8}$-, $3\frac{9}{16}$-, and $4\frac{5}{8}$-in.-diameter shafts were purchased from each of the three manufacturers. No attempts were made to compare or evaluate the seals of different manufacturers. The parameters varied were the shaft size, the shaft speed, and the system pressure. The reference gives a good discussion of the various types of mechanical seals available commercially and of the recoverable and non-recoverable leakage. The recoverable leakage is, in general, that leakage which is recovered by means of a seal-flange gland drain. This drain is located between the last and next-to-last bushing in the pump. The nonrecoverable leakage is then defined as that leakage which

passes the last bushing in the pump and is lost into the atmosphere. Quite often this may be vapor.

The nonrecoverable leakage losses on two of the pumps tested are shown in Table VI-1. The recoverable leakage losses were found to vary widely in each test and between tests, with the average being less than 2 lb/day. The runs, however, were of short duration, from about 25 hr to about 200 hr.

Investigations of leakage characteristics are reported in reference 4 for gasketed joints and pump seals that have been proposed for use in the Heavy-Water Components Test Reactor (HWCTR). The pump that was tested had a conventional mechanical seal with a Stellite rotating face and a carbon stationary face. The test pump circulated deionized water at 260°C and 850 psig at the suction nozzle. The shaft diameter was 2 in., and the rotational speed was 3600 rpm. The duration of the run was 149 days (3576 hr).

Table VI-1   NONRECOVERABLE LEAKAGE LOSSES[3]

Test conditions		Seal for a $2\frac{5}{8}$-in.-diameter shaft		Seal for a $3\frac{9}{16}$-in.-diameter shaft	
Nominal shaft speed, rpm	Pressure, psig	Duration, hr	Average leakage, lb/year	Duration, hr	Average leakage, lb/year
3600	1000	25	4.02	24	14.56
		41	19.83		
2500	1000	24	4.96	24	5.80
		48	11.77		
1500	1000	24	1.90	24	1.34
		48	10.11		
800	1000	46	8.89	24	0.57
575	1000	24	2.03		
3600	750	85	8.91	24	0.32
3600	500	50	11.40		
3600	300	58	7.86		

Table VI-2   SUMMARY OF LEAKAGE RATES (POUNDS PER YEAR) FROM A PUMP MECHANICAL SEAL[4]

	Days of operation					
	0–20	21–41	42–81	82–113	114–149	0–149
Vapor leakage, lb/year:						
Average	3.3	1.1	1.8	1.0	0.7	1.4
Maximum	22	4.8	13	8	7	22
Minimum	0.02	0.2	0.04	*	0.3	*
Average liquid leakage, lb/year	2900	2100	670	220	90	910

*Less than 0.005 lb/year, which is the minimum sensitivity of the measuring instrument.

The particular pump tested (Pacific $8 \times 10\frac{1}{2}$ NVC pump with a BJD-2250 mechanical seal) did not have a seal-flange gland drain, and the leakage was collected by forming an enclosure around the shaft and seal with a rubber cylinder. Vapor leakage was swept out of the collection chamber with a stream of nitrogen, and liquid leakage was trapped in a "catch bottle." Measurements were then performed on the amount of leakage of vapor and liquid. These data are shown in Table VI-2. Although the liquid loss rates are somewhat high (2.5 lb/day average) and quite time dependent, the liquid could be recovered with appropriate piping and pumps; the vapor losses are low and do represent, in all probability, true losses because recovery would be difficult.

Turbine Shaft Seals

The turbine shaft seal (Fig. VI-1) investigated by Sargent and Lundy[3] was developed for the Experimental Boiling-Water Reactor (EBWR) turbine and was designed for possible use with D_2O. Tests of this seal were performed on the EBWR turbine. A modification of this seal has been considered by Sargent and Lundy for application to direct-cycle boiling-D_2O power plants.[5] Relative to conventional labyrinth turbine shaft seals, the EBWR seal contains additional labyrinths and sealing fluids to reduce the leakage of D_2O steam to the atmosphere. At the low-pressure end of the turbine, inleakage of light water which could contaminate the D_2O was controlled by the same methods.
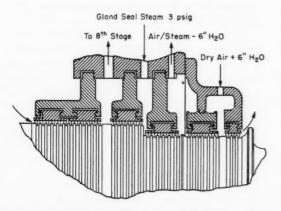

Gland Seal Steam 3 psig

To 8th Stage   Air/Steam - 6" H_2O

Dry Air + 6" H_2O

Fig. VI-1   EBWR turbine shaft seal showing the high-pressure end.[3]

At the high-pressure end of the turbine, dry air is introduced at the atmospheric end of the seal. This air will leak in both directions through the labyrinth glands; that which leaks to the outside mixes with the atmospheric air and does no harm. The air that leaks inward into the next space mixes with outward-leaking steam and is drawn off; the steam is recovered by condensation. The next space is a gland where sealing steam is introduced at 3 psig and leaks outward, as above, and inward to mix with the driving steam from the turbine which leaks through its own labyrinth gland. This mixture is carried off to the eighth stage of the turbine, where the pressure will allow re-entry. This arrangement assures that only air can leak back into the turbine-room atmosphere.

Two tests were run, one with and one without the vapor-recovery system in operation. These tests demonstrated that the EBWR turbine seals leak approximately 1.3 lb of H_2O per month; if the fluid were D_2O, this would be reduced to about 0.65 lb/month. During the tests the H_2O inleakage rate was 5.48 lb/month, although the reactivating cycle of the seal makeup-air desiccator was malfunctioning during the test periods. The reference concludes that turbine seal inleakage would be insignificant if the air desiccator were functioning properly.

Gaskets and Valve Stems

Valve-stem leakage is another potentially important source of loss from D_2O systems. Ordinary packed valve stems cannot be made tight unless the packing is tightened so much that the valve cannot be operated. The valve stem may also be galled if the packing is too tight. One method of eliminating these drawbacks is by installing a "lantern ring" fairly close to the working fluid. This lantern ring is provided with a leakoff to a recovery system, and the pressure drop across the remaining packing rings is so small that leakage is minimized. Bellows-sealed valves and diaphragm-sealed valves have also been considered for such applications, but there are limitations on each type of valve which make it unsuitable for general use. Absolutely zero leakage can be obtained only with a hermetically sealed valve: one in which a cap is welded over the stem. In the event that the valve must be operated, this cap must be removed, and it must be replaced

after the operation is complete. Vapor condenses in the cap, and provision must be made to drain it off before opening if loss of the fluid is to be prevented. Operation of such a valve becomes a major task, and therefore the scheme is usually impractical. The results of valve tests at Savannah River were reviewed in the September 1961 issue of *Power Reactor Technology*, Vol. 4, No. 4, page 70.

Mockups of typical joints using commercially available gaskets were tested in the program described in references 4 and 6. These joints included an asbestos gasket with a stainless-steel jacket, a spiral-wound gasket made of stainless steel and asbestos, and some pipe-to-tubing joints. In addition, joints for the bayonet fuel housings were tested. These included two conventional quick-disconnect couplings, a breech lock joint with a spiral-wound gasket, and a specially designed joint with a gold gasket between the Zircaloy and stainless-steel sections of the bayonet housing. These joints were tested through 100 cycles with a maximum pressure of 1500 psig and a maximum temperature of 250°C. Conditions were varied to simulate the actual conditions to which the joints would be subjected and were brought down to minima of atmospheric pressure and ambient temperature. Leakage was collected in a chamber constructed around each joint under test. This moisture was removed by passing a stream of dry nitrogen through the chambers and conducting both the inlet and effluent streams through hygrometers of the Keidel type.[7]

The average leakage rate for the gasketed joints was less than 0.25 lb/(year)(in.), although this rate increased to 0.46 lb/(year)(in.) during the last 25 to 100 cycles for the Flexitallic gasket in the control-rod cluster housing. In specifying the leakage per inch, the length of the gasket was measured around the inside circumference. The leakage from the tubing fittings was less than 0.13 lb/(year)(in.) for the worst case. The leakage rates for the bayonet joints were quite small, the maximum being 0.03 lb/(year)(in.), but the bayonet top-closure leakage was considerably larger, about 0.18 lb/(year)(in.). The gold gasket joint joining the Zircaloy and stainless steel had a leakage rate of 0.002 lb/(year)(in.).

References

1. Ebasco Services, Inc., Investigation of Types of Seals for Main Coolant Pumps for Large Pressurized Water Reactor Nuclear Plants, USAEC Report NYO-9321, June 1960.
2. Pumps for Water-Cooled Power Reactors, *Nucleonics*, 19(7): 55 (July 1961).
3. W. A. Chittenden and G. F. Hoveke, Heavy Water Reactor Plant Leakage, USAEC Report SL-1874, Sargent and Lundy, June 30, 1961.
4. F. C. Apple, Leakage of Water from Gasketed Joints Proposed for the HWCTR (Part II), and Pump Mechanical Seal Vapor Leakage, USAEC Report DP-611, Savannah River Laboratory, August 1961.
5. Sargent and Lundy and Nuclear Development Corp. of America, Heavy-Water Moderated Power Reactor Plant, Preliminary Design of the Prototype Plant, USAEC Report TID-8503(Pt. 2), July 1959.
6. F. C. Apple, Leakage of Water from Gasketed Joints Proposed for the HWCTR (Part I), USAEC Report DP-487, Savannah River Laboratory, July 1960.
7. F. A. Keidel, Determination of Water by Direct Amperometric Measurement, *Anal. Chem.*, 31: 2043−2048 (1959).

Design Practice: Hallam

General Description

The Hallam Nuclear Power Facility (HNPF)[1-6] consists of a 240-Mw(t) sodium graphite reactor (SGR) and the associated equipment for producing superheated steam to operate the turbine generator of the Sheldon Power Station located near Hallam, Nebr. Until the HNPF is completed, the steam demands are being met by a conventional coal-fired boiler.

The reactor (Fig. VII-1) is fueled with slightly enriched uranium-molybdenum alloy. The graphite moderator is contained in stainless-steel cans, and liquid sodium is used as the reactor coolant. Reactivity control is obtained by moving neutron-absorbing shim-safety-regulating rods into or out of the core. When necessary, these rods can be dropped by gravity into the core to shut down (scram) the reactor. The core and its supporting structures are contained in a stainless-steel reactor vessel that is surrounded by a thermal shield, a reactor outer vessel, thermal insulation, a gastight water-cooled cavity liner, and a concrete biological shield.

Three identical sodium heat-transfer circuits carry the heat generated in the reactor to the steam generators. Each circuit consists of a radioactive primary loop and a nonradioactive secondary loop coupled through a sodium-to-sodium intermediate heat exchanger. Steam from all three steam generators is fed into a common header that serves a single turbine generator. The required steam rate at the turbine throttle is 710,000 lb/hr at 800 psig and 825°F. The nominal net electrical output of the station is 75 Mw.

A building of conventional industrial construction is used to house the reactor. Within the reactor building, regions of potential radioactive contamination are maintained at slightly less than atmospheric pressure to prevent the outward release of contaminants.

Reactor Core

The reactor core consists of a matrix of moderator elements (Fig. VII-2) into which are suspended fuel elements, control rods, and miscellaneous other elements. The moderator assembly is approximately in the form of a right-circular cylinder 17 ft in diameter by 17 ft high. The initial fuel loading forms approximately a cylindrical core, 13 ft in diameter and 13.5 ft high, surrounded by a graphite reflector approximately 2 ft thick.

The primary sodium inlet pipes enter the reactor cavity just above the tops of the moderator assemblies and run downward to the lower part of the reactor vessel. The major portion of the sodium enters the lower plenum between the grid plate and the bottom of the reactor vessel and flows upward through the fuel-element process tubes to the sodium pool above the core, thus removing heat from the fuel elements. The remaining sodium (~5 per cent) is routed by a parallel piping system to the plenum between the grid plate and the bottom of the moderator elements. From here it flows upward through the gaps between the moderator elements into the upper sodium pool. This sodium removes the heat generated in the moderator. The gap between moderator elements is nominally 0.160 in. wide and is maintained by spacer fittings that are fastened to the top heads of the cans.

Moderator Elements

Each moderator element consists of a log of graphite enclosed within a stainless-steel can.

Iron-Limonite Concrete
265 cu ft

Loading Face Shield
405 Stainless Steel

Cavity-Liner
Cooling Coils

Gallery Seal
Gastight

Vent Line

Upper Cavity Liner
405 Stainless Steel

Iron-Magnetite
Concrete, 265 cu ft

Reflective Insulation

Reactor Bellows
321 Stainless Steel

Concrete Biological
Shield

Thermal Shock Liner

Carbon Steel Thermal
Shields

Carbon Steel Cavity
Liner

Grid Plate

Low Alloy Steel
Outer Vessel

Reactor Vessel
304 Stainless Steel

Pipe Support
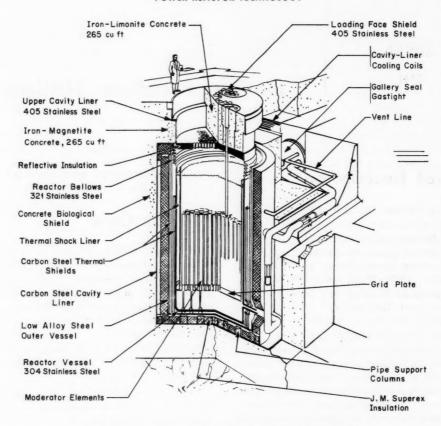Columns

Moderator Elements

J. M. Superex
Insulation

Fig. VII-1   Cutaway view of the HNPF reactor structure.[1]

The graphite is a prism of hexagonal cross section with a longitudinal scallop on each edge. The total assembly of moderator elements makes up the core and reflector graphite assembly. The edge scallops form the circular process channels for fuel elements, control rods, and miscellaneous core elements; in the reflector region the process channels are filled by canned graphite filler elements. The moderator elements are supported by a bottom grid plate, which is perforated by holes under the process-channel locations so as to accept the ends of fuel assemblies, control-rod thimbles, and miscellaneous core elements. There are 205 of these holes, and the boundary of the hole-containing region is the nominal boundary of the core. However, the initial core does not utilize all the available channels, about 45 of which are filled by dummy elements. The proper gap between moderator elements is maintained by spacers fastened to the top head of each element. Core clamps, supported by an internal ring welded to the pressure vessel, surround the matrix of moderator elements and support the top heads of the elements to prevent lateral movement.

Moderator material	Graphite (mold grade)
Sheath material (can wall)	Type 304 stainless steel, 0.016 in. thick
Upper and lower can heads	Type 304 stainless steel, ½ in. thick
Atmosphere within can	Helium, plus gases released from graphite; pressure <1 atm
Getter, for gases released from graphite	Zirconium sponge in cavity at top of log
Number of moderator elements	141
Shape	Hexagonal prism with scalloped edges
Number of process channels (including those containing graphite filler elements)	205

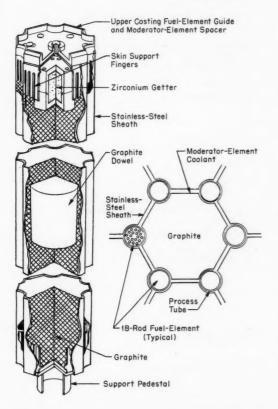|	
Width across flats	16 in.
Length	17 ft
Sodium gap between elements	0.160 in.
Cooling	Upflow of sodium in gap
Weight per element	2400 lb
Vertical support	Bottom support by pedestals on grid plate

Fig. VII-2 Moderator reflector element for the HNPF.[1]

Fuel Assemblies

The fuel for the first core loading is contained in 18-rod fuel bundles (Fig. VII-3). Each bundle consists of an outer ring of 12 rods and an inner ring of 6 rods, enclosed in a Zircaloy-2 process tube. A hollow central tube carries spacers, located at 1-ft intervals, which maintain the spacing between rods. A fuel rod consists of solid cylinders of uranium—10 wt.% molybdenum, 0.590 in. in diameter and 3 to 12 in. long, in a type 304 stainless-steel tube with welded end caps. At the upper end of each rod

is an 18-in.-long empty space to allow for potential growth of the fuel under irradiation and for the buildup of fission-product gases. The tube wall along this gas space is supported internally by a coil spring. The design requirements for the gas space are to allow 6 vol.% fuel growth and 2 vol.% fission-gas release.

The fuel rods are assembled into a bundle by hanger castings at each end. The upper hanger casting also joins the bundle to a hanger support which, in turn, connects the bundle to the hanger tube. The process tube is connected separately to the hanger tube by three disconnect pin assemblies that permit reuse of the process tube.

The process tube confines the main coolant flow to the fuel bundle. It seals the elements to a nozzle in the lower grid plate by means of piston rings carried on a lower extension of the process tube. This sliding seal allows for thermal expansion of the fuel element.

Each fuel element and process tube is supported from a shield plug in the loading-face shield by a perforated hanger tube. A variable orifice is incorporated into the lower end of the hanger tube to allow adjustment of the sodium flow in the individual coolant channels in order to obtain uniform coolant outlet temperatures during reactor operation. The orifice drive mechanism is located in the shield plug. It is operated manually from the loading face by a special tool. The lower tip of each orifice plug contains two thermocouples that measure the fuel-channel-outlet sodium temperature about 2 ft above the top of the fuel.

Number of fuel assemblies in initial core	137
Type	18-rod cluster
Fuel material	U−10 wt.% Mo alloy
Uranium enrichment	3.6 wt.% U^{235}
Active length of fuel rod	13.25 ft
Fuel diameter	0.590 in.
Jacket tube material	Type 304 stainless steel
Jacket dimensions	0.660-in. outside diameter and 0.01-in. wall
Fuel-jacket gap	0.025 in. on radius (nominal)
Material in gap	Sodium
Design limit:	
Maximum fuel temperature	1250°F
Maximum power per foot of fuel rod	19.4 kw
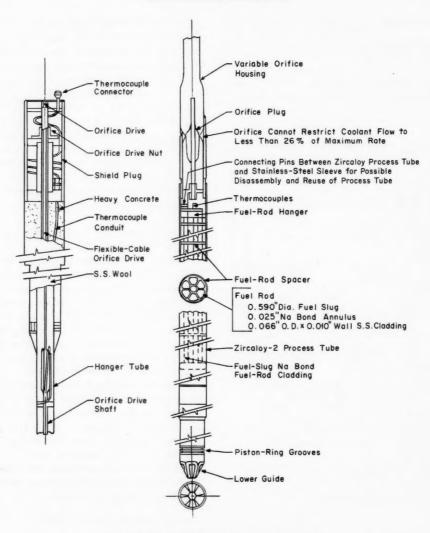
Fig. VII-3   HNPF fuel-element assembly.[1]

Maximum power per fuel assembly	2.5 Mw
Expected maximum fuel temperature	1184°F
Maximum fuel burnup	15,000 Mwd/metric ton of uranium
Average fuel burnup	8000 Mwd/metric ton of uranium

Control Rods

Nineteen gadolinium and samarium oxide control rods serve as combination shim-safety-regulating rods. The hollow cylindrical poison column, which constitutes the control rod proper, is connected to the drive mechanism by a group of three pull rods; the poison column and the pull rods are contained in a long vertical helium-filled Zircaloy-2 thimble that is supported from the loading face and extends downward into the bottom grid plate. The rod actuators, which consist of ball nuts and screws housed within gastight tubes communicating with the control-rod thimbles, are bolted to the loading-face shield (see Fig. VII-1) and extend up into a control-rod support structure (not shown in Fig. VII-1).

Number of control rods	19
Poison-column material	$Gd_2O_3 - Sm_2O_3$
Jacket for poison column	Hastelloy X
Column construction	$\frac{1}{8}$-in.-thick annular poison cans*
Active length	12.5 ft
Maximum worth of 1 rod	1.5 to 2% Δk
Total reactivity worth of rods	14.0% Δk
Rod speed	12.4 in./min
Maximum rate of reactivity insertion (19 rods)	0.03% Δk/sec
Rod drop time (full up to snubber)	0.9 sec
Rod travel	13 ft
Scram release	Magnetic latch at top of rod
Thimble atmosphere and pressure	Helium, 15 psig
Rod buffer	Three snubber cushions
Rod actuator	$1\frac{1}{4}$-in.-diameter ball screw that drives a ball nut and rod latch assembly
Torque restraint	Ball nut riding in square actuator housing
Position indication	Selsyn on drive-gear train for position increments of 0.1 in.
Rod operation	Individual or bank operation manually or automatically
Core access	All actuators are unbolted from the loading face and raised into the support structure; then the entire control-rod structure, drives, and actuators are moved from the loading face

Miscellaneous Core Elements

Various core elements are initially used in the core process channels that do not contain fuel

---

*The outside diameter of the poison can appears to be about 2.5 in., but this dimension is not given explicitly in the safeguards report.

elements. All these elements are attached to the shield plug on the loading face by hanger tubes.

Dummy element (45)	Cylindrical graphite log which is contained in a stainless-steel jacket and which is used to displace sodium from the unused core position
Neutron source (1)	Beryllium cylinder with an antimony tetroxide capsule supported at center of loading face; peak temperature 1310 °F; instrumented with thermocouples to measure coolant temperatures
Sodium level instruments (not in active core) (2)	Each position has four thimbles, contains sodium-level alarm and scram instruments; reactor scrams if two out of three level scram signals are received
Sodium temperature element (3)	Detects moderator-coolant temperature profile; consists of graphite logs clad in thermocoupled stainless-steel jacket
In-core nuclear instruments	Fission-chamber neutron detectors suspended from loading face in stainless-steel thimbles; used in empty fuel channels during initial loading and low-power experiments

Reactor Vessel Structure (Figs. VII-1 and VII-4)

Reactor vessel dimensions	19 ft in diameter by 33 ft high
Material	Type 304 stainless steel
Shell thicknesses	2 in. thick at inlet and outlet nozzle connections; $\frac{3}{4}$ in. thick at core; 1 in. thick above outlet nozzles
Operating pressure	1 to 6 in. H_2O

Nozzle schedule:

Type	Quantity	Size, in.	Location
Sodium inlet nozzles	3	14	28 in. above vessel base
Moderator coolant nozzles	1	6	$4\frac{1}{2}$ ft above vessel base
Sodium outlet nozzles	3	16	23 ft above vessel base

Reactor vessel bellows:

Flexible seal connection between the upper cavity liner and reactor vessel; bellows design pressures are 5 psig external and 15 psig internal at operational temperature.

Thermal-shock liners:

Upper and lower liners are made of type 304 stainless steel and are $\frac{1}{4}$ in. thick; they are supported at the core clamp, approximately 22 ft above the base of the vessel; stagnant sodium gap acts as thermal barrier.

Grid plate:

18 ft in diameter by 1 in. thick, stainless steel; supports and positions moderator elements; is located 42 in. above vessel base and is supported by pedestals and a ring around the inside of the reactor vessel.

Thermal shield:

Two concentric carbon steel cylinders that are $2\frac{3}{4}$ in. thick; they are placed outside the vessel to protect the biological shield.

Reactor outer vessel and insulation:

Carbon steel tank that is 20.67 ft in diameter by 35.5 ft high; it has a $\frac{1}{2}$-in.-thick shell and has 12 in. of external fibrous thermal insulation.

Cavity liner (Fig. VII-4):

Gastight enclosure around reactor; is made of $\frac{1}{2}$-in.-thick carbon steel plate; serves as an external boundary for sodium pipe chases and as an inner concrete form for the biological shield; is filled with a helium atmosphere at 0.25 psig; diaphragm seals separate the nitrogen atmosphere in the outer pipe tunnels from the helium atmosphere in the reactor cavity.

Loading-face shield:

Single-step reinforced-concrete plug; weighs approximately 300 tons; is 19 ft 2 in. in diameter and is 7 ft 3 in. in over-all depth; the lower $10\frac{1}{2}$ in. is reflective insulation of polished stainless-steel sheets; has a Cerrobend (frozen metal) seal between shield periphery and upper cavity liner; has 207 openings for $6\frac{1}{4}$-in.-diameter single-step shield plugs to support fuel elements, control rods, miscellaneous elements, and instrumentation assemblies; each shield plug has a double quad-ring cover gas seal; three 58-in.-diameter step openings are for moderator element removal.
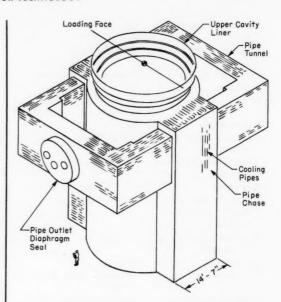

Fig. VII-4 HNPF reactor cavity liner.[1] The upper cavity liner supports the loading-face shield; the structure will be gastight; all surfaces will be cooled with 1-in. pipes; the cavity liner will be completely surrounded by biological concrete.

Heat Removal and Steam Generation

The sodium heat-transfer system consists of three independent heat-transfer circuits, each of which is directly connected to the reactor vessel. Each circuit consists of a radioactive primary loop that transfers thermal energy from the core to an intermediate heat exchanger and a nonradioactive secondary loop that carries the heat from the heat exchanger to a steam generator. The reactor can be operated with two of the three circuits in operation. In the event of failure of two circuits, the reactor will be shut down, and the third circuit will provide shutdown cooling.

A flow diagram of one of the three heat-transfer circuits is shown in Fig. VII-5. The primary loop includes a variable-speed centrifugal pump, an intermediate heat exchanger (IHX), power-actuated valves in the reactor inlet and outlet lines, and a check valve in the inlet line. The inlet-line throttling valve serves as a flow-control valve. The reactor vessel serves as an expansion tank. Vessel pressure is maintained
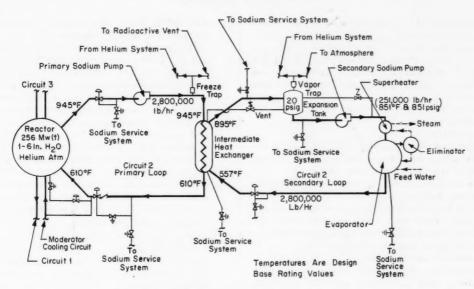
Fig. VII-5   Sodium heat-transfer circuit[1] of the HNPF.

at a positive pressure of 1 to 6 in. H₂O by a helium-gas cover above the surface of the sodium pool.

Each secondary sodium loop contains an IHX, an expansion tank, a variable-speed centrifugal pump, a steam generator, and a power-actuated throttling valve. The expansion tank provides space for sodium volume changes and a free surface for liberation of entrained gas and serves as a pressurizer at 20 psig.

All piping and equipment in direct contact with sodium in the sodium heat-transfer system are stainless steel except for the steam generators, which are chrome-molybdenum steel. Because the melting point of sodium is 208°F, the system is equipped with electrical preheating facilities that are capable of producing and maintaining a temperature of 350°F. The steam side of the steam generators is supplied with service steam at 110 psig and 338°F for pre-heating.

Primary system:

Reactor coolant-flow orificing	Individual variable orifices at each fuel element, minimum setting 26% of full flow
Core inlet temperature	610°F
Core outlet temperature	945°F
Δt through core	335°F
Primary sodium flow	2.8×10^6 lb/hr per loop

Total primary sodium flow	8.4×10^6 lb/hr
Primary flow control	Variable pump speed adjusted to maintain desired secondary coolant temperature

Secondary system:

Secondary sodium IHX inlet temperature	557°F
Secondary sodium IHX outlet temperature	895°F
Δt through IHX	338°F
Secondary sodium flow	2.8×10^6 lb/hr per circuit
Secondary flow control	Variable pump speed adjusted to maintain constant steam pressure

Steam conditions at steam generator:

Temperature	850°F
Pressure	850 psig
Flow rate (full power)	251,000 lb/hr per steam generator

Steam conditions at turbine throttle:

Temperature	843°F
Pressure	800 psig
Flow rate (full power)	752,000 lb/hr

Sodium pumps:
    Vertically mounted, overhung, centrifugal, free-surface type. Primary pumps are permanently mounted in the shielded heat-exchanger cells, and motors are mounted in the reactor room at floor

level; internal parts are removed through the top without disturbing pump case or piping. Secondary pumps are located in the unshielded steam-generator room. Primary and secondary pumps are nearly identical; each pump is driven by an a-c induction type motor through a variable-speed electromagnetic coupling; continuous speed range is 0 to 102 per cent of the rated number of revolutions per minute.

Sodium valves:

Primary sodium blocking valves are split wedge gate valves; the primary and secondary throttle valves are Venturi ball type valves. Each valve has a frozen-sodium stem seal and a backup stem packing. Valves can be operated automatically by an air motor drive or manually by handwheel operation. These valves were reviewed in the September 1961 issue of *Power Reactor Technology*, Vol. 4, No. 4, pages 54–56.

Intermediate heat exchangers:

Transfer heat from primary sodium to secondary sodium; shell (secondary) and tube (primary); counter flow design; vertically mounted; entirely type 304 stainless-steel construction. Designed for 100 psig at 1000°F; design pressure drop 5 psi tube side and 7 psi shell side; an expansion bellows is installed at the midpoint of the shell, preventing failure from differential expansion between tubes and shell.

Steam dumping system:

Capable of desuperheating, condensing, and subcooling 110,000 lb/hr of steam at 800 psig and 825°F (15 per cent reactor power); provides means of conserving feed water while dissipating reactor power when a turbine outage occurs during periods of low power testing, during hot transfer to the fossil-fired boiler, or for dissipating reactor heat following a shutdown.

Emergency feed-water system:

Emergency feed-water system provides a means of supplying feed water to the steam generators, in the event of outage of the main feed-water pumps or loss of plant power. Emergency feed water is supplied from the condensate storage tank through the deaerator to the steam generators until the shutdown heat generated can be dissipated.

Steam generators (Figs. VII-6 and VII-7):

Each steam generator consists of an evaporator and superheater of shell-and-tube design and a moisture eliminator; duplex bayonet heat-transfer tubes are utilized in the evaporator and superheater to form a double-walled barrier for separation of sodium and water. The duplex construction of the bayonet tubes is accomplished by roller-expanding the inner tube tightly against the outer tube. The outer surfaces of the inner tubes are grooved axially (Fig. VII-7). The grooves terminate in the space between the caps at one end of the tube and in the space between

tube sheets at the other end, thus providing the third-fluid monitoring chamber. The core tubes that direct the flow of sodium in the duplex tube are also double-walled tubes with the annular space between tubes filled with an inert gas and sealed to reduce heat transfer in the radial direction. Helium space between the grooved inner tube and outer tube serves as an intermediate chamber for the leak-detection system; evaporator is kettle design with water level slightly above the uppermost tube. The first stage of steam separation occurs in the shell, thus eliminating a steam drum; a moisture eliminator scrubs the remaining moisture from the steam. The superheater construction is similar to the evaporator but uses orifice baffles on the shell side to improve heat-transfer rates to the steam.

Evaporator portion of steam generator:

Duplex tubes	$2\frac{1}{4}$% Cr – 1% Mo steel
Core tubes	Type 304 stainless steel
Core tube bellows	Type 321 stainless steel
Sodium tube sheet	$2\frac{1}{4}$% Cr – 1% Mo steel
Steam tube sheet	$2\frac{1}{4}$% Cr – 1% Mo steel
Shell, water end	ASME-SA-212 grade B
Shell, sodium end	$2\frac{1}{4}$% Cr – 1% Mo steel

Superheater portion of steam generator:

Duplex tubes	5% Cr – $\frac{1}{2}$% Mo steel
Core tubes	Type 304 stainless steel
Core tube bellows	Type 321 stainless steel
Sodium tube sheet	5% Cr – $\frac{1}{2}$% Mo steel
Steam tube sheet	$2\frac{1}{4}$% Cr – 1% Mo steel
Shell, steam end	$2\frac{1}{4}$% Cr – 1% Mo steel
Shell, sodium end	5% Cr – $\frac{1}{2}$% Mo steel

Sodium Service System

Equipment for filling, draining, and flushing of the sodium heat-transfer loops and the purification of the sodium system consists of the sodium melt stations, primary and secondary fill tanks, electromagnetic fill and service pumps, plugging meter and cold-trap equipment for sodium purification, and carbon (hot) trap with sodium sampler. All sodium piping and equipment can be electrically preheated to 350°F.

Filling

Two sodium melt stations are provided for system filling. One station is for tank-car quantities and is used during initial filling; the other is for small quantities (110 gal) and is used for system makeup. Sodium from the melt stations is transferred by the electromagnetic fill pump, through filters, to either the primary or secondary fill tanks. Filling of the reactor
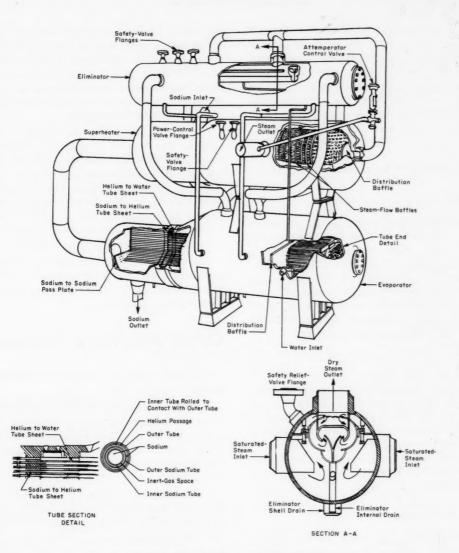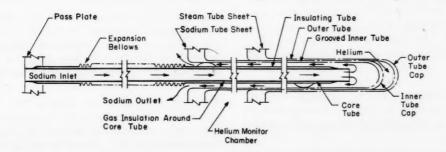
Fig. VII-6   HNPF steam generator.[1]

Fig. VII-7   Bayonet tube of the HNPF steam generator.[1]

vessel and the primary loops is accomplished by gravity flow and by the primary service pumps from five primary fill tanks located in a shielded cell. The secondary loops are filled by using the electromagnetic secondary service pump or by pressurizing the secondary fill tanks. Cover gas (helium) is maintained over all free surfaces. The high points in the primary loop and cold-trap piping are vented through freeze traps to prevent liquid sodium from entering the vent and helium systems.

Draining

The sodium in the reactor vessel and in the primary loops can be drained to the primary fill tanks by using either of the primary service pumps. The primary loops can be drained either simultaneously or separately. The secondary loops can be drained to the secondary fill tanks by using the secondary service pump. Each secondary loop is equipped with a radiation monitor that actuates an alarm circuit.

Flushing

Radioactive contaminants can be flushed from the primary loop so that an equipment cell can be entered. The flushing operation consists of alternately filling the loop with nonradioactive sodium and draining it to one of the other primary fill tanks. This can be accomplished several times with the amount of sodium stored in one fill tank.

Sodium Purification

The purification equipment in the sodium service system consists of two primary and one secondary circulating type cold-trap and plugging-meter assemblies and a primary circulating type carbon trap with a sodium sampler. Normally, cold- or carbon-trapping of sodium from the fill tanks is done only prior to filling the system. The function of the cold trap is to remove sodium oxides from the sodium and thereby prevent possible formation of plugs of sodium oxide in piping, fuel channels, orifices, etc. This is accomplished by cooling the sodium to a temperature at which the oxide precipitates and then passing the sodium through a wire-mesh filter.

The plugging meters are provided to indicate the oxide concentration. As the temperature of

the sodium flowing through the orifice is slowly decreased, a point will be reached where the oxide precipitates and begins to plug the orifice, thus causing a sudden reduction in flow. The oxide concentration is determined by a temperature and flow valve comparison with sodium oxide saturation temperatures.

The carbon trap removes carbon from the sodium. The sodium is heated to 1200°F and passed across stainless-steel foil in the carbon trap. At this elevated temperature the carbon migrates from the sodium into the stainless steel, thus carburizing the foil and removing the carbon from solution. The removal of carbon from the sodium reduces possible carburization and embrittlement of the fuel cladding.

The sodium sampler, located on the inlet to the carbon trap, provides a means of removing small quantities of sodium from the system for carburization analysis.

Other Auxiliary Systems

The other auxiliary systems include the following:

1. The cooling-water systems. These are for those miscellaneous cooling functions where water can be used. Two systems are used; one is for regions where radioactive contamination may occur, and the other is for regions where it is unlikely.

2. The helium system. This serves as an inert-gas atmosphere for the reactor, piping, and other metal surfaces in contact with sodium.

3. The nitrogen system. This provides an inert-gas atmosphere for the pipe and heat-exchanger cells and for cooling the primary cold-trap and plugging-meter assemblies and the freeze seals of valves.

4. The shield cooling system. The main biological shield is cooled by water, in cooling coils attached to the outside of the reactor cavity liner; the loading-face shield is cooled by a nitrogen system that rejects its heat in water-cooled exchangers.

5. The instrument air supply. The air is filtered and dried at 100 psi and is for pneumatic instruments and controls and for the pneumatic transmission of data. It is also used for emergency operation of the main sodium valves, which are normally operated by service air.
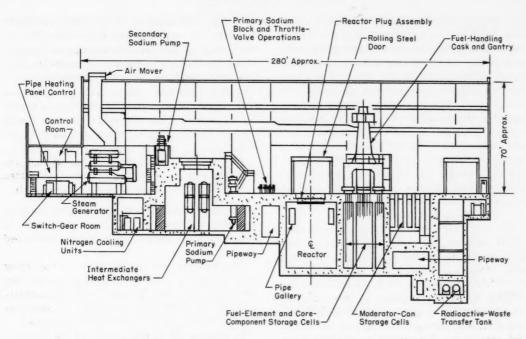
Fig. VII-8 Vertical section through the HNPF reactor building.[1]

Reactor Plant Building and Facilities

The reactor building houses the reactor, the heat-transfer system, the reactor service systems and equipment, and miscellaneous maintenance and service areas (see Fig. VII-8). The conventional plant turbine room and fossil-fired steam-generating equipment are located in adjacent buildings.

Reactor building construction	Steel frame covered with insulated steel roof decking and insulated steel wall panels
Dimensions	278 ft long, 80 ft wide, 75 ft high (high bay)
Design inleakage rate	3120 cfm at $\frac{1}{8}$ in. H_2O internal pressure
Access	Conventional personnel and cargo doors with weather-strip seals to minimize leakage; no windows. Railroad spur at cargo door of high bay
Overhead cranes	60-ton (high bay) and 25-ton (low bay)
Fuel-handling machine	Gantry mounted, operating between reactor and fuel cleaning and storage area
Maintenance cell	For disassembly, reassembly, and packaging for shipment of radioactive components
Control room	Common to both the conventional and reactor plants
Building ventilation	Serves general heating and ventilation requirements but maintains a negative pressure to promote inleakage of outside air. All building exhaust air from potentially radioactive areas is routed through filter systems to exhaust stack

Fuel- and Component-Handling Facilities

The fuel-handling machine consists of a tapered shielded cylinder about 50 ft high with

two internal hoists and grapple mechanisms to raise and lower core components, a gas lock to prevent the escape of any radioactive gases to the high-bay area, and an indexing device for proper positioning of the fuel-handling machine over the reactor core and storage cells. The machine and its operators' control panel are supported and transported by a trolley that rides on a gantry crane. A movable lead-shot-filled skirt, which can be raised and lowered by four hydraulic cylinders, provides shielding whenever an element is entering or leaving the machine. The handling-machine shielding is designed to limit radiation to the operator to 7.5 mr/hr during fuel transfer.

Internally there are two grapples, each suspended between two continuous roller chains. Each grapple is capable of picking up fuel elements when it is rotated into the pickup position directly above the port in the bottom of the machine. When the machine is traveling, the fuel element is carried in the position 180° away from the pickup position, and the empty grapple is kept in "traveling" position above the port at the bottom of the machine. Thus only one element can be in the machine while it is moving. The grapples are operated in two parallel guide tubes that run the full height of the machine. A variable-speed electric motor supplies power to each of the two hoist mechanisms. The grapple fingers are air operated. At the bottom of the machine are located the gas lock for sealing at the reactor face, a helium blower for fuel-element cooling, a photoelectric cell to monitor the grapple load, a gate valve for sealing the chamber, and three television cameras for remote viewing. The fuel element is cooled by the circulating helium, which transfers the heat to the walls of the machine where it is picked up by water circulating in cooling coils.

Before fuel-handling operations can proceed, the reactor must be shut down and the control-rod support structure, with the drive mechanisms, must be removed from the loading face. The fuel-handling machine must contain an atmosphere of helium and must have a fuel-storage-cell plug in the fuel-travel position. The sequence is as follows:

1. The fuel-element shield plug is uncovered, and the pickup cup is installed.

2. The handling machine is located over the element position of the loading face.

3. The gas lock is lowered and purged with helium, and then the movable shield is lowered.

4. The fuel element is grappled, raised to the full "up" position, and then rotated 180° to the traveling position. The storage-cell plug is above the empty core position. The shield plug is lowered to seal the loading-face opening.

5. The movable shield and gas lock are raised, and the fuel-handling machine is moved to the storage cell. The fuel element is cooled by the helium blower while in transit to the cell.

6. The storage-cell plug is withdrawn into the handling machine; then the fuel element is rotated into position and lowered into the storage cell.

A fresh fuel element in the handling machine may be exchanged with an exposed element in the reactor by steps similar to those described above.

The machine may also be used for transferring control rods, control-rod thimbles, dummy fuel elements, and other in-core items. By installation of a conversion assembly, it becomes capable of handling the moderator elements.

In addition to storage cells for the fuel elements, cleaning cells are also provided in the concrete substructure of the reactor building. These cells are essentially cylindrical steel-lined wells, about 40 ft deep, provided with steam, water, nitrogen, helium, vacuum, and vent services. Steam is usually used for fuel-element cleaning.

Reactor Instrumentation and Control

Nine channels of nuclear instrumentation are used to monitor neutron flux and to generate power and period signals for the plant control and protection system. Three channels of movable in-core nuclear instrumentation are used for flux monitoring during core loading and for flux mapping at low power.

Two source-range channels (BF_3 chambers) indicate and record reactor power level from about 6×10^{-9} to 6×10^{-4} per cent rated power. They provide the nuclear signal for the startup interlock of the protection system. The chambers are movable within their instrument thimbles and will be withdrawn at high power levels to avoid damage by high neutron flux.

Two channels (compensated ionization chambers) provide neutron-flux-level signals in the

intermediate range from about 6×10^{-5} per cent to 10 per cent power.

Three channels (uncompensated ionization chambers) are used with the power-range protective system. The outputs of these channels feed directly into the plant protective system, where they are used in the power flow circuit to provide alarm, setback, and scram action.

Two channels (uncompensated ionization chambers) are provided for the plant control system. Signals from these are either auctioneered or averaged for use in the flux control subsystem.

All nine chambers are located in sealed thimbles which extend from the reactor room floor downward to a position outside the cavity liner near the mid-height of the reactor core.

The sodium systems are provided with instrumentation to measure flow rates, liquid levels, sodium leaks, pressures, and temperatures. All instrument parts exposed to sodium are fabricated from stainless steel and are of all-welded construction.

Sodium flow rates are measured by permanent-magnet flowmeters. The sodium-level-measuring instrumentation consists of a continuous-reading, induction-coil level gauge and/or one or more induction-coil alarm points for each tank or vessel. Sodium leak detectors are located in the cells of the primary loops on piping, valves, pumps, and other components where leakage might occur or be readily detected.

The sodium-pressure instrumentation consists of NaK-filled diaphragm sensing elements, capillary tubes, transmitters, relays, and receivers.

Reactor-core thermocouples are located as follows:

Assembly	Number of thermocouples
Fuel-element sodium flow outlet (all)	2
Source element (1)	16
Instrument moderator can (1)	16
Temperature elements (3)	16
Instrumented fuel elements (2)	18
Instrumented control rod	16

The sodium temperature at the outlet of each fuel channel in the reactor core is monitored by the reactor fuel-channel-outlet temperature scanner which consists of two 192-point multibank recorders scanning the same set of thermocouples, 96 points apart. Each channel point is monitored once every 6.4 min. Identification and alarm lights are displayed in the core pattern on the control board.

References

1. Atomics International, Final Summary Safeguards Report for the Hallam Nuclear Power Facility, USAEC Report NAA-SR-5700, Apr. 15, 1961.
2. Atomics International, Revision for Section 5 of Final Summary Safeguards Report for the Hallam Nuclear Power Facility, September 1961.
3. Atomics International, Safeguards Report on Dry, Zero-Power Experiments in HNPF, USAEC Report NAA-SR-5700(Suppl. 1), Sept. 22, 1961.
4. Atomics International, Additional Information on Dry, Zero-Power Experiments in HNPF, USAEC Report NAA-SR-5700(Suppl. 2), September 1961.
5. Atomics International, Additional Safeguards Information for Hallam Nuclear Power Facility, USAEC Report NAA-SR-5700(Suppl. 3), November 1961.
6. Atomics International, Additional Safeguards Information for Hallam Nuclear Power Facility, USAEC Report NAA-SR-5700(Suppl. 4), Dec. 1, 1961.

Organic-Cooled Reactors

Coolant Radiolysis

The problems associated with the decomposition of organic liquids when they are used as reactor coolants or moderators have been discussed frequently in *Power Reactor Technology*, the most recent article having appeared in the September 1961 issue of *Power Reactor Technology*, Vol. 4, No. 4. Discussions on this subject have appeared in two British publications.[1,2] Reference 1 is a survey of the unclassified information that was available up to July 1959 on organic liquids as reactor coolants. It is primarily a compilation and review of previously published information, including much U. S. information, but it does contain some previously unpublished data. The appropriate organics are covered with respect to physical properties, heat-transfer performance, compatibility characteristics, radiation stability, cleanup and disposal, and operating experience. The discussion here will cover only the subject of radiation damage.

An essential point made in reference 1 is that the *G* value* of the organics for neutrons is higher than that for fast electrons. In estimating radiation damage, workers in this country (according to reference 1) have assumed this not to be the case, although the possibility has always been recognized.

The Santowax R loop data taken in the Materials Testing Reactor (MTR) at high-boiler (HB) contents from about 3 to 23 per cent, and at temperatures from 550 to 700°F, give *G*

*The *G* value is the number of molecules affected by the radiation per 100 ev of radiation energy absorbed by the organic. Appropriate *G* values may be used to designate the amount of organic damaged or to designate the amount of product formed.

values ranging* from 0.22 to 0.26 molecule destroyed per 100 ev of total absorbed energy. The corresponding value for fast electrons is 0.14, and this difference is interpreted in reference 1 as support for the statement that neutrons "do more damage" than other kinds of radiation. The assumption made in reference 1 is that the effects of neutrons and gammas are additive, i.e.,

$$G = G_n f_n + G_\gamma f_\gamma$$

where G is the over-all value for the radiation-damage parameter, and G_n and G_γ refer to the mean neutron and mean gamma values, respectively. The terms f_n and f_γ represent the fractions of energy deposited by the neutrons and gammas, respectively.

Evidently, if the total G is known for a particular reactor and if G_γ is taken to be a known value, independent of the characteristics of a specific reactor, then G_n can be derived for the reactor in question. In reference 1 this type of estimate is given for BEPO, in which some of the British decomposition tests have been made, and for the Organic-Moderated Reactor Experiment (OMRE). When a G_γ value of 0.19 was used, G_n values of 0.47 and 0.73 were calculated for OMRE and BEPO, respectively. The difference between these G_n values is stated to be caused by neutron-spectrum differences, the OMRE having a harder spectrum than that present in the BEPO experimental holes. In support of the above results, experimental work with alpha particles, recoil lithium atoms, and protons indicates that the G values increase as the initial energy of the particle decreases. With

*This value includes both pyrolytic and radiolytic damage, but the former is negligible at temperatures below 800°F.

Table VIII-1   AMOUNT OF MATERIAL DESTROYED AND CONTRIBUTION TO POWER COST IN A REACTOR,[1]
BASED ON INITIAL *G* VALUES,* FOR SANTOWAX R AT 300°C

	10% of total reactor energy deposited in coolant	7.5% of total reactor energy deposited in coolant	5.0% of total reactor energy deposited in coolant	3.5% of total reactor energy deposited in coolant
BEPO Data ($G_\gamma = 0.19$; $G_n = 0.73$)				
Molecules destroyed per 10^4 ev of total reactor energy:				
From gammas	1.43	0.95	0.48	0.19
From neutrons	1.83	1.83	1.83	1.83
Total	3.26	2.78	2.31	2.02
Pounds of weight destroyed/Mwd(t)	148	126	105	91.6
Metric tons/100 Mwd(t)	6.7	5.7	4.75	4.15
Cost in mills/kw-hr(e)† (at \$0.21/lb and 25% thermal efficiency)	5.1	4.4	3.6	3.2
OMRE Data ($G_\gamma = 0.19$; $G_n = 0.47$)				
Molecules destroyed per 10^4 ev of total reactor energy:				
From gammas	1.43	0.95	0.48	0.19
From neutrons	1.18	1.18	1.18	1.18
Total	2.61	2.13	1.66	1.37
Pounds of weight destroyed/Mwd(t)	118	96.6	75.0	62.0
Metric tons/100 Mwd(t)	5.36	4.38	3.40	2.82
Cost in mills/kw-hr(e)† (at \$0.21/lb and 25% thermal efficiency)	4.2	3.4	2.7	2.2

G value means number of molecules destroyed per 100 ev of absorbed energy. Subscript refers to type of radiation.

†Costs are converted from values in pence/kw-hr which are given in the original (reference 1) table.

these values of G_n, the coolant damage rates for various assumed fractions of gamma-energy deposition were calculated for reactors having neutron-energy spectra that are similar to those in BEPO and OMRE. This is shown in Table VIII-1. For operation at an HB content of 30 per cent, as is usual for an organic-cooled and -moderated reactor, the reference recommends that the coolant replacement rates shown in Table VIII-1 be cut in half; these revised damage rates are shown in Fig. VIII-1.

Comments from reference 1 on the performance of the OMRE coolant are as follows:

Some part of the good performance of the coolant in OMRE may be due to loss of neutron kinetic-energy by inelastic scattering in uranium and other core metals. This energy would be thereby converted into the less damaging gamma radiation. The available information on inelastic scattering is inadequate for assessment of the magnitude of the resultant improvement. The matter deserves serious study in appropriate quarters.

Detailed energy-deposition and radiation-damage calculations for organic-cooled reactors are given in reference 2. The energy deposited by neutrons, by gamma radiation, and by beta particles is analytically derived, and use of the formulas is illustrated by calculations of the organic replacement rate for three reactors:

Case I, the O.M.R.E. ... The fuel is fully enriched UO_2 in the form of fuel plates consisting of a 20-mil-thick central matrix of UO_2 and stainless steel, clad on each side with 5 mils of stainless steel. The plates are separated by a 134-mil coolant gap. Each element is assembled from 16 fuel plates, 2 inactive end plates, and 2 side closure plates so as to form a rectangular box 2.8×2.9 in. in cross section. The active dimensions of the fuel plates are 36 by 2.5 in. The plates are supported by end boxes which are positioned in a $4\frac{1}{2}$-in.-square lattice. There are 31 active fuel elements, with a total U^{235} content of 25.5 kg, and 5 dummy elements. The active region of the core is cylindrical with diameter and height of roughly 34 in. and 37 in., respec-
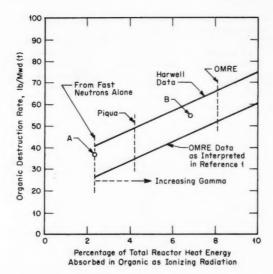
Fig. VIII-1 Estimates for coolant replacement rate due to radiolytic damage in an organic-cooled and -moderated reactor.[1] Bulk c o o l a n t temperature = 572°F. HB concentration = 30 per cent. All kinetic energy of fission neutrons transferred to moderator (2.5 per cent of total heat output). (*A*), case II reactor, reference 2. (*B*), case I reactor, reference 2.

tively. Further details can be obtained from the references.

Case II, a design of an organic cooled and moderated reactor, using $4C_0$ UO_2 fuel[*] in the form of rods of diameter 0.4 in., assembled into bundles of 19 rods. The rods are canned in stainless steel of thickness 0.010 in., with a minimum clearance between the cans of 0.060 in. The volume between the rods is filled with organic liquid, and the assembly of 19 rods with coolant is contained within a hexagonal, coolant channel box of wall thickness 0.040 in. The distance across the flats of a coolant channel box is 2.2 in. The bundles are separated by organic liquid. The height of the active region of the core is roughly 4.5 ft, and the diameter is 4.4 ft.

Case III, a design of graphite-moderated and organic-cooled reactor, with the same details of bundle design as for case II. In this case the coolant channel boxes are separated by graphite on a pitch of 6.5 in. The effective height and diameter of the active region of the core are both roughly 7.9 ft.

The results of the energy-deposition calculations for case I (OMRE) are illustrated in

---

*$4C_0$ refers to fuel having four times the natural U^{235} content, i.e., $4C_0$ corresponds to 2.87 per cent enrichment. — *The Editor*

Table VIII-2, and a summary for the other two cases is given in Table VIII-3. The calculations include the effect of inelastic scattering, although the reference states that "unfortunately the current state of information on the inelastic scattering process does not allow more than an approximate estimate to be made of the value $\overline{\sigma \Delta E_i^{in}}$."*

The results were used in conjunction with the reported decomposition rates in OMRE to derive values of G and G_n for that reactor. The resulting value of G was 0.18. To deduce the value of G_n, it was necessary to know the values of G_β and G_γ. These were assumed to be identical (as is confirmed by experiment) and were taken as 0.083, a value derived from beta and gamma irradiation experiments. The resulting value for G_n was 0.37.

Note that the values given above are intended to apply to the OMRE coolant when it contains 30 per cent high-boiler residue (HBR). This accounts for most of the difference between these results and those previously cited from reference 1, which were for fresh coolant. However, there is also a difference in the basis of the total G values, that of reference 1 being, evidently, an Atomics International value based on a higher estimate of the total energy deposition in the organic. If the G values were computed on a consistent energy-deposition basis, the difference between the values for fresh organic (reference 1) and organic with 30 per cent HBR (reference 2) would become larger. The important quantities given in the two references are as follows:

	Reference 1	Reference 2
Total energy deposition, Mev/fission		13.1
$f_{(\gamma+\beta)}$	0.70	0.66
f_n	0.30	0.34
$G_{\gamma,\beta}$	0.14	0.083
G_n	0.47	0.37
G	0.24	0.18

These differences are reflected in Fig. VIII-1, where the results of the reference 2 calculations for case I and case II are spotted on the

---

*$\overline{\sigma \Delta E_i^{in}}$ is the product of the inelastic scattering cross section and the energy lost in such a collision, averaged over all possible excitation levels for the ith nuclear species.

Table VIII-2   BREAKDOWN OF THE RATE OF ENERGY DEPOSITION IN OMRE[2]

Source of energy	Location of organic liquid	Rate of energy deposition, Mev/fission
Fission neutrons	Moderator and coolant	3.9
	Reflector	0.5
	Entire organic liquid	4.4
Prompt fission, fission-product decay gammas, and radiative capture in core	Moderator, coolant, and reflector	6.9
Radiative capture in reflector (including plenums)	Entire organic liquid	0.58
Radiative capture in thermal shield and reactor tank wall	Entire organic liquid	0.06
Inelastic scattering of fast neutrons	Entire organic liquid	0.14
All gamma sources	Entire organic liquid	7.7
All beta sources	Entire organic liquid	1.0

Table VIII-3   SUMMARY OF RESULTS OF THE CALCULATED ENERGY DEPOSITION RATES IN ORGANIC LIQUID[2]

Source of energy	Energy deposited, Mev/fission		
	Case I	Case II	Case III
Neutrons	4.4	3.7	0.8
Gamma radiation	7.7	1.4	0.8
Beta particles	1.0	0.05	0.05
Total	13.1	5.15	1.65

Table VIII-4   VALUES OF THE ORGANIC DECOMPOSITION RATE[2]

Radiation causing decomposition	Decomposition rate, lb/Mwd		
	Case I	Case II	Case III
Neutron	37	32	7.0
Beta + gamma	16	3	1.7
Total	53	35	8.7

curves from reference 1. Thus the case I point, which applies to the OMRE, falls to the left of the OMRE energy-deposition line, and the case II point happens to fall on the "neutrons only" energy-deposition line, even though fast neutrons actually deposited only 72 per cent of the energy (Table VIII-3).

If it is assumed that the G_n value for OMRE is typical of that to be expected in the other two reactor types investigated, then it is possible to compute, from the energy-deposition breakdowns (Table VIII-3), the decomposition rate in each reactor type. The results of such a computation are given in Table VIII-4.

These British reports focus attention on the importance of examining closely the modes of energy deposition in the organic, both for interpreting the results of irradiation experiments and for applying them to the prediction of decomposition rates in other reactors. As an immediate consequence of this approach, they infer somewhat higher total G values from the OMRE results than previous analyses had indicated.

A recent Atomics International report[3] treats organic-coolant decomposition rates and makeup costs for organic-moderated and -cooled reactors. This reference updates developments in the field since about 1959 and reports on recent experimental work designed to measure organic-coolant decomposition rates under a variety of conditions. This recent work includes capsule irradiations at the Curtiss-Wright Research Reactor (CWRR) and the Oak Ridge Graphite Reactor (OGR), work done at Harwell in BEPO, operation of the OMRE, and a series of irradiations with Po^{210} alpha particles. In addition, analytical energy-absorption calculations have been performed for several different organic-cooled and -moderated reactors. These reactors are summarized in Table VIII-5.

Figure VIII-2 summarizes the results of the various experimental programs. Values for G_e are given in Fig. VIII-3, and the ratio G_n/G_γ is illustrated in Fig. VIII-4. The reference states that the equivalence of G_e and G_γ has been demonstrated experimentally. As is evident from Fig. VIII-4, the two types of experiments give markedly different results for the effect of temperature on the G ratio. It is to be noted that the curve based on in-pile experimental data was drawn through a series of points, each of which was obtained in a different reactor, under different conditions, and using a different calorimetry technique. It is therefore subject to fairly large uncertainties. The reference discusses this point quite thoroughly; it concludes by using both of the curves in Fig. VIII-4 to compute coolant makeup costs. Table VIII-6 shows the power absorbed in the coolant moderator, and Table VIII-7 is a summary of the coolant makeup costs for several of the reactors.

The makeup rates shown in Table VIII-7 do not differ greatly from an earlier estimate, 27 lb/Mwd(t), quoted in the Proceedings of the Organic Cooled Reactor Forum[4] (reviewed in the September 1961 issue of *Power Reactor Technology*, Vol. 4, No. 4, page 77), despite the fact that the earlier estimate was based on the assumption of equal damage per unit of energy absorbed from various types of ionizing radiation. This should not be interpreted to imply that the G_n/G_γ ratio is unimportant; it apparently comes about because of a compensating change in the estimate of the effect of inelastic scattering of neutrons. Reference 5 points out the importance of accuracy in assessing the inelastic scattering and the modes of energy deposit in the organic, as well as in establishing the G values, and concludes that more thorough investigation is in order.

Auxiliary Systems

The importance of controlling the particulate-matter concentration in organic-reactor coolant loops has been demonstrated by the experience with fouling in the OMRE. Reference 6 is a report on the design and construction of the new OMRE particulate-removal loop. The following

Table VIII-5   REACTOR DESIGN PARAMETERS[3]

	POPR*	PNPF†	150-Mw(e) OMR	300-Mw(e) OMR	OMRE
Thermal power, Mw	160	45.5	475	891	6
Electric power, Mw (net)	51.3	11.4	159	312	
Core inlet temp., °F	644	519	572	604	600
Core outlet temp., °F	700	575	622	700	609
Total circulating coolant volume, gal	45,000	13,300	125,250	102,300	6,000
Type of fuel element	UO_2, cylindrical rods	U–3.5 wt.% Mo–0.1 wt.% Al, concentric tubes	U–10 Mo, plates	UO_2, cylindrical rods	UO_2 (25 wt.%) + S.S. (75 wt.%), plates
Fuel-element cladding	Finned APM	Finned Al	Finned Al	Finned APM	Flat S.S.
Core geometry:					
Radius, cm	68.5	74	134	Not available	35.9
Height, cm	244	137	305	Not available	91.5
Core composition, atom density, atoms/cm^3 ($\times10^{24}$):					
Hydrogen	0.01599	0.0231	0.0182	0.01599	0.02992
Carbon	0.02087	0.0302	0.0238	0.02087	0.03906
Oxygen	0.00939			0.00939	0.00038
Aluminum	0.0182	0.00723	0.01513	0.0182	
Iron	0.000194	0.00085	0.00429	0.000194	0.00673
Molybdenum		0.000661	0.00154		
Uranium	0.004698	0.00738	0.00553	0.004698	0.00190
Weight fraction organic	0.133	0.149	0.125	0.133	0.539
Organic volume/fuel volume	2.69	3.95	3.87	2.69	11.1

*Prototype Organic Power Reactor.
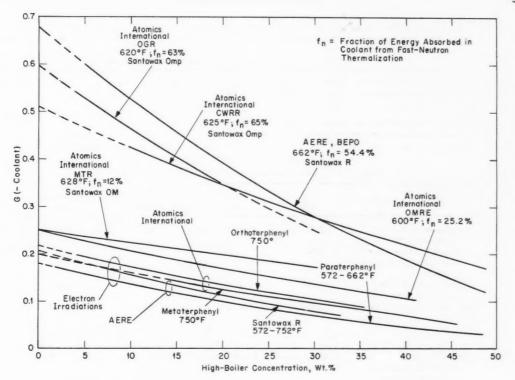†Piqua Nuclear Power Facility.

Fig. VIII-2   Decomposition rate of terphenyls: summary of experimental results.[3]
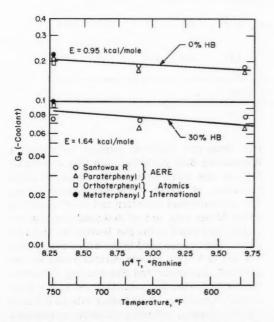

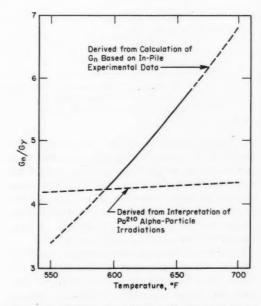Fig. VIII-3   Effect of temperature on electron radiolysis of terphenyls.[3]

Fig. VIII-4   Effect of temperature on the relation between G_n (−coolant) and G_γ (−coolant) at 30 per cent HB.[3]

Table VIII-6   PER CENT OF TOTAL POWER ABSORBED BY COOLANT MODERATOR[3]

Radiation type	OMRE	PNPF	POPR	150 Mw(e)	300 Mw(e)
Neutron	2.28	1.72	1.50	1.58	1.50
Gamma	6.04	1.22	1.26	1.12	1.26
Beta	0.72	—	—	—	—
Total	9.04	2.94	2.76	2.70	2.76

Table VIII-7   OMR COOLANT MAKEUP RATES AND COSTS[3]

	POPR		PNPF		150-Mw(e) OMR		300-Mw(e) OMR	
Average in-core temperature, °F	672		547		597		653	
Per cent of total reactor fission energy absorbed in coolant	2.76		2.94		2.70		2.76	
f_m, fraction of absorbed energy due to neutrons	0.543		0.585		0.585		0.543	
G_γ (−coolant), at 30% HB	0.0796		0.0677		0.725		0.0778	
	A*	B†	A	B	A	B	A	B
G_n (−coolant), at 30% Hb	0.480	0.346	0.226	0.285	0.312	0.310	0.431	0.337
Total G (coolant)	0.297	0.224	0.160	0.195	0.213	0.211	0.270	0.219
Radiolytic decomposition rate, lb/Mwd(t):								
From neutrons	32.9	21.0	17.8	22.4	22.5	22.4	29.6	23.1
From beta and gamma	4.6		3.8		3.7		4.5	
Total	37.5	25.6	21.6	26.2	26.3	26.1	34.0	27.6
Pyrolytic decomposition rate, lb/hr	0.3		0.00008		0.02		0.6	
Total decomposition rate, lb/hr at full power	250	171	40.9	49.7	520	517	1265	1024
Thermal efficiency, %	32.1		25		33.3		35	
Coolant makeup cost, mills/kw-hr(e)‡	0.83	0.56	0.61	0.74	0.56	0.56	0.69	0.56

*A: according to G_n values derived from in-pile experiments.
†B: according to G_n values derived from Po^{210} alpha irradiations.
‡Coolant cost assumed to be $0.17/lb.

coolant-processing systems were selected for inclusion in the loop: sintered media filtration, centrifugation, magnetic separation, cold trapping, glass cloth filtration, glass spool filtration, precoat filtration, and adsorption. The loop was constructed on a concrete slab adjacent to the OMRE facility buildings; no building or other shelter for the loop was constructed.

Reference 7 updates information on the Piqua reactor HB handling system. Previous information was reviewed briefly in the March 1961 issue of *Power Reactor Technology*, Vol. 4, No. 2, page 83. The HB was successfully burned[7] in the prototype of the HB combustion system to be employed at the Piqua OMR plant. The origi-

nal stack-gas filtering system employed a dacron-bag dust collector, and this was modified to use woven-glass filter bags, to allow operation at higher stack-gas temperatures. The primary dust collector had an efficiency of about 90 per cent, and no detectable particulate matter was found in the gas leaving the absolute filter. The burner used in the experiments with HB was a Vortex burner manufactured by the Thermal Research and Engineering Corporation. A Hydro burner, manufactured by the Utah Hydro Corporation, was tested with an HB substitute, Montar, and more complete combustion was achieved than with any other burner tested. The economics of the HB combustion process

are discussed, and a total annual cost of about $3800 is predicted to burn 216,000 lb of HB from the Piqua plant. At a plant factor of 0.80, this corresponds to an approximate cost of 0.05 mill/kw-hr.

References

1. K. Maddocks (Comp.), Organic Liquids as Reactor Coolants, Review of Technological Information Available July 1959, British Report AERE-R-3633, April 1961.
2. J. D. Jones, Energy Deposition and Radiation Damage in Organic Cooled Reactors, British Report AEEW-R-52, September 1960.
3. R. H. J. Gercke and J. F. Zack, Jr., Coolant Decomposition Rates and Make-up Costs for Organic Reactors, USAEC Report NAA-SR-6920, Atomics International (to be published).
4. R. H. J. Gercke, Status of Organic Coolant Technology, in Proceedings of the Organic Cooled Reactor Forum, October 6–7, 1960, USAEC Report NAA-SR-5688, Atomics International, December 1960.
5. Ad Hoc Committee of Argonne National Laboratory, Organic Nuclear Reactors: An Evaluation of Current Development Programs, USAEC Report ANL-6360, May 1961.
6. H. Cataldo, Design and Construction of the OMRE Particulate Removal Loop, USAEC Report NAA-SR-6646, Atomics International, Dec. 30, 1961.
7. R. R. Stiens, Disposal of OMR High Boiler by Combustion, USAEC Report NAA-SR-5410, Atomics International, Nov. 15, 1961.

Gas-Cooled Reactors

Thermal Behavior of EGCR Type Fuel Elements

Reference 1 describes an experimental apparatus at Oak Ridge National Laboratory to simulate the thermal conditions in single Experimental Gas-Cooled Reactor (EGCR) type fuel elements. The EGCR element is made up of cylindrical, hollow-core, UO_2 pellets jacketed in a thin-walled stainless-steel tube. In the reactor the fuel elements are assembled into seven-rod clusters, but the apparatus described in the reference is intended for investigation of the characteristics of single fuel elements.

The apparatus takes advantage of the hollow-core design of the fuel element to simulate electrically the in-pile heating. A single tantalum-rod heater element is located within the hollow core of an open-ended fuel-element rod. The jacket surface is cooled by a surrounding gas gap and an aluminum shell which in turn is cooled by flowing water. Maximum central UO_2 temperatures up to $3000-4000°F$, with cladding temperatures less than $1500°F$, can be obtained, and the effects of rapid heating and cooling rates can be investigated. Measurements of axial and radial growth, including relative growth between the fuel and cladding, can be made at operating temperatures by radiography and/or extensometers. Temperature measurements are made with thermocouples.

The apparatus has been utilized to study the dimensional behavior of the EGCR fuel element.[2] Particular emphasis was placed on determining the relation between the fuel temperature and axial expansion and on the radial expansion characteristics of the fuel, the interaction of fuel and cladding due to thermal cycling, the degradation of the UO_2 pellets due to temperature gradients and thermal cycling, and cumulative effects in the fuel element due to thermal cycling.

The investigation showed that the behavior depends on whether a radial gap exists between the cladding and the fuel pellets before and during operation. In fuel elements that have radial gaps between the cladding and the fuel pellets, the components responded in much the same way as if they were separately subjected to the same thermal conditions. Measurements on fuel elements having radial gaps showed that both the axial and radial thermal expansions of the fuel were very nearly functions of the inner surface temperature of the pellet rather than of a mean temperature. It was demonstrated that the axial expansion of the fuel-pellet column can be reduced appreciably by "dishing" either one or both ends of the pellets, but the report[2] concludes that the reduction is important only at the higher temperatures or when the radial thermal gradient becomes quite large.

When the cladding is collapsed onto the UO_2 pellets so that no radial gap exists, the pellets and the cladding may interact, to a degree depending on the pressure between the cladding and the pellets and on the temperatures involved. In such cases the thermal expansions are not singularly dependent on either the cladding temperature or the central temperature of the UO_2; instead, they are dependent on both of these and on the number of thermal cycles and other factors. Gaps may appear between pellets during thermal cycling, and circumferential ridges may form in the cladding at positions that correspond to interfaces between pellets and cracks in the pellets. These ridges are not large, generally being only about 1 to 3 mils in height; no test fuel element has been known to fail as a result of such ridging. Experimental measurements demonstrated that, if a high contact pressure exists between the collapsed cladding and the

fuel, axial extension of the fuel element will occur with thermal cycling, as a result of plastic strain of the cladding, and will increase as a linear function of the number of cycles. The magnitude of the plastic strain apparently depends on the upper and lower temperature limits of the thermal cycle, on the heating and cooling rates of the cycle, and particularly on the hold time at the high temperature. As a result of this axial extension of the fuel element, gaps grow between the fuel pellets with continued cycling, and openings as large as 0.040 in. have been observed.

The above results were obtained with flat-end pellets or with pellets that were dished a relatively small amount compared to the axial thermal expansion involved. The results of other investigators have indicated that axial distortion of the fuel element can be controlled by distributing the required axial clearance throughout the stack of UO_2 pellets by dishing the ends of the pellets to a depth of about 10 to 25 mils/in.

Compatibility of Ceramics with Gaseous Coolants

An evaluation of (1) the results of thermodynamic calculations and (2) information in the technical literature is given in reference 3 for the interaction between a selected group of gas coolants and a number of ceramic materials. The study is primarily intended as an aid to the development of high-temperature gas-cooled reactors utilizing ceramic or coated-particle nuclear fuels. Helium is the gaseous coolant generally favored for such an application because it is chemically inert. However, helium does have certain disadvantages, such as limited supply and high cost, and presents operating problems having to do with leakage and the maintenance of the extremely high purity required. Moreover, other coolants such as steam are of interest for direct-cycle use. This study considered the compatibility of helium, steam, air, nitrogen, CO_2, CO, and hydrogen coolants with UO_2, carbon, Al_2O_3, BeO, MgO, Nb_2O_5, SiC, ZrC, and ZrO_2. On the basis of the thermodynamic calculations performed, which were correlated where possible with experimental results reported in the literature, the study concluded that nitrogen is the gas coolant that appears to be compatible with the widest variety of ceramic

materials. It is the only coolant besides helium that appears to be useful in oxidizable systems containing graphite or carbides and in hybrid systems combining both oxides and graphite or carbides. Oxygen and air are compatible, even at very high temperatures, with all the oxide ceramics considered except UO_2. CO_2 is similarly inert toward the oxides. The effects of radiation on these systems are not well known. Radiation is prone to form metastable and reactive products in the gas phase which may increase attack on the ceramic structures. The course and extent of such reactions cannot be predicted theoretically and would require experimental study.

Peach Bottom Reactor

Reference 4 reports on a conference devoted exclusively to the High-Temperature Gas-Cooled Reactor (HTGR). The HTGR is being designed and constructed, as part of the Power Reactor Demonstration Program, under a cooperative agreement between AEC, Philadelphia Electric Company, and General Dynamics Corporation. General Atomic Division of the General Dynamics Corporation is the reactor designer. The plant is to be built at Peach Bottom, Pa., by Bechtel Corporation. The cost of design and construction of the plant is being shared by Philadelphia Electric and 51 other utilities comprising the High Temperature Reactor Development Associates, Inc. This plant was previously discussed briefly in the September 1960 issue of *Power Reactor Technology*, Vol. 3, No. 4, page 58. Additional data are given in reference 5.

The HTGR is fueled with approximately 150 kg of 93 per cent enriched uranium and about 8 to 10 times that much thorium fertile material, both in the form of dicarbides dispersed in a graphite matrix. The gas coolant is helium, which enters the reactor core at 660°F, and is heated to an average mixed temperature of 1380°F. The hot helium gas flows to two steam generators in independent loops where steam is produced at 1000°F and 1450 psi. A conventional steam generator produces 40 Mw(e) net from the 115-Mw(t) output of the reactor. Table IX-1 is a summary of the Peach Bottom Atomic Power Station characteristics, and Fig. IX-1 is the flow diagram for the plant.

The essential, characterizing, feature of the HTGR is its fuel element. It consists of a disper-

Table IX-1　SUMMARY OF HTGR ATOMIC POWER
STATION CHARACTERISTICS

Reactor data:

Thermal power, Mw	115
Helium pressure, psia	350
Helium inlet temp., °F	660
Helium outlet temp., °F	1380
Total helium flow at full power, lb/hr	~400,000
Active core height, ft	$7\frac{1}{2}$
Active core diameter, ft	9
No. of fuel elements	820
No. of control rods	37
Average power per fuel element, kw	150
Average power density in core, kw/liter	8
Average specific power in fuel, kw/kg U[235]	~800
Uranium to thorium atom ratio	1:8 to 1:10
Uranium inventory in core, kg	150
Initial conversion ratio	0.5
Maximum fuel temp., °F	3150
Average exposure of fuel, Mwd/ metric ton of uranium + thorium	70,000
Average life of core at 80% plant-load factor, months	36

Steam- and turbine-generator data:

Plant net electrical output, kw	40,000
Steam pressure at turbine throttle, psig	1450
Steam temperature at turbine throttle, °F	1000
Feed-water temperature at full power, °F	425
Steam flow at full power, lb/hr	398,000
Main generator output voltage	13.8 kv, 60 cps
Net plant heat rate, Btu/kw-hr	9800

sion of uranium and thorium dicarbides in graphite compacts that are contained in a can of low-permeability graphite about $\frac{1}{4}$ in. thick. These are located within a $3\frac{1}{2}$-in.-OD graphite sleeve, about $\frac{3}{8}$ in. thick, as shown in Fig. IX-2. This sleeve is also made of low-permeability graphite. Some 820 of these 12-ft-long fuel elements are arranged in a closely packed, equilateral triangular lattice to form the core, which is roughly a cylinder about $7\frac{1}{2}$ ft in diameter. The elements are supported by a core support plate within a pressure vessel, 14 ft in diameter by 35 ft high. Coolant-gas flow is upward in the spaces between the nearly touching cylindrical fuel elements. The resulting all-ceramic core operates at quite high temperatures, from which the carbon steel pressure vessel is protected by baffling the incoming coolant gas so that the vessel is exposed only to the inlet gas temperature of about 660°F.

The low-permeability graphite that encloses the fuel-bearing compact is the only barrier against the release of fission-product activity to the helium-gas coolant, but a scavenging gas flow is provided to enhance the effectiveness of the barrier. A small fraction, less than 1 per cent, of the helium-gas coolant flow passes inward through the graphite cladding as a result of a pressure differential, and this small amount of helium flows along the surface of the fuel compacts to sweep away any volatile fission products that escape from the compacts. These volatile fission products are carried by the helium purge stream to the lower, cooler end of the fuel element and through an internal fission-product trap. The internal trap consists of an adsorbent material, such as activated charcoal and silver, which is cooled by the incoming 660°F helium coolant gas. A large portion of the condensable fission products is expected to be taken up by this internal trap. The permanent gases and the remaining fraction of volatile elements such as iodine and bromine will then be collected by a header system and carried out of the reactor vessel by the helium purge stream to an external trapping system. The external trapping system will probably also consist of a series of adsorption beds that operate at successively lower temperatures. The condensables are thereby removed first, and the holdup period for xenon and krypton gases is sufficient for their activity to decay in the trapping system. The helium purge gas is then returned to the primary coolant system.

These measures are not expected to be completely effective in keeping radioactive fission products out of the primary coolant system; a circulating activity level of about 35 curies of total activity is anticipated. The specifications on the radioactivity of the primary circuit are that any gas which leaks out of the plant should not constitute a hazard either on or off site and that the radioactivity which plates out in the coolant system should be of low enough intensity to permit direct maintenance.

The secondary containment vessel, which is around the entire nuclear steam-supply system, is another barrier against the release of radioactivity. It is expected that there will be some helium and fission products leaking out of the primary coolant system into the containment vessel. These fission products will eventually be released to the atmosphere via the ventilating

stack, but the level of this activity is to be held well within the allowable limits.

Another method of alleviating the fission-product problem is being investigated in the HTGR project. This is a coating for the uranium dicarbide fuel particles, such as a thin layer of pyrolytically deposited carbon, to serve as a primary barrier against the release of fission products. This coating is not intended to retain the more volatile fission products permanently in the compact but is intended to delay their release so that some of the shorter-lived species
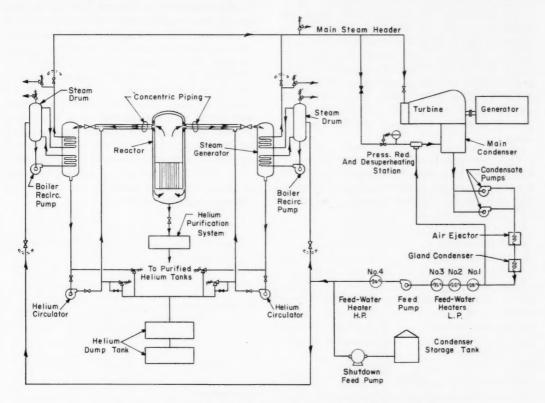
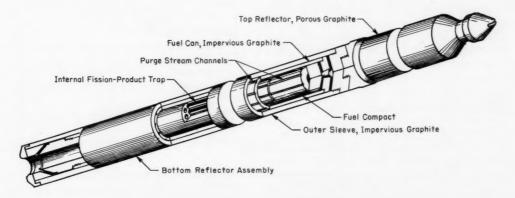Fig. IX-1   Flow diagram of the Peach Bottom Atomic Power Station.[5]

Fig. IX-2   Pictorial view of the HTGR fuel element.[5]

will decay in the fuel element. The total activity to be deposited in the internal and external adsorption systems could thereby be considerably reduced. Current reports on the development of such a fuel-particle coating appear to be favorable.

Approximately 37 control rods enter the HTGR core from the bottom of the reactor, as shown in Fig. IX-3. The neutron-absorbing portions of the control rods consist of compacts of boron carbide-loaded carbon attached to gas-cooled metal structural members that operate within graphite guide tubes. The control-rod drives, which are of the hydraulic type, are located below the biological shield in a subpile room.

Fuel handling is carried out only after the reactor has been shut down and cooled off and the primary system pressure has been reduced. The top of the reactor pressure vessel is penetrated by several components of the fuel-handling equipment as shown on Fig. IX-4. One such component is a transfer machine that is used to move fuel elements around within the reactor vessel. It consists of a radius arm that can reach any one of the core positions, pick up a fuel element by a suitable knob on the top of the element, and transfer it to a position from which it can be withdrawn from the vessel. Withdrawal is accomplished by a separate charge machine that is used to insert and remove fuel elements from the reactor pressure vessel. The spent fuel elements are then canned in a metal container by another separate machine and finally are transferred to a spent-fuel-element storage pit for cooling. Auxiliary fuel-handling equipment, which also operates through the top of the reactor pressure vessel, includes (1) a television machine for viewing the inside of the reactor after shutdown and (2) a failed-fuel-element locating machine.
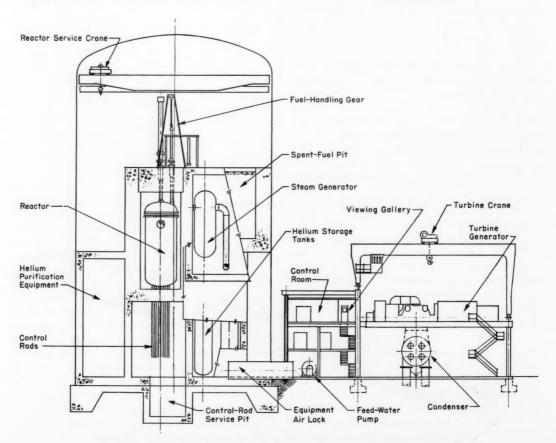
Fig. IX-3   Longitudinal section of the Peach Bottom Atomic Power Station.[5]

Supporting the HTGR design effort is a major research and development program. Areas receiving particular effort under this program are the proposed fuel-element materials, the in- and out-of-pile fission-product trap systems, the helium-coolant-gas purification system, the control rods and drives, and the fuel-handling equipment. General Atomic began operation of an HTGR critical experiment facility in July 1960.
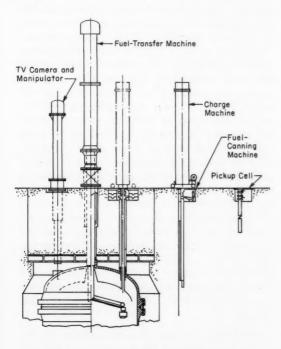

Fig. IX-4 HTGR fuel-handling system.[4]

The construction permit hearing was conducted in December 1961, and the construction permit was issued. Construction was expected to begin early in 1962; the earliest possible date for completion of construction was expected to be March 1964, and the earliest date for operation was expected to be June 1964.

Coolant-Temperature Measurement

The provision of coolant-temperature monitors for the individual fuel channels can contribute substantially to the maximum performance of a large gas-cooled reactor. Reference 6 is a discussion of a system which is being designed for the EGCR and which employs pneumatic temperature probes. These probes employ sonic flow through two nozzles in series and take advantage of the principle that the velocity of sound in a given gas is proportional to the square root of the absolute temperature. For two nozzles in series, the following relation holds if sonic flow occurs in both:

$$T_1 = K T_2 \ (A_1/A_2)^2 \ (P_1/P_2)^2$$

where A_1 = throat area of primary nozzle, sq ft
A_2 = throat area of secondary nozzle, sq ft
P_1 = absolute pressure upstream of primary nozzle, lb/sq ft
P_2 = absolute pressure upstream of secondary nozzle, lb/sq ft
T_1 = absolute temperature of gas upstream of primary nozzle, °R
T_2 = absolute temperature of gas upstream of secondary nozzle, °R
K = calibration constant

This relation holds even if heat is added to or taken from the gas in the region between the two nozzles. Consequently the second nozzle may be located at a convenient place and may handle relatively cool gas. The technique is to measure experimentally the pressure of the gas entering both nozzles and the temperature of the gas entering the second nozzle. In the EGCR each fuel channel is equipped at its exit with a length of $\frac{1}{2}$-in. tubing which incorporates the primary nozzle and which leads out through the pressure vessel and the biological shield, through a valve, to a manifold. The secondary nozzle is in the manifold line in an instrumentation room; thus one secondary nozzle is needed to monitor all the channels in sequence. After flowing through the second nozzle, the gas enters a surge tank and is pumped back into the main coolant system. The temperature of the gas entering the second nozzle in the instrumentation room is held to 100°F by suitable heat-exchange equipment. The pressure upstream of the primary nozzle is assumed to be that in the outlet plenum of the reactor and is measured by a single transducer located within the reactor vessel. The only other measurement required, therefore, is that of the pressure upstream of the secondary nozzle. The pneumatic temperature-monitoring (PTM) system design conditions are given in Table IX-2.

Table IX-2   EGCR PNEUMATIC TEMPERATURE
MONITORING SYSTEM DESIGN CONDITIONS[6]

Reactor coolant	Helium
Fuel-channel exit gas temperature range, °F	800–1200
Accuracy, °F	15
Minimum monitoring time per fuel channel, sec	8
Sample gas flow at a fuel-channel outlet gas temperature of 1050°F, lb/sec	0.006
Sample gas flow range between 800 and 1200°F, lb/sec	0.008–0.004
Reactor outlet plenum pressure, psia	303
Gas pressure upstream of secondary nozzle, psia	225
Surge tank pressure, psia	120
Compressor power required (PTM system only), hp	10

This system is of particular interest to the EGCR, as compared to the use of thermocouples, because it is integrated with the burst slug detection (BSD) system. The BSD system requires a gas sample from each fuel channel, and both operations are carried out simultaneously.

A more comprehensive discussion of the pneumatic temperature probe may be found in the September 1960 issue of *Nuclear Safety*, Vol. 2, No. 1.

Graphite Oxidation

Reference 7, an evaluation of chlorine as an inhibitor for graphite oxidation, cites runaway graphite oxidation as one of the most serious potential hazards of the gas-cooled graphite-moderated reactor. It visualizes as a possible accident a rupture of the primary coolant system during high-temperature operation. This would depressurize the reactor and displace the normal coolant by air; the combination of drastic reduction of cooling capacity and the presence of oxygen in the hot reactor might lead to runaway oxidation (combustion) of the graphite, with severe reactor damage and possibly widespread contamination.

The reference reports on a test program that investigated the effects of chlorine as an inhibitor of graphite oxidation. The test results show that chlorine apparently functions as a gas-phase inhibitor to retard oxidation by chemisorption on active carbon sites on the graphite surface. Chlorine was tested as an oxidation inhibitor in both the presence and absence of

ionizing radiation and with both dry and moist air. Tests were also conducted under combustion conditions to study the effect of chlorine on ignition temperatures and in extinguishing combustion of graphite.

The test results show that chlorine is apparently equally effective as an inhibitor of graphite oxidation, whether ionizing radiation is present or not. They also show that chlorine is not nearly so effective in moist air as it is in dry air. The minimum amount of chlorine that must be added to the oxidizing air flow, in order to approach saturation of the inhibiting effect, was shown to be a function of the temperature of the graphite and the moisture content of the air. For a practical application, it probably would be necessary to assume that the air would contain considerable moisture. For the typical conditions of 650°C graphite and moist air, the test results show that about 20 to 25 vol.% chlorine must be added to the air to reduce the oxidation rate by approximately a factor of 4. There is some question as to whether it would be practical to provide for such a large chlorine fraction in a large reactor installation. The results of the tests under combustion conditions did show, however, that a much smaller proportion of chlorine suffices to increase the ignition temperature of graphite or to extinguish established combustion. The addition of only 1 vol.% chlorine, for example, extinguished combustion of 1400°C graphite in a flow of pure oxygen.

The reference concludes that chlorine may be a potential safeguard for the prevention and control of runaway oxidation (combustion) in gas-cooled graphite-moderated reactors. Its effectiveness and low cost, and the relative simplicity of storage and application, would seem to make it particularly suitable for this function.

Reference 8, by the same author, is a report on a closely related subject—a program of tests on the oxidation of graphite under high-temperature reactor conditions by air and oxygen. The effects of environmental conditions, such as gamma radiation, neutron bombardment prior to oxidation exposure, prior oxidation, gas flow rate, the surface-to-volume ratio of the graphite, and impurities in the graphite, were investigated.

The results showed that, over the temperature range investigated (400 to 675°C) and at atmospheric pressure, graphite oxidation proceeds as

a near first-order reaction with respect to oxygen. The activation energy of the graphite tested was 50 ± 5 kcal/mole, but a wide difference in chemical reactivity between various nuclear-grade graphites was found. This was attributed to varying concentrations of impurities. Gamma radiation increased the oxidation rate significantly, at least up to the highest temperature (650°C) tested. The enhancement of the rate was observed to decrease with increasing temperature; at a temperature of about 600°C, an intensity of 1×10^6 r of Co^{60} gammas per hour increased the oxidation rate by about a factor of 3. Neutron bombardment of the graphite to an exposure of 4×10^{18} nvt ($E > 0.18$ Mev) at 550°C prior to oxidation had no discernible influence on oxidation rates.

Oxidation rates of preoxidized graphite exceeded those of unoxidized graphite. The rate of graphite burnoff increased steadily through about the first 1 per cent of burnoff at low temperatures and through about the first 10 per cent at 650°C or above. After this initial increase, the oxidation rate then generally stabilized over a wide burnoff range until the geometric area of the sample was substantially reduced. Increasing the flow rate of the oxidizing gas over the relatively low flow required to provide a stoichiometric oxygen concentration apparently had no effect on the oxidation rate. This would indicate that the mass transport of reacting gas and products through the relatively stagnant gas film at the surface of the graphite was not a determining factor in the rate of graphite oxidation. No changes in oxidation rates were observed with changes in the surface-to-volume ratio of the specimens used in these tests (surface/volume = 20 cm^{-1} to 8 cm^{-1}). This would indicate that the diffusion of reacting gas from the exterior surface to active sites beneath the surface, and of products in the opposite direction, also was not a determining factor under the conditions tested. The author injects a note of caution, however, that this would probably not be true for large graphite blocks such as those in an actual reactor application.

The effect of impurities on the rate of oxidation of reactor-grade graphites is also being investigated in Great Britain, and preliminary results of this investigation are reported in reference 9. This investigation also found that certain impurities greatly increase the rate of oxidation of graphite: especially copper, vana-

dium, and iron, and sodium when it is associated with vanadium. The rate of oxidation was found to be increased by factors of about 40, 28, 12, and 6 by concentrations of 10 ppm copper, vanadium, iron, or sodium, respectively. Magnesium, calcium, and titanium, however, had little effect on the oxidation rate. It was also found that the impurities in reactor-grade graphites tend to be concentrated into many small locations. These concentration sites are believed to be formed during the manufacture of the graphite and, specifically, at that phase in the process when it is heated to 2000°C. This localization of impurities can cause pitting of the graphite when it is oxidized.

Helium Purification

With the increasing interest in high-temperature gas-cooled reactors, a need is developing for efficient systems for removing contaminants from the coolant gas. In many cases the trace quantities of certain impurities may be corrosive to the moderator or the fuel elements, or they may be undesirable for other reasons. Further, if any fission products are released into the coolant system, an effective way of removing them is highly desirable. Most of the contaminant-removal systems available today introduce a high impedance to the flow of the gases and usually require that the gas be cooled well below the operating temperature in the primary coolant loop. Practical considerations, therefore, always require that only a small fraction of the total coolant flow be bypassed through the cleanup system, and the result is that the equilibrium contaminant concentration remains relatively high.

The removal of contaminants from helium gas is of particular interest because helium appears to be the only suitable gas for some of the higher-temperature applications and because the presence of significant quantities of contaminants may nullify the most important advantage of helium: its chemical inertness.

Reference 10 is a report on preliminary feasibility experiments on a technique of concentrating contaminants into a bypass stream, thereby reducing the equilibrium concentration in the primary coolant loop. The principle of operation is illustrated in Fig. IX-5. The coolant gas issuing from the reactor will be partially ionized because of its exposure to the reactor
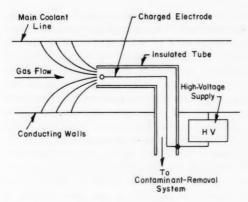
Fig. IX-5   Diagram of an electrostatic separation system.[10]

radiations. It is presumed that the fractional ionization of the impurities will be greater than that of the helium because the ionization potential of helium is higher than that of other atoms. The charged electrode, whose electrostatic field extends across the entire cross section of the coolant duct, is expected to collect ions from the entire duct; after the ions reach the electrode, they will be neutralized and will act as normal gas molecules, but they will not be able to return to the main coolant circuit if the gas velocity in the concentrator tube is substantially greater than the rate of diffusion of the neutralized atoms.

The experiments performed indicated that separation of contaminants from helium is possible by this technique. The experiments were, however, of a preliminary nature, and the author concludes that further experimentation is necessary to establish more accurately the attainable increase in contaminant concentration and to investigate whether the technique would be practical for reactor applications.

Internal Thermal Insulation

Reference 11 presents the results of a test program on the effectiveness of several gas-gap type thermal insulations intended particularly for use in gas-cooled-reactor coolant systems. The work is applicable to the internal insulation of coolant ducts, whether these ducts lie outside the reactor, or, as in the pressure-tube concept, form the coolant channels of the reactor itself. This type of insulation restricts

heat flow by enclosing gas in one or more narrow layers by thin metal barriers, thus simultaneously inhibiting convection heat flow and reducing radiation heat transfer by reflection from the thin metal barriers that divide the gas gaps. The theoretical ultimate configuration of this type would therefore be one that would restrict heat flow to the relatively low level due to conduction by the gas.

Seven configurations were tested. Each consisted of an annular cylindrical region that was subdivided into thin gas layers by thin metal barriers. This insulation annulus was installed in a vertical pressure pipe in such a way that the hot gas flow passed through the cylindrical duct formed by the insulating annulus but not through the insulating gas layers. Spacing between the thin metal barriers was maintained by either metal lugs, glass-fiber cloth tape, or corrugated metal strips. Two gases were used in the tests: helium and carbon dioxide.

The test results indicated that conduction and convection heat transfer across one, or a series, of the vertical annular gas spaces can be predicted with a fair degree of accuracy by appropriate nondimensional correlations of the usual kind. These correlations are of the form:

$$N_{\text{Nusselt}} = f\left(N_{\text{Grashof}} \times N_{\text{Prandtl}}\right)$$

If the product of $N_{\text{Gr}} \times N_{\text{Pr}}$ is below 2000, convective heat transfer will in general be negligible. For typical values of temperature and gas pressure that would exist in an actual reactor application, this would correspond to gas annuli of thickness about 0.2 in. for helium and 0.04 in. for CO_2, the difference being due largely to the difference in densities of the gases. Since the thermal conductivity of helium is approximately six times that of CO_2, one can conclude that gas annuli of equal effectiveness would be about six times as thick in helium as in CO_2; approximately the same number of annuli would be required for equal effectiveness in the two gases, and hence the total thickness of the insulation would also be five or six times as thick in helium.

Most of the test results given in reference 11 are presented in the form of curves, in which the effective thermal conductivity of each insulation configuration is plotted as a function of gas pressure and of temperature. Two effective thermal conductivities were evaluated in each case: the total or "gross" conductivity (including

conduction, convection, and radiation) and the partial or "net" thermal conductivity (including only conduction and convection).

Typical results for an insulating configuration of three 0.050-in. gaps evaluate the net thermal conductivity with helium at about the thermal conductivity of helium gas: 0.10 to 0.12 Btu/(hr)(ft)(°F). Moreover, the effective conductivity does not vary with gas pressure. Both of these results indicate that essentially no heat is being transferred by convection, as is to be expected with helium in such narrow gaps. The net thermal conductivity of the same configuration of three 0.050-in. gaps with CO_2 gas at atmospheric pressure also corresponds to the thermal conductivity of CO_2, about 0.02 Btu/(hr)(ft)(°F). This value increases with gas pressure to about 0.04 Btu/(hr)(ft)(°F) at 1000 psia, as convection heat transfer becomes more effective.

The values for the gross thermal conductivity (including the conduction, convection, and radiant heat transfer) which were evaluated for the configuration of three 0.050-in. gaps show that the heat transferred by radiation is approximately equal to that transferred by conduction and convection with either gas. The values for the gross thermal conductivity with helium ranged from 0.2 to 0.25 Btu/(hr)(ft)(°F), depending on the gas temperature. For CO_2 the value increased from about 0.05 at low pressures to 0.09 at 1000 psia, again because of the increase in convection.

Effective thermal conductivities were also evaluated for an insulation configuration, called the "ORNL type" by the investigators, which consisted of four 0.13-in. gaps. The values for the net and gross thermal conductivities with helium were about 0.15 and 0.19 Btu/(hr)(ft)(°F), respectively. The effective thermal conductivities with these thicker gas gaps increased slightly with pressure even in helium, and increased very considerably with pressure in CO_2. The results therefore confirm analytical predictions that these gaps would be satisfactory for helium but are too large for CO_2 because of convective heat transfer.

Using typical values of the effective gross thermal conductivities evaluated in these tests, and typical power densities that might be expected in a pressure-tube gas-cooled reactor, one may calculate that the heat loss through the insulation is only about 1 to 2 per cent of the power being produced in the tube. The gas-annuli-series type of thermal insulation there-fore appears to be an effective method of accomplishing this heat insulating function in pressure-tube reactors.

A summary of the above investigation was recently published in *Nuclear Science and Engineering*.[12] Although it gives less experimental detail than reference 11, it discusses the results and their significance more thoroughly.

Reference 13 also presents the results of a design and development program on thermal insulations, but for use in quite a different type of gas-cooled-reactor plant. In this case the intended application is that of aircraft nuclear propulsion, and the technology and design limits tend to be peculiar to this application. The operating temperatures are extremely high (up to 2000°F), as are the gas velocities (up to Mach 0.3). The lifetime requirements, however, are only of the order of 1000 hr.

In general, the problem was to provide thermal insulation on the inside of ducts and other components of the nuclear-powered gas-turbine power plant, between the hot gases and the structural material carrying pressure and other stresses. Except in a few special cases, the thermal insulation selected was fibrous insulation of the alumina-silica or silica families, such as Thermoflex (made by Johns Manville) or Refrasil (made by H. I. Thompson Fiberglass Company). These materials are used in pads having thicknesses of about 0.1 to 0.5 in. The fibrous insulation is protected from the high-velocity gas flow by thin metal covers which are about 0.015 in. thick and which are penetrated by small holes so that there are no pressure loads against them or the insulation. The metals used for these thin liners are varied with the operating temperature and corrosion conditions and include stainless steels, the Hastelloys, the Inconels, and even the noble metals and alloys: platinum-rhodium, palladium-rhodium, and palladium.

The method of holding the insulations and their cover sheets in place is by the use of metal fasteners. These fastening devices were one of the limiting features of the insulations, and therefore the design and development of satisfactory fasteners represented a substantial portion of the program.

References

1. W. R. Martin and J. R. Weir, A Device To Simulate the Service Thermal Conditions in EGCR

Type Fuel Elements, USAEC Report ORNL-3032, Oak Ridge National Laboratory, Jan. 12, 1961.

2. W. R. Martin and J. R. Weir, Dimensional Behavior of the Experimental Gas-Cooled Reactor Fuel Element at Elevated Temperatures, USAEC Report ORNL-3103, Oak Ridge National Laboratory, Aug. 2, 1961.

3. A. Levy and J. F. Foster, The Compatibility of Gas Coolants and Ceramic Materials in Coated-Particle Nuclear Fuels, USAEC Report BMI-1530, Battelle Memorial Institute, July 18, 1961.

4. General Atomic Div., General Dynamics Corp., Proceedings of the High-Temperature Gas-Cooled Civilian Power Reactor Conference, January 17–18, 1961, USAEC Report TID-7611.

5. Philadelphia Electric Co., Application of Philadelphia Electric Company for Construction Permit and Class 104 License, Part B, Preliminary Hazards Summary Report, Vol. I, Plant Description and Safeguards Analysis, Report NP-9115, July 1960.

6. L. L. Kintner et al., Pneumatic Temperature Probes for Gas-Cooled Reactors, *Nuclear Sci. and Eng.*, 11: 318–323 (November 1961).

7. R. E. Dahl, Evaluation of Chlorine Inhibition of Graphite Oxidation as a Gas-Cooled Reactor Safe-guard, USAEC Report HW-67255, Hanford Atomic Products Operation, April 1961.

8. R. E. Dahl, Oxidation of Graphite Under High Temperature Reactor Conditions, USAEC Report HW-68493, Hanford Atomic Products Operation, July 1961.

9. S. Keraudy et al., The Effect of Impurities on the Rate of Oxidation of Reactor Grade Graphite, British Translation DEG-Inf-Ser-112, July 1, 1959.

10. Tracerlab, Inc., Helium Contaminant Removal Feasibility Study, USAEC Report TID-12821, Nov. 30, 1960.

11. Orenda Engines, Ltd., Tests on Gas Space Reflective Insulations, USAEC Report TID-13441, November 1960.

12. R. E. MacPherson, Jr., and H. D. Stuart, The Performance of Metallic-Foil Insulations in Vertical Gas Spaces, *Nuclear Sci. and Eng.*, 12: 225–233 (February 1962).

13. T. D. McLay, Thermal Insulation Designs for Gas-Cooled Reactors, USAEC Report APEX-641, General Electric Co., Flight Propulsion Laboratory Dept., August 1961.

Section

X

Evaluations: Steam-Cooled Power Reactors

In early 1961 the U. S. Atomic Energy Commission was authorized to sponsor a program for the development of conceptual designs and engineering analyses of several different steam-cooled-reactor concepts. The AEC's Division of Reactor Development then contracted with several nuclear designers to complete independent design studies of nine steam-cooled reactors. The contractors for the different concepts are shown in Table X-1. The nuclear portions of the plant were to be designed to the point where estimates of capital, fuel-cycle, and operating costs could be made, and each study was to include an analysis of the research, development, and related costs necessary to substantiate the design features of the different

reactor plants. The plants were designed to generate a nominal 300 Mw(e), and a second design for a nominal 40 Mw(e) was to be accomplished at the option of the nuclear designers.

Subsequently Kaiser Engineers was engaged to prepare conceptual designs of the nonnuclear portions of the plants and to make cost analyses. Specifically they were to

1. Assist the Commission in developing basic parameters for normalizing capital costs, fuel-cycle costs, and operation and maintenance costs for each of nine steam-cooled-reactor concepts.

2. Cooperate with the nuclear designers in developing over-all plant layout, heat balance, etc.

Table X-1   STEAM-COOLED-REACTOR DESIGNS AND CONTRACTORS[1]

Design	Contractor
Graphite-Moderated Boiling and Superheating Reactor (GBSR)	Atomics International A Division of North American Aviation, Inc. Canoga Park, Calif.
Integral Boiling and Superheating Reactor (IBSHR)	Westinghouse Electric Corporation Atomic Power Department Pittsburgh, Pa.
Integral Nuclear Superheater Reactor (ISR)	General Nuclear Engineering Corporation Dunedin, Fla.
Mixed-Spectrum Superheater Reactor (MSSR)	General Electric Company Atomic Power Equipment Department San Jose, Calif.
Once-Through Superheater Reactor (OTSR)	General Electric Company Atomic Power Equipment Department San Jose, Calif.
Pressure-Tube Superheater Reactor (PTSR)	General Electric Company Hanford Atomic Products Operation Richland, Wash.
Steam-Cooled D_2O-Moderated Reactor (SCDMR)	Nuclear Development Corporation of America* White Plains, N. Y.
Steam-Cooled Fast-Breeder Reactor (SCFBR)	Nuclear Development Corporation of America* White Plains, N. Y.
Separate Superheater Reactor (SSR)	General Electric Company Atomic Power Equipment Department San Jose, Calif.

*Now called the United Nuclear Corporation.

Table X-2   SUMMARY OF PRINCIPAL PLANT CHARACTERISTICS

	GBSR*			IBSHR-NR*		IBSHR-R*		
	Boiler	Super-heater	Reheater	Boiler	Super-heater	Boiler	Super-heater	Reheater
Heat balance:								
Total reactor power, Mw(t)	760			820		820		
Gross turbine power, Mw(e)	330			341		355		
Net plant power, Mw(e)	318			322		334		
Net plant efficiency, %	41.8			39.3		40.8		
Turbine cycle conditions:								
Throttle pressure, psia	1815			1465		2415		
Throttle temperature, °F	1000			1000		1000		
Condensing pressure, in. Hg abs.	1.5			1.5		1.5		
Final feed-water temperature, °F	530			442		506		
Reactor vessel:								
Inside diameter, ft	51.3			26.6		26.6		
Inside height, ft	62.5			34.8		32.3		
Operating pressure, psig	20.0			100		100		
Reactor core:								
Total uranium loading, kg of U	60,000	60,000		30,012	24,705	24,385	14,820	9722
Specific power, kw(t)/kg of U	6.33	6.33		18.33	10.93	16.3	20.5	12.3
Power density, kw(t)/cu ft	20.2	20.2		193	101	172	190	79.1
Initial U^{235} enrichment, wt.%	1.80	2.72		1.94	2.65	1.95	2.50	1.89
Final U^{235} enrichment, wt.%	0.22	0.71		0.60	1.24	0.63	1.25	0.75
Fuel exposure, Mwd/metric ton (av.)	25,000	25,000		17,000	17,000	16,500	15,500	15,600
Reflector or blanket material	Graphite			Graphite		Graphite		
Moderator material	Graphite			Graphite		Graphite		
Coolant:								
Material	H_2O			H_2O		H_2O		
Outlet temperature, °F	645	1000	1000	613	1000	681	1000	1000
Inlet temperature, °F	613	645	660	603	613	676	681	698
Fuel elements:								
Fuel material	UO_2 in graphite			UO_2	UO_2	UO_2		
Geometry	Cylindrical			Annular		Annular		
Cladding material	Silicon carbide			Zircaloy-4	304 S.S.	Zircaloy-4	304 S.S.	304 S.S.
Maximum cladding temperature, °F				622	1250	686	1240	1250
Fuel assemblies:								
Total number	1296			256	240	208	144	136
Elements per assembly	10			7	5	7	5	4
Reactor control:								
Absorber material	B_4C			B_4C		B_4C		
Number of control elements	68			69		69		
Type of drive	Rack and pinion			Drum and cable		Drum and cable		

*GBSR, Atomics International; IBSHR-NR, Westinghouse Electric Corp.; IBSHR-R, Westinghouse Electric Corp.; ISR, General Nuclear Engineering Corp.; MSSR, General Electric Co.; OTSR, General Electric Co.; PTSR, Hanford Atomic Products Operation; SCDMR, Nuclear Development Corp. of America; SCFBR, Nuclear Development Corp. of America (now called the United Nuclear Corp.); SSR, General Electric Co.

FOR 300-Mw(e) (NOMINAL) STEAM-COOLED NUCLEAR POWER PLANTS[1]

ISR* Boiler	ISR* Superheater	MSSR* Boiler	MSSR* Superheater	OTSR* Boiler	OTSR* Superheater	PTSR* Boiler	PTSR* Superheater	SCDMR* Boiler	SCDMR* Superheater	SCFBR*	SSR* Boiler	SSR* Superheater
782		815		833		848		947		876	833	
333		331		316		332		308		316	316	
323		319		307		320		298		304	307	
41.3		39.1		36.8		37.8		31.5		34.7	36.8	
1465		1450		960		1387		765		1415	960	
1100		950		900		944		800		945	900	
1.5		1.5		1.5		1.5		1.5		1.5	1.5	
450		495		400		419		350		495	400	
13		12.5		12.5		39.4		22.2		10.67	11.08	8.50
49.0		41		49.5		36.7		18.2		31	42	43
1590		1800		1435		5				1860	1310	1310
18,800	26,180	39,330	6418 (U + Pu)	42,900		222,000		40,600	13,680	13,464 (U + Pu)	30,800	10,720
15.38	18.79	16	57	19.4		3.55		18.9	5.2	62	20.0	20.0
1070	1232	1010	6150	1138		41.5		323	72	5930	1385	1070
4.10	1.95	2.46	19.6 (Pu)	2.77		2.02		1.05	1.28	15.39 (Pu)	2.46	3.25
2.93	0.62	1.08	18.8 (Pu)	1.30		1.01		0.17	0.27	16.47 (Pu)	1.08	1.68
14,300	18,400	17,200	33,400	17,200		11,000		15,000	15,000	33,000	17,500	17,500
H₂O	H₂O	H₂O	Depleted UO₂	H₂O		Graphite			D₂O	Depleted UO₂	H₂O	H₂O
H₂O	H₂O	H₂O	None	H₂O		Graphite			D₂O	None	H₂O	H₂O
H₂O	H₂O	H₂O	H₂O	H₂O		H₂O		H₂O		H₂O	H₂O	H₂O
601	1100	600	950	900		644	950	525	803	950	553	900
580	601	592	600	400		572	517	532	524	610	535	553
UO₂	UO₂	UO₂	UO₂-PuO₂	UO₂	UO₂	U in Mg		UO₂	UO₂	UO₂-PuO₂	UO₂	UO₂
Rod	Double annular	Rod	Rod	Rod	Annular	Tubular		Rod	Rod	Rod	Rod	Annular
304 S.S.	Inconel X and 347 S.S.	S.S.	S.S.	Zr	S.S.	304 S.S.		Zircaloy-2	S.S.	Inconel X	S.S.	304 S.S.
	1350				1250	670	1025	560	1100	1350	580	1250
114	169	96	132	109		1448	532	242	273	326	164	52
84	6	136 and 225	416, 82, and 81	36	49	6	6	37	31	127	143	49
Boron-S.S.		Boron-S.S. fuel		Boron-S.S.		Boron-S.S.				B₄C	Boron-S.S.	Boron-S.S.
126		60	4	52		241		38	38	14	69	24
Rack and pinion		Locking piston	Twin screw	Locking piston		Ball screw		Lead screw and nut		Lead screw and nut	Hydraulic locking piston	

3. Evaluate and normalize the reactor complex and reactor-associated equipment, fuel-cycle, and operation and maintenance cost estimates prepared by the nuclear designers for each reactor concept.

4. Design the nonnuclear portion of the plant in sufficient detail to determine the probable capital cost of the conventional power-plant equipment for the various reactor plants.

5. Use the information developed in items 3 and 4 to determine the net power generation cost for each reactor plant.

To a large extent the cost study drew on work already under way under the nuclear superheat program (described in *Power Reactor Technology*, Vol. 4, No. 3), although the group of contractors was not identical. The results of the Kaiser Engineers study have been published as reference 1, and the summary of the evaluation, prepared by the AEC's Division of Reactor Development, is given in reference 2. Many of the designs of the individual nuclear contractors have been issued and are cited as references 3 to 11. The principal characteristics of the plants are summarized in Table X-2. This review will characterize briefly each of the several reactor concepts and will conclude with a summary of cost data.

Graphite-Moderated Boiling and Superheating Reactor[3] (GBSR)

This pressure-tube reactor is of novel design in that the fuel elements and the coolant tubes are buried, separately, in the graphite moderator. Heat flows, primarily by radiation, from the fuel element across a 0.1-in. clearance gap to the graphite, and it is conducted by the graphite to the coolant tubes. Boiling, superheating, and reheating occur in separate regions of the core; the boiling region is centrally located and is surrounded, in turn, by concentric annular superheating and reheating regions. The saturated steam is separated in an external drum before flowing to the superheat region. The vertical core of the reactor is roughly a right cylinder which is composed of full-length (41 ft) graphite columns that are 22 in. square in cross section. Each column is penetrated (lengthwise) by four fuel channels (4.2 in. in diameter) which contain the 4-in.-diameter fuel slugs. Each fuel channel is surrounded by four vertical coolant-pressure tubes that are buried in the graphite. The diameter of the coolant tubes differs in the different regions of the reactor; the internal diameter is about

0.7 in. in the boiling region, 0.625 in. in the superheat region, and 1.25 in. in the reheat region. Coolant flow is single-pass in the boiling region and two-pass in the superheat and reheat regions. Inconel X is specified for the superheat and reheat tubes; whereas both zirconium alloys and stainless steel (PH 15-7 Molybdenum) are considered for the boiling region. The fuel elements consist of unclad slugs of a uranium dicarbide–graphite dispersion (50 per cent UC_2 by weight) and are coated with silicon carbide. Helium is circulated slowly through the core and over the fuel elements and to a continuously operating purification system for the removal of off-gases and fission products. On-power refueling is provided by means of a fuel-handling machine located beneath the core. Refueling is expected to be simplified by the circumstance that the fuel elements are not in the high-pressure coolant stream. Commercial, mold-grade graphite rather than nuclear-grade graphite is specified as moderator because of its lower cost. The commercial graphite differs from the nuclear-grade graphite in that it has a higher neutron-absorption cross section—due primarily to high cross-section impurities which burn out in time—and a higher gas content.

It is noted in Table X-2 that this reactor is quite large and that the specific power is low. Despite the combination of low specific power and substantial fuel enrichment, the fuel use charge is not extremely high when computed according to the ground rules of the study. The reactor type has, in fact, the lowest total estimated fuel cost of any of the reactors considered.

Integral Boiling and Superheating Reactor[4] (IBSHR)

The IBSHR is also a graphite-moderated pressure-tube reactor, but both fuel and coolant are contained within common pressure tubes in the more conventional way. The graphite moderator is contained in a large, low-pressure (80 psi) vessel and is operated at 1200 to 1500°F; heat deposited in the moderator is removed by a helium blanket system and is utilized partially for feed-water heating. Since the moderator is at a relatively high temperature, part of the deposited energy (25 per cent) also flows back into the coolant inside the pressure tubes. Two reactor plants have been examined: one with reheat and one without reheat. The IBSHR employs a central boiling region which discharges

to a steam drum for steam-water separation. The saturated steam then flows to a peripherally located superheater; the reheat region, where employed, is located in concentric rings of pressure tubes just outside the superheating region. The pressure-tube materials for the reheat (IBSHR-R) plant are different from the nonreheat plant (IBSHR-NR), since the latter operates at a considerably lower pressure (see Table X-2). The IBSHR-R employs

Reheat
Thru — Tube

Superheat
Re-entrant Tube

Boiling
Thru — Tube

Fig. X-1   Annular fuel assemblies[4] for the IBSHR-R.

zirconium—3 aluminum—0.5 molybdenum alloy for the pressure tubes in the boiling and superheating sections; whereas the reheat pressure tubes use a niobium-base alloy that is presently under development. The fuel elements for the IBSHR-R are shown in Fig. X-1. The superheat elements are of the reentrant type in that steam flows downward in an annular space adjacent to the pressure-tube wall and then upward through the fuel assemblies. The clad materials and dimensions are also shown in Fig. X-1. The annular elements are fabricated of UO_2 by means of vibratory compaction. The shroud and baffle shown (Fig. X-1) for the superheater element serve to contain a layer of stagnant, saturated steam for thermal insulation. The pressure tubes for the IBSHR-NR are fabricated of Zircaloy-4. Rod type elements containing UO_2 are under consideration for fuel, as well as the annular type shown in Fig. X-1. Both reheat and nonreheat plants use a wet refueling system which employs a fuel-handling pool located over the reactor.

Integral Nuclear Superheater Reactor[5] (ISR)

The ISR is a light-water-cooled and -moderated thermal reactor with boiling, steam separation, and superheating accomplished within a single pressure vessel. The plant was designed in two sizes: 300 and 40 Mw(e). Characteristics of the plants are given in Tables X-2 and X-3. Both designs employ a central region of double-annular fuel assemblies which superheat steam in the internal flow passages and boil water on the external heat-transfer surfaces; surrounding the boiler-superheater section of the core is a concentric ring of rod type fuel elements in which only boiling occurs. This concept is reviewed in detail in the June 1961 issue of *Power Reactor Technology*, Vol. 4, No. 3, page 76.

Mixed-Spectrum Superheater Reactor[6] (MSSR)

This reactor concept employs a core consisting of four concentric regions within a single pressure vessel:

1. An inner, unmoderated superheating region
2. An inner, unmoderated buffer region
3. An outer, moderated buffer region
4. An outer boiling region

The name of the reactor was derived from the fact that the neutron spectrum varies from thermal in the boiling region to fast in the superheater region and assumes an intermediate distribution in the buffer regions. The function of the buffer regions is to avoid very high power densities at the boundaries of the fast and thermal regions while preserving sufficient reactivity coupling between the regions to give a reasonably long effective neutron lifetime for the composite reactor and without wasting an excessive fraction of the neutrons. Water is boiled in the outer buffer and boiling regions; the buffer region differs from the boiler proper in that the fuel rods are larger and the fuel is depleted in U^{235} (0.3 per cent). The fuel cladding in these regions is either stainless steel or a zirconium alloy. After passing through an internal steam-separation system that employs radial-flow separators, the saturated steam generated in the boiling regions passes through the inner superheating regions of the core. The

Table X-3 SUMMARY OF PRINCIPAL PLANT CHARACTERISTICS OF 40-Mw(e) (NOMINAL) STEAM-COOLED NUCLEAR POWER PLANTS[1]

	ISR*		SCDMR†		SCFBR†
	Boiler	Superheater	Boiler	Superheater	
Heat balance:					
Total reactor power, Mw(t)	112		131		127
Gross turbine power, Mw(e)	41.7		43.7		46.8
Net plant power, Mw(e)	40		40		40
Net plant efficiency, %	35.8		30.5		31.5
Turbine cycle conditions:					
Throttle pressure, psia	1200		765		1415
Throttle temperature, °F	1000		800		920
Condensing pressure, in. Hg abs.	1.5		1.5		1.5
Final feed-water temperature, °F	450		350		575
Reactor vessel:					
Inside diameter, ft	7.75		13.8		8.33
Inside height, ft	29.5		12.0		16.67
Operating pressure, psig	1300				1860
Reactor core:					
Total uranium loading, kg of U	3260	3160	6410	1230	1482 (U + Pu)
Specific power, kw(t)/kg of U	14.6	17.2	15.4	18.7	79.5
Power density, kw(t)/cu ft	1050	1240	360	317	8680
Initial U^{235} enrichment, wt.%	4.6	2.75	1.13	1.50	17.6 wt.% Pu
Final U^{235} enrichment, wt.%	3.40	1.33	0.20	0.39	16.3 wt.% Pu
Fuel exposure, Mwd/metric ton (av.)	11,100	16,000	15,000	15,000	32,500
Reflector or blanket material	H_2O	H_2O	D_2O		Depleted UO_2
Moderator material	H_2O	H_2O	D_2O		None
Coolant:					
Material	H_2O	H_2O	H_2O		H_2O
Outlet temperature, °F	573	1000	525	803	925
Inlet temperature, °F	560	573	532	524	610
Fuel elements:					
Fuel material	UO_2	UO_2	U_2O	U_2O	UO_2-PuO_2
Geometry	Rod	Double annular	Rod	Rod	Rod
Cladding material	347 S.S.	Inconel X and 347 S.S.	Zircaloy-2	S.S.	Inconel X
Maximum cladding temperature, °F		1250	560	1120	1350
Fuel assemblies:					
Total number	66	37	72	19	67
Elements per assembly	84 and 24	6	31	31	127
Reactor control:					
Absorber material		Boron-S.S.			B_4C
Number of control elements	188				10
Type of drive		Rack and pinion		Induction motor	Induction motor

*General Nuclear Engineering Corp.

†Nuclear Development Corp. of America (now called the United Nuclear Corp.).

superheating fuel elements of the fast and inner buffer zones are jacketed with stainless steel. Upper and lower reflectors of depleted UO_2 are provided on this central, unmoderated zone of the core. In the equilibrium fuel cycle, PuO_2 (mixed with $U^{238}O_2$) is considered as the fuel for the unmoderated region. Table X-4 gives fuel compositions and fuel-rod diameters for the MSSR. In order to avoid the problem of a very large reactivity gain upon flooding of the unmoderated superheater region, the plan is to incorporate epithermal absorbers, such as hafnium, in that region. Neutron absorption by such a material would normally be small, but it would increase greatly if the neutron spectrum were degraded by the addition of water moderator.

Once-Through Superheater Reactor[7] (OTSR)

The water in the OTSR is not recirculated as in a conventional boiling-water reactor; the water is evaporated and superheated, without steam separation, in three continuous passes through the core. The thermal design of the reactor has been discussed in the December 1961 issue of *Power Reactor Technology*, Vol. 5,

No. 1, and that issue should be consulted for additional details. Briefly, the reactor is designed to operate with one pass in the low-quality boiling regime, a second pass in the transition-boiling regime, and a third pass in the super-heating regime. Zircaloy-clad UO_2 fuel rods are utilized for the first-pass fuel elements; whereas the second and third passes are made around the outside and the inside, respectively, of stainless-steel-clad annular UO_2 fuel elements. The core is a "mixture" of these two types of elements; the annular elements are surrounded by Zircaloy process tubes to define the flow channels. The steam-water mixture generated by the rod type elements enters at the tops of the process tubes and flows down between the tube and the outer surface of the annular fuel element. This region operates in the transition-boiling regime and produces steam of about 100 per cent quality. The steam then reverses and flows up the center of the annular element where superheating takes place. Other details of the plant are given in Table X-2.

Pressure-Tube Superheater Reactor[8] (PTSR)

The PTSR utilizes the features of the Russian Beloyarsk[13] (Ural) Power Station. The reactor

Table X-4   FUEL-ROD DIAMETERS AND AVERAGE ISOTOPIC COMPOSITIONS[6]
OF FUEL EQUILIBRIUM CYCLE* (MSSR)

[Balance Is Always U^{238} (No Fission Products)]

Region	Isotope	Initial enrichment, at.% based on initial loading	Final enrichment, at.% based on final loading	Initial loading, kg	Final loading, kg	Fuel-rod diameter, in.
Fast core	Pu^{239} and Pu^{241}	13.00	12.51	4,020	3,840	0.24
	Pu^{240} and Pu^{242}	0	1.21			
Boiling-water core:						
Standard rods	U^{235}	2.3	0.91	30,700	29,850	0.392
	Pu^{239} and Pu^{241}	0	0.57			
	Pu^{240} and Pu^{242}	0	0.20			
Corner rods	U^{235}	1.8	0.53	3,910	3,800	0.370
	Pu^{239} and Pu^{241}	0	0.81			
	Pu^{240} and Pu^{242}	0	0.20			
Slow buffer	U^{235}	0.30	0.30	4,720	4,720	0.750
	Pu^{239}	0	0.64			
Fast buffer	U^{235}	5	1.51	258	246	0.24
	Pu^{239}	0	2.57			
Axial reflector	U^{235}	0.30	0.30	2,120	2,120	0.50
	Pu^{239}	0	2.10			

*Burnup for a fast core:
 Standard rods   38,500 Mwd/metric ton
 Fast buffer   38,500 Mwd/metric ton
 Reflector   56 months at 80% load factor

 Burnup for a boiling core:
 Standard rods   18,700 Mwd/metric ton
 Corner rods   20,900 Mwd/metric ton
 Slow buffer   56 months at 80% load factor

is graphite-moderated and contains 1980 vertically oriented fuel channels. Boiling takes place in 1448 of the channels and superheating in the remaining 532. The fuel element is a bayonet assembly inserted from the top of the reactor, of the same design for boiling or superheating; see the cross section in Fig. X-2. The active

two-phase mixture are cooled with a "fog" of light water dispersed in steam. The fog enters the coolant channels at about 15 per cent quality and leaves at about 35 per cent quality. This fog cooling keeps the light-water inventory in the pressure tubes to a minimum. The design of the pressure tubes and fuel elements is shown in
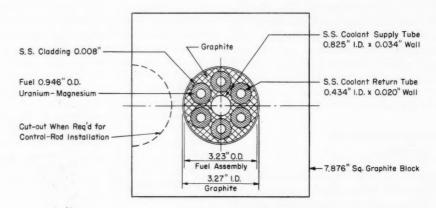
Fig. X-2   Fuel element for the PTSR.[8]

length is about 26 ft. The stainless-steel cladding shown in Fig. X-2 is a Russian alloy similar to type 321; the thicknesses are approximately double those of the Russian design so as to conform to applicable codes in the United States. The design used for the cost estimates incorporated the magnesium-matrix fuel typical of the Russian design, although some studies were done with a 9 wt.% molybdenum—uranium alloy. A distinctive feature of the reactor is the use of an indirect cycle for the production of steam; the steam is then superheated by a pass through the reactor and is fed directly to the turbine. Fuel handling is done in a single batch at about two-year intervals.
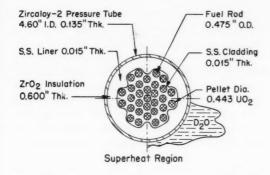
Steam-Cooled D$_2$O-Moderated Reactor[9] (SCDMR)

The SCDMR is a two-region reactor in which nonpressurized, low-temperature D$_2$O is contained in a calandria tank penetrated by vertical Zircaloy pressure tubes. An inner region of 19 fuel clusters constitutes the superheater section; saturated steam is generated in 72 fuel clusters located in an annular ring around the superheater. The reactor is not a boiling reactor, as such, since those elements cooled by a

Fig. X-3. It can be noted that, whereas external insulation (calandria) is used for the fog-cooled pressure tubes, internal insulation is utilized in the superheat tubes to avoid high tube-wall temperature. The design presented in reference 9 employs enriched fuel in both the superheating and fog-cooled zones, although operation with natural uranium is discussed. Since steam is introduced at the entrance to the fog-cooled elements, it is necessary to provide steam circulators to pump saturated steam back to a sufficiently high inlet pressure. Data on both the large and small reactors are given in Tables X-2 and X-3. The fuel elements for the large and small reactors have lengths of 15.2 and 7.8 ft, respectively.

Steam-Cooled Fast-Breeder Reactor[10] (SCFBR)

The SCFBR is a pressure-vessel reactor that is cooled entirely by steam. About one-third of the superheated steam discharged from the reactor is fed directly to the steam turbine, and the remainder is utilized to produce saturated steam in a Loeffler boiler; this steam is then pumped into the superheating reactor by steam circulators. The fuel is composed of
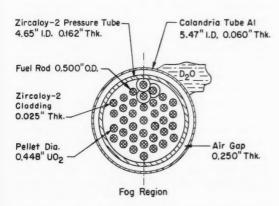
Fig. X-3 Fuel-element pressure-tube arrangement[9] for the SCDMR.

Inconel-clad rods (0.25 in. in outside diameter) of PuO_2-UO_2, arranged in hexagonal clusters. The core is enclosed by axial and radial blankets that are fabricated of stainless-steel-clad depleted UO_2. Breeding ratios of about 1.5 are predicted for the plutonium-fueled equilibrium cycle. An inward radial-shift refueling program is used, with refueling approximately every 50 days. The steam coolant flows downward through the core and axial blankets, with about 10 per cent of the steam flowing in parallel through the radial blanket. The reactor is controlled by stainless-steel-clad B_4C rods; the reference states that the reactor can be flooded with water for refueling and for other shutdown operations. Reactivity rise upon flooding is prevented by incorporating resonance absorbers, such as hafnium and indium, in the fuel. Preliminary calculations indicate that the temperature and void coefficients of the 300-Mw(e) reactor are positive, although no detailed studies of the consequences are reported in the reference.

Separate Superheater Reactor[11] (SSR)

This concept employs two separate H_2O-moderated reactors: one for the production of saturated steam and one for superheating. The superheating reactor has been described in the June 1961 issue of *Power Reactor Technology*, Vol. 4, No. 3, page 72, and will not be treated here. The Boiling-Water Reactor (BWR) is a forced-circulation reactor that employs Zircaloy-clad UO_2 rods arranged on a square pitch. Both the BWR and the SSR employ systems for the location of failed fuel elements. These consist of systems of tubes located to take saturated or superheated steam samples from the fuel bundles in either reactor for radiochemical analyses. The BWR, in addition, is provided with internal steam separation and drying equipment. The radial-flow steam separators are located above the core, and the dryers are located in the reactor-pressure-vessel head.

Power Costs and Potentials

Normalized power cost estimates were derived from the individual studies by Kaiser Engineers. A considerable amount of normalizing apparently was done, since the "nominal" 300-Mw(e) plants as submitted by the contractors ranged in size from 298 to 334 Mw(e) (net). Various containment concepts were originally employed, but all plants except the MSSR were normalized to vapor suppression by Kaiser Engineers to remove this cost variable. End results are shown in Figs. X-4 and X-5. The BWR reference plant included in Fig. X-5 was taken from reference 12. The fuel-cycle costs indicated in the figures apply only after fuel-cycle equilibrium is attained.

The 40-Mw(e) plants studied do not appear to be competitive with the conventional plant; their estimated power costs were not as low as those forecast for nonsuperheat boiling reactors in the same power range. Seven of the 315-Mw(e) plants (GBSR, IBSHR, ISR, MSSR, OTSR, SCFBR, and SSR) do yield estimated power costs in the range competitive with the estimated conventional plant, which uses coal at a cost of $0.35 per million Btu, and lower by 0.3 to 1.1 mills/kw-hr than the estimated cost for a nonsuperheating boiling nuclear plant. In the AEC summary report,[2] the latter estimated cost differential is considered to have significance, but the spread among the seven steam-cooled estimates is
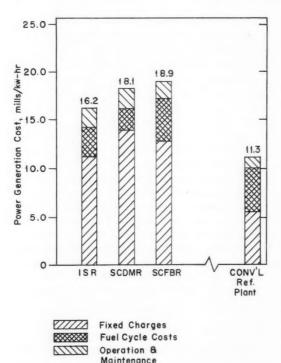
Fig. X-4 Power generation costs, 40-Mw(e) plants.[1] Fixed charges include: capital cost, 14 per cent; working capital, 12.5 per cent; interim replacements, 0.3 per cent; and nuclear insurance. Plant operating factor = 80 per cent. Reference conventional plant is coal fired with a unit fuel cost of $0.35 per thousand Btu.

considered too small to be valid in consideration of the uncertainties in the estimates.

Under the ground rules of the study, the designs and cost estimates were intended to be consistent with the possibility of operation of the plant by June 30, 1967. Substantial research and development programs appear necessary for the more attractive plants. The estimated research and development costs, as given in references 3 to 11, are summarized in Table X-5. The research and development cost estimates are complicated by the circumstance that some of the programs are presently being partially funded under existing research and development programs financed by private and public funds. If the recommended programs were carried out and if they proved successful, all or any of the plants could, no doubt, be built for operation in 1967. Some of the plants, however, represent rather drastic departures from current practice,

and, in these cases, the likelihood that a 300-Mw(e) plant actually would be built on such a schedule appears rather small.

Inasmuch as two nuclear superheat reactors (Pathfinder and BONUS) have already reached advanced stages of construction, it is perhaps a little surprising that some of the approaches considered in the study for achieving nuclear superheat are so unconventional. Aside from the natural tendency to explore many approaches to such a broadly defined objective as the nuclear superheating of steam, the reason for this phenomenon appears to be that, whereas the basic feasibility of nuclear superheat can be demonstrated in a rather straightforward way, the development of a superheating reactor, which will be a strong competitor against the conventional boiling- or pressurized-water reactors, is not so straightforward.

The characteristics of the two power reactors and the reactor experiment currently under way in the nuclear superheat program (Pathfinder, BONUS, and BORAX-V) are summarized in Table X-6. From the developmental point of view, the main function of these reactors (at least in the early stages of their operation) is
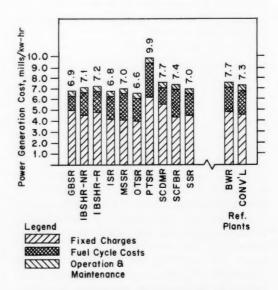

Fig. X-5 Power generation costs, 315-Mw(e) plants.[1] Fixed charges include: capital cost, 14 per cent; working capital, 12.5 per cent; interim replacements, 0.3 per cent; and nuclear insurance. Plant operating factor = 80 per cent. Reference conventional plant is coal fired with a unit fuel cost of $0.35 per thousand Btu.

Table X-5   RESEARCH AND DEVELOPMENT
COSTS FOR STEAM-COOLED POWER-REACTOR
EVALUATION STUDY

| Reactor concept | Cost, millions of dollars | |
	Research and development	Reactor experiment
GBSR	8.8	7.5
IBSHR	16.5	None
ISR	15.0	None
MSSR	9.5	7.4
OTSR*		
PTSR†	5.0	None
SCDMR‡	1.0	None
SCFBR‡	3.9	8.2
SSR§	12.7	7.8

*Research and development cost data are included with SSR development program.

†Some research and development costs will be charged to production.

‡The data are for incremental costs above existing development programs.

§Reactor experiment is the hook-on superheat reactor at VBWR.

to demonstrate solutions to those problems which are inherent in the concept of the direct-cycle superheating of steam. The major problems of this type are as follows:

1. *Problems of radioactive carryover.* Although the feasibility of the direct-cycle boiling reactor has been adequately demonstrated, the carryover problem may be more severe in the direct-cycle superheat reactor. In the boiling reactor the evaporation process affords a very substantial decontamination factor, which, in combination with cleanup systems for the coolant water, keeps the radioactive carryover to the turbine low. In the superheat reactor the possibility exists that materials may deposit upon the coolant-channel surfaces, where they may be activated and subsequently swept out into the turbine. Serious carryover of fission products from failed fuel elements, if failures should occur, is also a possibility.

2. *Performance of available materials, in the relatively thin sections that must be used for fuel cladding and coolant-channel structures, in the superheat environment.* This question is not simply one of corrosion and erosion resistance to superheated steam. The possibility of the deposition of other materials, such as chlorides (which may cause stress corrosion), also exists. Further, some departures from current water-reactor fuel-element technology appear to be necessary. The use of a free-standing fuel

jacket, for example, appears unattractive because of the reduced strength of the cladding materials at the high temperatures used for superheating.

3. *Control and power-split problems.* The requirements of properly proportioning the power generation between boiler and superheater, over the life of the reactor, and of avoiding dangerous reactivity changes upon flooding or unflooding of the superheater, present difficult design problems. Further, the effects of the superheater upon the stability and control of the reactor, although not expected to present significant new problems, remain to be met in practice.

A number of other problems, which are related to and which interact with the above problems, can affect strongly the economic performance of the reactor, but they cannot properly be considered as problems of basic technical feasibility. These problems apparently are the ones that have played a rather large part in determining the designs considered in the evaluation study. The more important ones are:

1. *Parasitic neutron absorption.* The parasitic absorption in superheat reactors tends to be high because (1) low cross-section materials capable of operation in superheated steam are not available, (2) the strengths of materials are lower at the high temperatures required, and (3) in many of the concepts, thermal insulation must be provided between the superheated steam and the liquid water that is present in the reactor. These considerations, for example, account for the use of annular fuel elements, cooled on the inside by steam and on the outside by boiling water, which, in effect, use the oxide fuel as thermal insulation between the two phases. As mentioned above, the same considerations in many cases dictate the use of relatively thin "collapsed clad" fuel jackets. An alternate approach to the neutron-conservation problem is to design the superheating portion of the reactor as a fast-neutron system, as is done in the mixed-spectrum and fast-breeder reactors. In such a case, relatively large amounts of steel may be used, and free-standing fuel jackets are possible.

2. *Power density.* Unless particular pains are taken with the design, the power density in the superheat reactor tends to be lower than that in a pressurized-water or boiling-water reactor, simply because of the poorer heat-

Table X-6   SUPERHEATING REACTOR PLANTS UNDER CONSTRUCTION[2]

	BORAX-V	Pathfinder	BONUS
Location	NRTS, Idaho	Sioux Falls, S. Dak.	Puerto Rico
Net plant power, Mw(e)	3.5	66	17.3
Total plant costs, not including site or switchgear (estimated)	$1,700,000	$21,300,000	$11,150,000
Status	Construction	Construction	Construction
Owner of reactor	USAEC	NSP	USAEC
Owner of power plant	USAEC	NSP	PRWRA
Prime contractor	ANL	AC	GNEC
Reactor designer (nuclear)	ANL	AC	GNEC
Architect-engineer	Norman Fink Engineers	Pioneer Services and Engineers	Jackson and Moreland, Inc.
Operating contractor	ANL—Idaho	NSP	PRWRA
Function	Power experiment	Electric power	Electric power
Reactor type	Thermal neutron, H_2O moderated	Thermal neutron, H_2O moderated	Thermal neutron, H_2O moderated
Reactor system	Integral boiling-superheating reactor	Integral boiling-superheating reactor	Integral boiling-superheating reactor
Plant steam cycle	Direct	Direct	Direct
Location of superheating region	Central or peripheral	Central	Peripheral
Location of boiling region	Central or peripheral	Peripheral	Central
Start research and development program	Continuing	August 1957	July 1959
Start design	January 1959	January 1959	February 1960
Start construction	October 1959	November 1959	August 1960
Achieve criticality	April 1961	June 1962	December 1962
Reach full power	July 1961	October 1962	December 1962
Gross turbine power, Mw(e)	3.5	66	17.3
Net plant power, Mw(e)	3.5	62	16.3
Total reactor power, Mw(t)	40	203	50.0
Nominal operating pressure on reactor, psig	600	600	900
Turbine throttle steam pressure, psig	350	450	850
Saturated-steam temperature, °F	489	489	534
Superheated-steam temperature, °F	850	825	900
Power to boiling, Mw(t)	16.6	164	38.6
Power to superheating, Mw(t)	3.4	39	11.4
Gross cycle efficiency, %		32.5	34.6
Net cycle efficiency, %		30.5	32.6
Maximum fuel-centerline temperature in boiling region, °F	2700	4400	4400

Table X-6   (Continued)

	BORAX-V		Pathfinder		BONUS	
Maximum fuel-cladding temperature in superheater region, °F	1110		1250		1140	
Total reactor steam flow, lb/hr	88,800		615,000		152,000	
	Boiler	Superheater	Boiler	Superheater	Boiler	Superheater
Effective outside core diameter, ft	3.25	Central SH, 1.0	6.0	2.5	3.34	4.71
Core height, ft	2.0	2.0	6.0	6.0	4.54	4.55
Structural material (active core)	Al (X-8001)	S.S.	Zircaloy-2	S.S.	Zircaloy-2	S.S.
Fuel type	Rod	Plate	Rod	Double tubular	Rod	Rod
Fuel material	UO_2	UO_2-S.S. cermet	UO_2	UO_2-S.S. cermet	UO_2	UO_2
Fuel enrichment	5, 10, and 20	93	1.85	93	2.40 and 0.71	3.25
Cladding material	304 S.S.	304 S.S.	Zircaloy-2	316L S.S.	Zircaloy-2	316 S.S.
Control-rod shape	Cruciform and "T" blades	Cruciform and "T" blades	Cruciform	Annular	Cruciform	Slab
Control-rod material	Boral	Boral	2 wt.% boron in S.S.	2 wt.% boron in S.S.	2 wt.% boron in S.S.	2 wt.% boron in S.S.
Control-rod entry in core	Bottom	Bottom	Top	Top	Top	Top
No. of steam passes in core		2		1		4

transfer and heat-transport properties of steam. The problem is not as difficult as that in an indirect-cycle gas-cooled reactor because the available pressure drop for coolant flow can be rather large without resulting in large pump requirements and the temperature drop in the intermediate heat exchanger is voided. Nevertheless, the desire, at least in the pressure-vessel type reactors, is to use small coolant channels and highly subdivided fuel in the superheater in order to achieve power densities comparable to those in the nonsuperheat water-cooled reactors. Such an approach again leads to high parasitic neutron absorption, unless the problem can be circumvented by clever design. An alternate approach is, of course, the use of the tube type reactor rather than the pressure-vessel type, in which the consideration of power density is presumably less important.

3. *Steam separation and drying.* These problems are linked very closely to the basic superheat problems discussed above, and the degree of perfection that must be attained in separating and drying the steam will probably not be known until some operating results are available. However, the problem of separating the steam-water mixture within the reactor vessel is a difficult one for large boiling reactors, even when superheat is not applied, and the problem can have a relatively large effect on the overall reactor design. It can, of course, be solved in a straightforward way by the use of external steam drums, but usually at some additional cost. The OTSR represents a method of eliminating the problem if the concept proves to be feasible. It would appear, however, that this approach would be particularly susceptible to any troubles that might result from the deposition of solids as the steam evaporates, and, basically, it is a fear of these troubles that accentuates the concern about steam separation and drying in all superheat reactors.

References

1. Kaiser Engineers Div., Henry J. Kaiser Co., Steam-Cooled Power Reactor Evaluation Capital and Power Generation Costs, USAEC Report TID-12747, Mar. 17, 1961.

2. Steam-Cooled Power-Reactor Evaluation, USAEC Report TID-8536, November 1961.
3. Atomics International, Steam-Cooled Power Reactor Evaluation. Graphite-Moderated, Boiling Water, Steam-Superheat Reactor, USAEC Report NAA-SR-6100 (Vols. I and II).
4. Westinghouse Electric Corp., Atomic Power Dept., Graphite Moderated Integral Boiling and Superheating Pressure Tube Reactor, USAEC Report WCAP-1674 (Rev.), February 1961.
5. General Nuclear Engineering Corp., Steam-Cooled Power Reactor Evaluation. Integral Nuclear Superheat Reactors, USAEC Report GNEC-150, Apr. 30, 1961.
6. Bertram Wolfe, Steam-Cooled Power Reactor Evaluation. Mixed Spectrum Superheater, USAEC Report GEAP-3590(Rev.1), General Electric Co., Atomic Power Equipment Dept., November 1960.
7. R. T. Pennington, Steam-Cooled Reactor Evaluation. Study of 300 Mw(e) Once-Through Superheater Reactor, USAEC Report GEAP-3633, General Electric Co., Atomic Power Equipment Dept., January 1961.
8. Hanford Atomic Products Operation, Steam-Cooled Power Reactor Evaluation—Beloyarsk (Ural) Reactor, USAEC Report HW-67473, April 1961.
9. G. Sofer et al., Steam-Cooled Power Reactor Evaluation, Steam-Cooled D_2O-Moderated Reactor, USAEC Report NDA-2161-2, Nuclear Development Corp. of America, Apr. 15, 1961.
10. G. Sofer et al., Steam-Cooled Power Reactor Evaluation, Steam-Cooled Fast Breeder Reactor, USAEC Report NDA-2148-4, Nuclear Development Corp. of America, Apr. 15, 1961.
11. R. T. Pennington, Steam-Cooled Power Reactor Evaluation for 300 Mw(e) Separate Superheater Reactor, USAEC Report GEAP-3589(Rev.1), General Electric Co., Atomic Power Equipment Dept., November 1960.
12. Civilian Power Reactor Program, Part II, Economic Potential and Development Program as of 1959, USAEC Report TID-8517(Pt.II), 1960.
13. N. A. Dollezhal et al., Uranium-Graphite Reactor with Superheated High Pressure Steam, *Proceedings of the Second United Nations International Conference on the Peaceful Uses of Atomic Energy, Geneva, 1958*, Vol. 8, p. 398, United Nations, New York, 1958.

Reactor Experiments

A report has been issued that lists in detail the as-constructed characteristics of the SPERT-III reactor system.[1] Several pertinent engineering calculations and tables of experimental reactor design data are included in this report. Earlier reports outlined the whole Special Power Excursion Reactor Test (SPERT) program, including the participation of the SPERT-III reactor.[2] The over-all SPERT program involves various reactor power excursion tests that are designed to obtain experimental data on the kinetic behavior of water-cooled and -moderated reactors. The SPERT-III system is designed to continue the SPERT program research at operating pressures, temperatures, and power-density levels characteristic of power reactors. The facility was completed and accepted for operation by the Phillips Petroleum Company in October 1958; criticality was achieved in December 1958, and SPERT-III has been engaged in kinetics testing since March 1960.

The SPERT-III facility includes all buildings, instrumentation, vessels, cooling systems, and other auxiliaries that are necessary for the testing of reactor cores at power levels up to 60 Mw(t). It is an addition to the SPERT-I and SPERT-II facilities which are located at the National Reactor Testing Station (NRTS) in Idaho. The core vessel and primary coolant system components are designed for operation at pressures up to 2500 psig and at temperatures up to 650°F. Both boiling and nonboiling (pressurized) cores may be tested. All reactor energy is dumped through heat exchangers by vaporization of secondary coolant system water. Reactor control is accomplished from a remote center that is located approximately $\frac{1}{2}$ mile from the reactor building. A list of the major reactor and initial core parameters is given in Table XI-1.

The core that has been used thus far in the tests contains uranium enriched to 93.5 per cent U^{235} as UO_2 powder, which is uniformly dispersed in sintered type 304 stainless steel. This ceramic-metal fuel is in the form of plates and is clad with type 304L stainless steel. Three types of fuel assemblies are used. These are (1) the standard assembly, which has 38 fuel plates per assembly; (2) a smaller assembly, which has 32 plates per assembly; and (3) the fuel sections of control rods, each of which contains 32 plates. Each of the 38 plates contained in the 40 standard assemblies consists of a 0.020- by 1.155- by 36.0-in. fuel plate that is clad with 0.005-in.-thick stainless steel. The four smaller fuel assemblies contain 0.020- by 0.918- by 36-in. fuel plates that are also clad with 0.005-in.-thick stainless steel. The eight fuel-containing control-rod sections contain fuel plates identical to those of the smaller fuel assembly. The three groups of fuel plates contain 16.8, 13.8, and 12.93 g of U^{235} per plate, respectively. Cooling water flows upward through all fuel assemblies. A schematic section of the core vessel is shown in Fig. XI-1.

Control of the reactor is accomplished by eight combination poison-fuel assemblies. These are yoked together in pairs and are positioned by four motor-positioning air-scram drives that are located on the core vessel head. The fuel sections are positioned below the boron—stainless steel poison sections. Cooling water flows upward through the fuel and then through the boxlike poison sections. A cruciform transient rod with 5.025-in.-wide 0.187-in.-thick blades is positioned in the center of the core. This rod is positioned by a fifth drive unit.

A brief description of the BORAX-V reactor was given in the December 1960 issue of *Power*

Table XI-1   DESIGN DATA FOR THE SPERT-III
REACTOR[1] (INITIAL CORE)

|	
Maximum steady-state power level (for a maximum of 30 min), Mw(t)	60
Maximum operating pressure, psig	2500
Maximum operating temperature, °F	650
Maximum primary coolant flow rate (2 loops, 4 pumps), gal/min	20,000
Core diameter, in.	24
Core height, in.	36
Number of fuel assemblies (all types)	52
Number of full-sized fuel assemblies	40
Number of small-sized fuel assemblies	4
Number of combination control-fuel assemblies	8
Fuel material (cermet)	93.5% enriched UO_2–stainless steel
Total number of fuel plates (includes three types of assemblies)	1904
Fuel-plate dimensions (approximate), in.	$36 \times 1 \times 0.020$
Fuel-cladding thickness, in.	0.005
Water in core, vol.%	73.5
Stainless steel in core, vol.%	25.2
UO_2 in core, vol.%	1.3
Fuel-assembly water-channel width (nominal), in.	0.128
Maximum power density, kw/liter	217
Number of control rods (combination, box shaped)	8
Control-material composition	Boron (1.35% B^{10}) in 18-8 stainless steel
Number of transient (control) rods	1
Transient-rod material	Boron (1.35% B^{10}) in 18-8 stainless steel
Transient-rod travel, in.	42
Transient-rod drop time, sec	0.2
Number of control-rod drives (control rods are yoked in pairs)	4
Type of control-rod drives	Unbalanced air-piston drive, with motor-driven acme-screw drive positioning, air scrammed
Reactor-vessel inside diameter, in.	48
Over-all reactor-vessel length (approximate), ft	24
Inside diameter of inner thermal shield, in.	$34\frac{1}{4}$
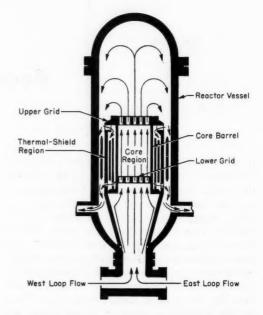
Fig. XI-1   General coolant-flow pattern through the SPERT-III core vessel.[1]

Reactor Technology, Vol. 4, No. 1. The design and hazards summary report[3] for BORAX-V, which has recently become available, contains more detailed design information. A comparison of the SPERT-III and BORAX-V facilities and their test programs can be summarized as follows:[2-5]

1. The SPERT-III program deals primarily with transient reactor behavior, whereas the BORAX program will cover normal operating conditions and determine operational limits.

2. Pressurized and boiling cores are being investigated under the SPERT-III program. Boiling and superheating cores may be investigated in the BORAX reactor.

3. The SPERT-III pressure vessel and primary coolant loops are designed for higher pressure operation than are the BORAX-V components.

References

1. R. E. Heffner and T. R. Wilson, SPERT-III Reactor Facility, USAEC Report IDO-16721, Phillips Petroleum Co., Oct. 25, 1961.

2. W. E. Nyer and S. G. Forbes, SPERT Program Review, USAEC Report IDO-16634, Phillips Petroleum Co., Oct. 19, 1960.

3. Argonne National Laboratory, Design and Hazards Summary Report, Boiling Reactor Experiment V (BORAX-V), USAEC Report ANL-6302, May 1961.

4. F. Schroeder, SPERT-III Hazards Summary Report, USAEC Report IDO-16425, Phillips Petroleum Co., Jan. 14, 1958.

5. C. R. Montgomery et al., Summary of the SPERT-I -II, and -III Reactor Facilities, USAEC Report IDO-16418, Phillips Petroleum Co., Nov. 1, 1957.

Variable-Moderator Reactor

The variable-moderator reactor (VMR) concept being investigated for AEC by Advanced Technology Laboratories, a division of American-Standard, was reviewed briefly in the December 1960 issue of *Power Reactor Technology*, Vol. 4, No. 1. Reference 1 is a report of a study of the feasibility and economic potential of the reactor type. The concept considered differs from that previously described in *Power Reactor Technology* in that the moderator flow circuit is entirely separate from the coolant circuit (see Fig. XII-1). Separation of moderator and coolant flow within the core region is achieved by a calandrialike structure (Fig. XII-2), wherein each fuel bundle (conventional UO_2 rod type elements) is contained and cooled by water (H_2O) flow within an individual, hexagonal vertical tube; moderator water (H_2O) surrounds each of the fuel-containing tubes.

The study[1] is directed at the technical feasibility and economic potential of the VMR concept; the results of physics critical experiments are given, and a cost comparison of the reactor part of an electric plant is made with a boiling-water reactor of about the same power [71.5 Mw(t), 19.3 Mw(e)]. The cost comparison indicates a saving of 0.38 mill/kw-hr with the VMR. The report[1] states that for plants of smaller output the cost saving due to the VMR concept is expected to be larger and implies that the VMR cost saving would be less for larger plants. Other things being equal, core power density tends to be lower for the VMR concept because the average water-to-fuel ratio is somewhat higher; in the higher-output reactors, this consideration appears to become controlling. With respect to purely technical questions, the reference reports that the critical experiments have, in general, confirmed the calculational methods used in the VMR design. No insurmountable problems were indicated by the

feasibility study; however, a research and development program is required. A discussion is given on one possible hazard peculiar to the VMR: an unplanned increase in reactivity caused by coolant-water leakage into the moderator-water region of the core. After careful study of all applicable hardware, it is concluded that the VMR scram system, which works by dumping the moderator from the core, is of adequate capacity to accommodate all anticipated accidental coolant-to-moderator leaks.

Among the attractive features of the VMR concept is the absence of moving parts within the reactor. Reactivity control is accomplished by manipulation of an external flow loop that is made up of more or less standard hardware such as pumps, valves, heat exchangers, piping, tanks, and a water cleanup system. Because this equipment is external to the reactor, it is hoped that maintenance could be simplified and that the availability of the reactor would show an improvement over that of more conventional types.

With regard to reactor performance, the basic idea of reactivity control by adjustment of water-to-fuel ratio has always held out the hope of improvements in the areas of neutron economy and power distribution. The first of these is based on the expectation that reactivity adjustment by this means would result primarily from adjustment of the fraction of neutrons absorbed in the neutron resonances of U^{238}, rather than from adjustment of the parasitic neutron absorption, whereas the second is based on the hope that changes in water-to-fuel ratio could be made rather uniformly over the core and that strong power-distribution distortions by the control system could be avoided. These hopes prove to be difficult of realization in a practical system. In the present case, the partial-height moderator proves to have an ef-
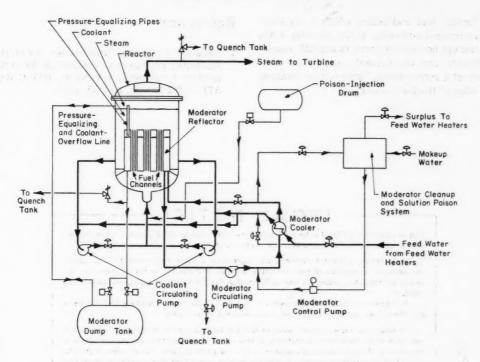
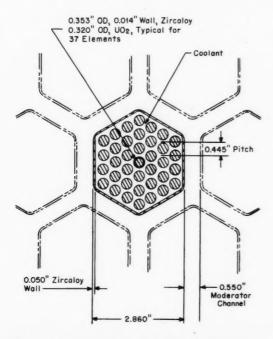Fig. XII-1 Coolant and moderator flow diagram for the VMR.[1]

Fig. XII-2 Structure showing separation of moderator and coolant flow for the VMR.[1]

fect much like that of a bank of partially inserted control rods, causing a bad skewing of the axial power distribution toward the bottom of the core. To avoid this effect, the designers resort to a variable concentration of neutron absorber (boric acid) in the moderator water for controlling the long-term reactivity swing due to fuel burnup and fission-product poisons. This does, of course, forfeit the basic neutron-economy advantage of the VMR concept. The reference points out that the use of a soluble poison in the VMR is more practical than it is in the conventional boiling reactor, where the absorber must be mixed with the circulating coolant.

The VMR of optimum design,[1] using soluble poison, does achieve a better power distribution than the "conventional" boiling reactor with which it was compared (which also uses soluble poison). The improvement, however, is all in the axial component of the distribution and appears to be due to the fact that the variable-moderator design uses forced circulation of the restricted amount of coolant available, whereas the conventional boiler uses natural circulation in the

more "open" fuel-rod lattice which it employs. The maximum-to-average power-density ratio in the hottest horizontal plane is actually somewhat higher for the variable-moderator core because of a rather large "water-hole" peaking at the edge of the fuel bundle.

Reference

1. Advanced Technology Laboratories, Technical Feasibility and Economic Potential of the Variable Moderator Reactor, Final Report, USAEC Report ATL-A-109(Rev. 1), Dec. 15, 1960.
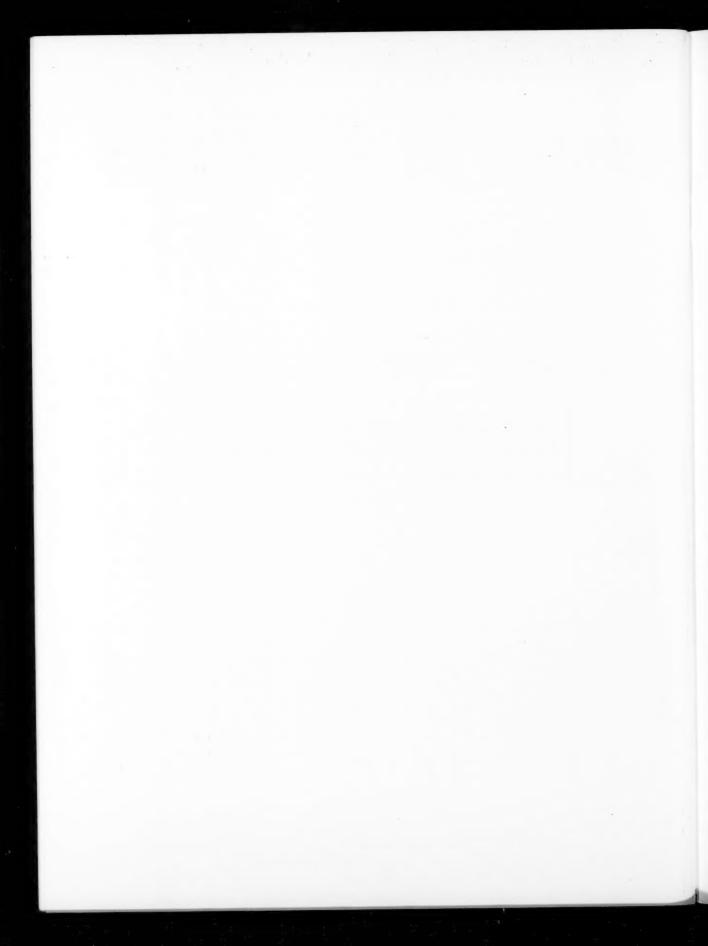
NUCLEAR SCIENCE ABSTRACTS

The U. S. Atomic Energy Commission, Division of Technical Information, publishes *Nuclear Science Abstracts (NSA)*, a semimonthly journal containing abstracts of the literature of nuclear science and engineering.

NSA covers (1) research reports of the U. S. Atomic Energy Commission and its contractors; (2) research reports of government agencies, universities, and industrial research organizations on a world-wide basis; and (3) translations, patents, books, and articles appearing in technical and scientific journals.

Complete indexes covering subject, author, source, and report number are included in each issue. These are cumulated quarterly, semiannually, and annually providing a detailed and convenient key to the literature.

Availability of NSA

SALE *NSA* is available on subscription from the Superintendent of Documents, U. S. Government Printing Office, Washington 25, D. C., at $22.00 per year for the semimonthly abstract issues and $15.00 per year for the four cumulated-index issues. Subscriptions are postpaid within the United States, Canada, Mexico, and all Central and South American countries, except Argentina, Brazil, British and French Guiana, Surinam, and British Honduras. Subscribers in these Central and South American countries, and in all other countries throughout the world, should remit $27.50 per year for subscriptions to semimonthly abstract issues and $17.50 per year for the four cumulated-index issues.

EXCHANGE *NSA* is also available on an exchange basis to universities, research institutions, industrial firms, and publishers of scientific information. Inquiries should be directed to the Division of Technical Information Extension, U. S. Atomic Energy Commission, P. O. Box 62, Oak Ridge, Tennessee.

TECHNICAL PROGRESS REVIEWS may be purchased from Superintendent of Documents, U. S. Government Printing Office, Washington 25, D. C. for $2.00 per year for each subscription or for $0.55 per issue. The use of the coupon below will facilitate the handling of your order.

POSTAGE AND REMITTANCE: Postpaid within the United States, Canada, Mexico, and all Central and South American countries except as hereinafter noted. Add $0.50 per year, or $0.15 per single issue, for postage to all other countries, including Argentina, Brazil, British and French Guiana, Surinam, and British Honduras. Payment should be by check, money order, or document coupons, and MUST accompany order. Remittances from foreign countries should be made by international money order, or draft on an American bank, payable to the Superintendent of Documents, or by UNESCO book coupons.

order form

SUPERINTENDENT OF DOCUMENTS
U. S. GOVERNMENT PRINTING OFFICE
WASHINGTON 25, D. C.

Enclosed:

document coupons ☐   check ☐   money order ☐

Charge to Superintendent of Documents No. _____

Please send a one-year subscription to

☐ REACTOR MATERIALS
☐ POWER REACTOR TECHNOLOGY
☐ NUCLEAR SAFETY
☐ REACTOR FUEL PROCESSING

(Each subscription $2.00 a year; $0.55 per issue.)

SUPERINTENDENT OF DOCUMENTS
U. S. GOVERNMENT PRINTING OFFICE
WASHINGTON 25, D. C.

(Print clearly)

Name _____

Street _____

City _____ Zone ____ State _____